

Biomechanical evaluation of intervertebral disc treatments

Andrew Robert Dixon

Submitted in accordance with the requirements for the degree of Doctor of
Philosophy

The University of Leeds
Institute of Medical and Biological Engineering
School of Mechanical Engineering
Faculty of Engineering and Physical Sciences

July 2022

The candidate confirms that the work submitted is his/her own, except where work which has formed part of jointly-authored publications has been included. The contribution of the candidate and the other authors to this work has been explicitly indicated below. The candidate confirms that appropriate credit has been given within the thesis where reference has been made to the work of others. Further details of the jointly-authored publications and the contributions of the candidate and the other authors to the work should be included below this statement.

Chapter 1 and parts of discussions in other chapters include elements from two jointly authored bodies of work:

Dixon, A.R., Warren, J.P., Culbert, M.P., Mengoni, M. and Wilcox, R.K. 2021. Review of in vitro mechanical testing for intervertebral disc injectable biomaterials. *Journal of the Mechanical Behavior of Biomedical Materials*.

Culbert, M.P., Warren, J.P., **Dixon, A.R.**, Fermor, H.L., Beales, P.A. and Wilcox, R.K. 2022. Evaluation of injectable nucleus augmentation materials for the treatment of intervertebral disc degeneration. *Biomaterials Science*.

This copy has been supplied on the understanding that it is copyright material and that no quotation from the thesis may be published without proper acknowledgement.

Abstract

Lower back pain, which has been associated with intervertebral disc degeneration, is a leading cause of disability worldwide and is associated with a large socioeconomic cost. A proposed treatment for disc degeneration is nucleus augmentation, where a biomaterial is injected into the nucleus pulposus of the disc aiming to restore disc height and biomechanics. Current laboratory test methods have not been adapted for evaluating soft tissue mechanics. The aim of this project was to develop and utilise a suite of methods to evaluate the mechanical properties and effects of injectable treatments on the intervertebral disc. A further goal was to develop a prototype delivery device to meet the unique requirements of the University of Leeds peptide hydrogel.

High magnitude loading was applied to bovine tail intervertebral discs in native, degenerated, and treated states. Discs were cyclically tested under high magnitude to 20,000 cycles aiming to exacerbate potential mechanical consequences across the different states. A rapid enzymatic degeneration procedure was performed to replicate an early stage degeneration state. Predictive modelling was applied to the 20,000 cycle data and showed the mechanical behaviour in the native and degenerate states can be estimated with approximately 1,000 to 5,000 cycles.

A further study was performed using 1,000 cycles which evaluated different parameters with respect to mechanical restoration. The test method found a strong relationship with the clinically measurable parameters volume injected ($r^2=0.7$) and change in disc height from the injection ($r^2=0.8$). The developed bovine tissue *in vitro* model was transferred to human tissue. Several issues with the transfer were addressed and a preliminary set of data was analysed.

Finally, a novel prototype device was developed that is able to deliver the University of Leeds patented hydrogel. *In vitro* and clinical studies were completed to evaluate the efficacy of the novel device. These studies examined the performance of the design and highlighted the need to assess the delivery requirements for injectable treatments.

Overall, a suite of tests has been developed that were able to mechanically evaluate the performance of injectable nucleus augmentation treatments. Mechanical testing was shown to be an important factor that can help optimise the surgical process, mitigate risks, and contribute towards clinical translation.

Acknowledgements

I would like to start by thanking my supervisors, Professor Ruth Wilcox and Dr. Marlène Mengoni, for their fantastic support during this PhD. Even during the trying times of a global pandemic, they have given me their time and guidance which has allowed me to complete my research and this thesis. I am incredibly humbled to have been a part of this team and feel privileged to have had them as my supervisors.

I would like to express my thanks to the members of iMBE who have helped me immeasurably throughout my project. I appreciate the support from the technical team in the institute, specifically, my thanks must go to Andrew Stockdale and Phillip Wood for all their technical assistance in the project. Additional thanks must go to Dr. Nagitha Wijayathunga for his assistance with MRI scanning, handling, and dissection of human tissue. I have to give special thanks to Dr. James Warren for his aid in the development of the degenerate model and for passing on his laboratory wisdom to me. I want to give a huge thank you to Mr. Matthew Culbert, who not only completed the rheological data in this project, but also provided me with a huge amount of support in the lab, even whilst I was injured. A special thank you goes to them both for all their aid in the biology lab as well!

I am extremely grateful to the human tissue donors and their families for their selfless donations which enabled the progression of my research. I would like to extend my gratitude to the partners involved in this project including the Medical Technologies IKC team, University of Cambridge, University of Nottingham, and the Royal Veterinary College. I would like to thank the UKRI and EPSRC for funding this research allowing me to complete this PhD.

I want to thank my colleagues, friends, and family for their support in my career, and most importantly I want to thank my wonderful partner, Natalia, who has pulled me through some of the toughest times in my PhD.

Table of Contents

1	Introduction.....	1
1.1	The spine.....	1
1.2	The Intervertebral disc.....	2
1.2.1	Structure and function.....	2
1.2.2	Nucleus Pulposus.....	4
1.2.3	Annulus Fibrosus.....	5
1.2.4	Endplates	5
1.2.5	Hydration and Cellular behaviour.....	6
1.2.6	Mechanical behaviour.....	7
1.3	Disc degeneration.....	10
1.3.1	Diagnosis.....	13
1.3.2	Treatment.....	16
1.3.3	Nucleus replacement and nucleus augmentation.....	17
1.4	Load estimation of intervertebral discs.....	19
1.4.1	Direct measurements of the disc for load estimation.....	20
1.5	<i>In vitro</i> testing	26
1.5.1	Mechanical loading.....	26
1.5.2	Specimen preparation.....	34
1.5.3	Test environment.....	35
1.5.4	Tissue models	36
1.5.5	Artificial degeneration	38
1.5.6	Freeze-thaw cycling.....	42
1.5.7	Nucleus augmentation	43
1.5.8	Biomaterial delivery	43
1.6	Summary and Conclusions.....	46
1.7	Aims and Objectives.....	47
1.8	Thesis structure	47

2	Materials and Methods	46
2.1	Introduction.....	46
2.2	Methods.....	46
2.2.1	General stock solution preparation	46
2.2.2	General <i>in vitro</i> testing approach	46
2.2.3	Bovine tail dissection methodology.....	47
2.2.4	Bovine bone-disc-bone unit biomechanical testing	49
2.2.5	Bovine bone-disc-bone unit artificial degeneration.....	51
2.2.6	Statistical testing.....	51
3	High cycle loading of bovine tail intervertebral discs	54
3.1	Introduction.....	54
3.2	Methods.....	55
3.2.1	Overview	55
3.2.2	Sham degenerate group	56
3.2.3	Treatment.....	56
3.2.4	Data Analysis	56
3.3	Results	60
3.3.1	Disc Mechanical Properties.	60
3.3.2	Stiffness comparison across states.....	63
3.3.3	Extrapolation modelling to 20,000 cycles.....	66
3.3.4	Application of extrapolation models	69
3.4	Discussion	70
3.4.1	Disc Mechanical Properties	70
3.4.2	Extrapolation modelling to 20,000 cycles.....	75
3.4.3	Application of extrapolation models	76
3.5	Conclusions.....	77
4	Injection parameter assessment in bovine tail intervertebral discs	76
4.1	Introduction.....	76

4.2	Methods.....	77
4.2.1	Overview	77
4.2.2	Treatment.....	77
4.2.3	Data Analysis	78
4.3	Results	79
4.4	Discussion	84
4.5	Conclusion.....	86
5	Application and adaptation of methods for human spinal tissue.....	86
5.1	Introduction.....	86
5.2	General Methods	87
5.2.1	Donor spine selection	87
5.2.2	Human tissue handling	87
5.2.3	Imaging of spines	87
5.2.4	Bone-disc-bone unit preparation.....	88
5.3	Method Development.....	89
5.3.1	Introduction.....	89
5.3.2	Methods	89
5.3.3	Results	90
5.3.4	Method development conclusion and recommendations.....	92
5.4	Methods.....	93
5.4.1	Overview	93
5.4.2	Additional bone-disc-bone unit preparation.....	94
5.4.3	Step 1, 2, 3, & 5: Biomechanical testing	94
5.4.4	Step 4: Treatment.....	95
5.4.5	Data analysis.....	95
5.5	Results	95
5.6	Discussion	101
5.6.1	Developed methodology.....	101

5.6.2	General mechanical behaviour	101
5.6.3	Effect of treatment	102
5.6.4	Injection end criteria	103
5.7	Conclusion.....	104
6	Delivery device design and evaluation.....	105
6.1	Introduction.....	105
6.2	Device design development.....	106
6.2.1	Nucleus augmentation general surgical workflow	106
6.2.2	Design requirements	106
6.2.3	Additional design details	107
6.3	Design development.....	109
6.4	<i>In vitro</i> needle puncture evaluation	113
6.4.1	Methods	113
6.4.2	Results	115
6.4.3	Discussion and conclusions.....	116
6.5	Rheological evaluation.....	117
6.6	<i>Ex vivo</i> surgical assessment.....	119
6.7	Discussion and Conclusions	120
7	Discussion and Conclusions	122
7.1	Introduction.....	122
7.2	<i>In vitro</i> testing for nucleus augmentation treatments.....	123
7.3	Treatment delivery and clinical implications	126
7.4	Future work and limitations	130
7.4.1	<i>In vitro</i> testing for nucleus augmentation treatments.....	130
7.4.2	Treatment delivery and clinical implications	130
7.4.3	Delivery device	131
7.5	Conclusions.....	132
	References.....	133

Appendix 1 – General stock solution preparation	123
8 General stock solution preparation	123
8.1 Sodium citrate.....	123
8.2 Phosphate buffer saline	123
8.3 Papain	123
8.4 Ebselen	123
8.5 Peptide hydrogel.....	124
Appendix 2 – Human tissue MRI scans	75
9 Human tissue MRI scans	75
9.1 Spine 2	75
9.2 Spine 3	78
10 Appendix 3 – Technical Drawings	160
10.1 Specialist needle technical drawing	160
10.2 Handling device technical drawings	161
10.2.1 Assembly.....	161
10.2.2 Device Top	162
10.2.3 Device bottom	163
10.2.4 Rear plate.....	164
10.2.5 Syringe attachment.....	165
10.2.6 Tekscan Press.....	166
10.2.7 Blanked syringe attachment.....	167

List of figures

Figure 1.1 – Lateral view of a vertebral column showing regions alongside number of vertebrae and intervertebral discs. Adapted from Servier Medical Art image bank (smart.servier.com), shared under CC by 3.0.	1
Figure 1.2 - Lateral and superior view of typical lumbar vertebra showing the vertebral body, neural foramen, and posterior processes. Adapted from Servier Medical Art image bank (smart.servier.com), shared under CC by 3.0.....	2
Figure 1.3– Basic diagrams showing anterior, lateral, or superior views for a disc going through: no movement (static), flexion/extension, lateral bending, and axial rotation. ...	3
Figure 1.4 - Illustration of the general structures in an intervertebral disc (Adapted from Dixon et al., 2021).....	4
Figure 1.5 - Sagittal cross section of health young adult disc (Reproduced from Adams et al., 2000).....	4
Figure 1.6 - Angled lamellae of the anulus fibrosus, $\alpha = 25^\circ$ to 45° (Adapted from Adams and Roughley, 2006)	5
Figure 1.7 - Single axis compression of intervertebral disc (Reproduced from Dixon et al., 2021)	9
Figure 1.8 - Progression of disc degeneration (A) non-degenerated disc (B) moderately degenerated disc (C) Severe degeneration (D) extreme degeneration (Reproduced from Kurtz and Edidin, 2006)	11
Figure 1.9 - The Charité intervertebral disc replacement (reproduced from Hall et al., 2006)	17
Figure 1.10 - Comparison of intradiscal pressure during standing, note: Corrected values are due to pressure transducer heating. (Reproduced from Dreischarf et al., 2016) ...	21
Figure 1.11 - Load axes for vertebral body replacement (left) and spinal fixator rods (right). (Adapted from Orthoload.com accessed 18 th Dec 2021).....	23
Figure 2.1 – Flow chart of testing completed including artificial degeneration and treatment. The bypassing arrows indicate testing where the native state can be treated directly, for example in vivo degenerate discs treated without any prior intervention. (Adapted from Dixon et al., 2021)	47
Figure 2.2 – Preparation of bovine bone-disc-bone units A) Full tail, B) Tail cut down from transverse cut along fifth disc, C) Tail with soft tissue removed, D & E) CT scans of cranial and caudal ends of the tail with bone-disc-bone unit measurements, F) Separated	

bone-disc-bone unit pre water piking, G) Separated bone-disc-bone unit post water piking, H) Isometric view of bone-disc-bone unit	48
Figure 2.3 - Preliminary testing which captured the full 24-hour data and was used as the basis for the length of the osmotic equilibrium portion of the main testing (Data from Dr. Ruth Coe and Dr. James Warren University of Leeds, UK), unpublished data shared through private communication).....	49
Figure 2.4 – Visual depiction of mechanical loading protocol for bovine bone-disc-bone units.....	50
Figure 3.1 - Summary flow chart of testing protocol	55
Figure 3.2 - Example curve for a single cycle with stiffness analysis.....	57
Figure 3.3 - Data comparison points for stiffness comparison at 1,000 cycles and using extrapolation analysis to compare at 20,000 cycles	58
Figure 3.4 – Example plot showing the actual data with the extrapolated confidence intervals for a restored specimen	59
Figure 3.5 - Categorisation and status of treated state stiffness based on native and degenerate state predictions, note: over-restored, damaged, restored and not restored occur in both categories.....	60
Figure 3.6 - Example of decreasing specimen height throughout duration of test (up to 1,000 cycles), data taken from specimen in 1 ml GAG:PEP group.....	60
Figure 3.7 - Change in specimen height from the cycle 1 to cycle 1000 for each specimen	61
Figure 3.8 - Decreasing size of hysteresis loop throughout length of test, A) example full hysteresis loops from different cycles, B) Example plot of hysteresis change over 1,000 cycles across multiple states.....	61
Figure 3.9 - A&B) Example plot of same specimen from 0.3 mL PEP:GAG group showing smooth increase throughout test: A) sample to 1,000 cycles, B) sample to 20,000 cycles, C) Example from 0.3 mL PEP:GAG group showing observed large shift exhibited by treated state specimens, D) Example from 0.3 mL PEP:GAG group showing small change in stiffness observed.....	62
Figure 3.10 - Example of lateral transverse plane motion from post-test CT scan, left) Post native test CT scan, right) Post degenerate test CT scan	62

Figure 3.11 – Degenerate state stiffness normalised to the native state stiffness for Individual discs, n=34 for degenerate state, n=6 for ‘sham’ degenerate state. Dashed lines are at 0, the native state and $\pm 10\%$ from the native.	64
Figure 3.12 – Degenerate and treated state stiffnesses normalised to the native state stiffness for individual discs, split by group. Dashed lines are at 0, the native state and $\pm 10\%$ from the native.	65
Figure 3.13 - Linear regression for all data comparing the low cycle stiffness to the stiffness at 20,000 cycles.....	66
Figure 3.14 – Example plot of function used to predict high cycle behaviour using a small dataset.....	67
<i>Figure 3.15 – Actual value at 20,000 cycles, predicted values based on 1,000 cycle test, and 95% confidence intervals for the A) native and B) degenerate groups.</i>	Error!
Bookmark not defined.	
Figure 3.16 – Two examples of predictive analysis, both plots from 0.3 mL PEP:GAG group, showing A) Stiffness restored, and B) Stiffness not restored.....	70
Figure 3.17 - Pictorial representation of fluid in/out flow and bone-disc-bone unit height through the duration of the test	71
Figure 4.1 – Treatment injection fixture set up (not to scale), BDBU stands for bone-disc-bone unit.....	77
Figure 4.2 – Example images from eliminated specimens A) No response to degeneration procedure native and degenerate stiffness profiles, B) Transverse profile of disc where injection was into the annulus CT image, C) Lateral profile of disc where coalesced microbubbles were identified.....	79
Figure 4.3 – Example typical injection force plot	80
Figure 4.4 - Typical stiffness plot for different states	80
Figure 4.5 - Comparison of stiffness in different states for all specimen.....	81
Figure 4.6 - A) Summary of stiffness differences compared to native state for low, medium, and high-volume specimens, B) Linear regression relationship between mechanical restoration, the ratio between the native state stiffness and the treated state stiffness, and volume injected/cross sectional area.....	83
Figure 5.1 - Prepared bone-disc-bone units prior to the being cleaned with the water pik.	88

Figure 5.2 - Change in disc height during the 24-hour hold period for the first two specimens	90
Figure 5.3 - The stiffness for Spine 1 T10-T11 throughout the duration of the test. The incorrect load control loop targets was applied to the specimen. The initial overshoot from the targets from the increase amplitude can be seen at the start of the test.....	91
Figure 5.4 – Stiffness profiles for two bone-disc-bone units that completed correct loading	91
Figure 5.5 – CT scan pre and post-test screenshots with bone damage circled	92
Figure 5.6 - Flow chart with details of testing completed	93
Figure 5.7 - Example of decreasing specimen height throughout duration of test, data taken from specimen Spine 2 T11-T12	95
Figure 5.8 -Summary of the change in height for specimens in the native and treated states.....	96
Figure 5.9 - Example of a typical change in hysteresis across the duration of the test, data taken from specimen spine 2 T11-T12	96
Figure 5.10 – Example typical change in stiffness over length of test from Spine 3 T12 to L1	97
Figure 5.11 – Stiffness change in specimens where drops were observed, A) Spine 2 T12-L1, B) Spine 2 L4-L5.....	97
Figure 5.12- Native and treated state stiffness for specimens alongside injection end criteria and control specimen (for which the cross is the first test and circle the second test).	98
Figure 5.13 - Injection force plots for different end criteria: A) typical driver slip, B) Typical leak, C) End of syringe.....	99
Figure 6.1 - Bevel needle orientations with representative inside diameters. A) M-shape orientation, B) parallel orientation, C) back-to-back orientation.	109
Figure 6.2 - Design development timeline, A) Phase 1: Development of initial concepts with clinical team feedback followed up a second wave of design concepts, B) Phase 2: Manufacturer development where it was possible to silver braise and bend small diameter needles, C) Phase 3: The agreed design for the in vivo study.....	110
Figure 6.3 - Solidworks renders of agreed design for in vivo study A) Disassembled and B) Assembled	112

Figure 6.4 - Methodology for the needle puncture evaluation, showing the order of the testing and the position of each needle puncture, starting posterior lateral and at approximately 120° for the two set of punctures. 114

Figure 6.5 – Stiffness in the native, 1 x puncture, 2 x puncture, and 3 x puncture states for all specimens..... 115

Figure 6.6 - Mean complex moduli for different needle configurations..... 118

List of Tables

Table 1.1 - Mechanical properties of the nucleus pulposus. *Biphasic-swelling model..	7
Table 1.2 - Grading system proposed by Thompson et al., 1990	15
Table 1.3 - Grading system proposed by Pfirrmann et al., 2001.....	15
Table 1.4 - Summary of load estimates from literature	25
Table 1.5 - Constant load review table, *Value reported as a force and converted to MPa using data from (Beckstein et al., 2008), ** Value reported in MPa and converted to a force using data from (Beckstein et al., 2008; Paul et al., 2012; Dreischarf et al., 2016), all converted values are italicised (Reproduced from Dixon et al., 2021)	27
Table 1.6 -Uniaxial cyclic loading table. *Values reported in MPa and converted to a force using data from (Beckstein et al., 2008), ** Values reported as a force have been converted to MPa using data from (Beckstein et al., 2008; Paul et al., 2012; Dreischarf et al., 2016), all converted values are italicised. One study applied uniaxial cyclic loading to failure of the disc whilst applying a 6 Nm flexion throughout (Lin et al., 2019). (Adapted from Dixon et al., 2021).....	29
Table 1.7 -Range of motion cyclic loading summary	31
Table 1.8 - Comparison of large animal intervertebral disc dimensions adapted from (Monaco et al., 2016) and human tissue dimensions adapted from (Pooni et al., 1986)	37
Table 1.9 - Artificial degeneration techniques applied across different studies, highlighting incubation times, annular damage, and nucleotomy details (Adapted from Dixon et al., 2021).....	39
Table 1.10 – Methods used to deliver augmentation material and maximum volumes injected (Adapted from Dixon et al., 2021)	44
Table 2.1 - Summary of loads applied during testing with the intradiscal pressure/activities the load represents. References for intradiscal pressure activities A - Wilke et al., 1999, B - Sato et al., 1999, and C -Nachemson and Morris, 1963. Bovine loads calculated using a correction factor of 0.66 as recommended by Dreischarf et al., 2016.	50
Table 3.1 – Groups, respective size, and end stage for different specimens. See Figure 3.1 for details on end stage or 20,000-cycle step. *two of the specimens in these groups were completed in a previous study by Dr. Ruth Coe and Dr. James Warren.	56

Table 3.2 - Observed disruptions to smooth stiffness data alongside the group and number of specimens	62
Table 3.3 - Statistical testing for the degenerate and 'sham' groups. The table contains data for the Shapiro-Wilk test p values, type of test used, and test outcomes. All statistically significant results are highlighted in blue.....	64
Table 3.4 – Shapiro-Wilk normality test p values and selected test for statistical comparison. All statistically significant results are highlighted in blue. *Specimens did not have normal distribution in all data but had an sample size of six meaning t-tests were chosen over Wilcoxon sign rank tests.	65
Table 3-5 – p values for the repeated measures ANOVA and follow up paired t-tests for the different treatment groups. All statistically significant results are highlighted in blue.	65
Table 3.6 –R squared values of the linear regression analysis between the actual 20,000 cycle data and reduced cycle numbers. Values above 0.8 have been highlighted in green to show strong relationships.	66
Table 3.7 - Root mean squared error of the linear regression analysis between the actual 20,000 cycle data and reduced cycle numbers. Values with an error of 10% or lower have been highlighted in green to show low errors	67
Table 3.8 – Root mean squared error comparing outputs from the exponential function fitting with reduced cycle numbers to the actual stiffness. Values with an error of 10% or lower have been highlighted in green to show low errors	68
Table 3.9 - Root mean squared error comparing outputs from the natural log function fitting with reduced cycle numbers to the actual stiffness. Values with an error of 10% or lower have been highlighted in green to show low errors	68
Table 3.10 - Root mean squared error comparing outputs from the power law function fitting with reduced cycle numbers to the actual stiffness. Values with an error of 10% or lower have been highlighted in green to show low errors	68
Table 3.11 – Status of treated specimens broken down by group.	70
Table 4.1 – Criteria and number of specimens for eliminated specimens.....	79
Table 4.2 - Shapiro-Wilk normality test p values and selected test for statistical comparison. All statistically significant results are highlighted in blue.....	81

Table 4.3 -- p values for the repeated measures ANOVA and follow up paired t-tests for the different treatment groups. All statistically significant results are highlighted in blue.	82
Table 4.4 – Relationship (linear regression) between parameters and treatment stiffness mechanical restoration.....	83
Table 5.1 -Donor details and segment lengths of selected segments for the study	87
Table 5.2 - Specimens used in testing and degeneration levels.....	88
Table 5.3 - Summary of preliminary testing hold location and test notes.....	92
Table 5.4 - Summary of loads applied during testing with the intradiscal pressure/activities the load represents based on (Nachemson, 1981; Wilke et al., 1999; Dreischarf et al., 2015).....	94
Table 5.5 – Summary of testing, specimens highlighted in light red were not used for further analysis.	98
Table 5.6 – Summary of human tissue testing showing stiffness difference, volume injected, maximum injection force, change in height from injection, and the end injection criteria for the given disc with location of leaks where appropriate.	100
Table 6.1 - Initial overview of user needs and intended uses with corresponding design inputs.....	107
Table 6.2 - Nominal needle outer diameter to mean disc height ratio for ovine, bovine and human tissue (disc heights taken from Monaco et al., 2016).....	108
Table 6.3 - Agreed design for in vivo study part manufacture details	112
Table 6.4 - Shapiro-Wilk normality test p values and selected test for statistical comparison. All statistically significant results are highlighted in blue.....	116
Table 6.5 - Statistical testing for needle puncture groups, tests where p value is below 0.05 are highlighted in blue.....	116
Table 6.6 – Statistical testing of various needle configurations, ANOVA with Bonferroni correction was used to compare all groups and student t-tests were used for the intergroup comparisons, statistically significant results are highlighted in blue (p<0.05).	118

1 Introduction

1.1 The spine

The spine is a complex structure responsible for providing movement and stability to the upper body. The spine consists of the vertebral column, ligaments, and spinal musculature. The vertebral column is separated into five regions known as cervical, thoracic, lumbar, sacrum and coccyx. The overall structure forms a double 's' shape consisting of 24 separate vertebrae (cervical, thoracic, and lumbar), and nine fused vertebrae (sacrum and coccyx). Other than the first two cervical vertebrae (C1 and C2) intervertebral discs lie between the non-fused vertebrae enabling motion. The spine has natural curvature which varies along the length based on anatomical differences. The curvature is referred to as either lordotic or kyphotic. A diagram of the vertebrae and the natural curvature of the regions is shown in Figure 1.1.


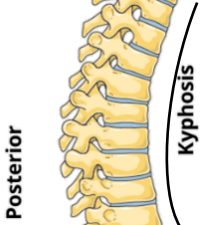
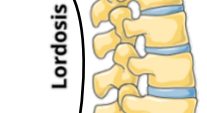

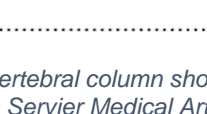
Spinal Region	Vertebral Column:	Region details
Cervical		Vertebrae: 7 (C1 - C7) Intervertebral discs: 6 (C2 - T1)
Thoracic		Vertebrae: 12 (T1 - T12) Intervertebral discs: 12 (T1 - T12)
Lumbar		Vertebrae: 5 (L1 - L5) Intervertebral discs: 5 (L1 - S1)
Sacrum		Vertebrae: 5 (fused) (S1 - S5) Intervertebral discs: None
Coccyx		Vertebrae: 4 (fused) (Co1 - Co4) Intervertebral discs: None

Figure 1.1 – Lateral view of a vertebral column showing regions alongside number of vertebrae and intervertebral discs. Adapted from Servier Medical Art image bank (smart.servier.com), shared under CC by 3.0.

The size and shape of vertebrae vary at different spinal levels but maintain a general structure consisting of a central body (attaching cranially and caudally to intervertebral

discs), a neural foramen (opening for spinal cord), and posterior elements. The posterior elements connect to the vertebral body via pedicles and include two transverse processes, a spinous process, two lamina, and superior/inferior articular processes. The transverse processes, spinous processes, and lamina act as attachment points for muscles or ligaments. The articular processes are the zygapophyseal (or facet) joints and connect adjacent vertebrae. The joints bear the loading and receive support from the muscles and ligaments. An example of a typical vertebrae is shown in Figure 1.2.

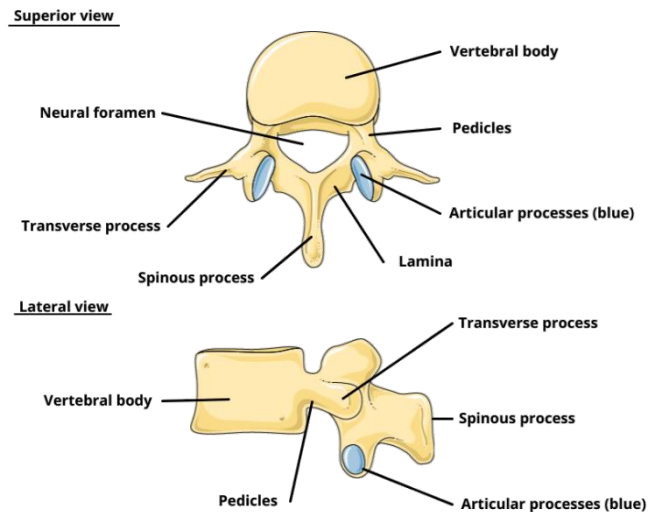


Figure 1.2 - Lateral and superior view of typical lumbar vertebra showing the vertebral body, neural foramen, and posterior processes. Adapted from Servier Medical Art image bank (smart.servier.com), shared under CC by 3.0.

1.2 The Intervertebral disc

1.2.1 Structure and function

Intervertebral discs sit between vertebrae and are responsible for transferring and supporting load across the vertebral bodies. The processes in conjunction with the intervertebral discs enable a wide set of motions including flexion/extension, lateral bending, and axial rotation as shown in Figure 1.3. The motions are often coupled together on an individual disc due to the natural curvature of the spine and the connections between vertebrae.

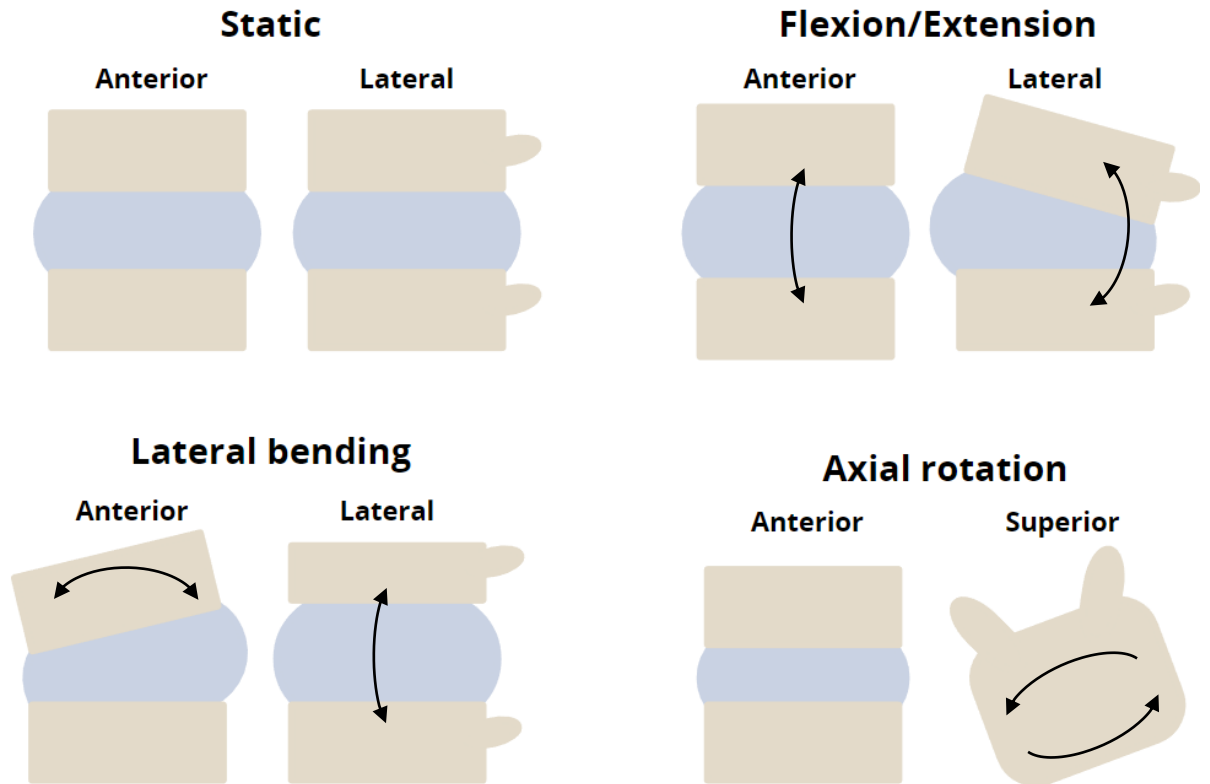


Figure 1.3– Basic diagrams showing anterior, lateral, or superior views for a disc going through: no movement (static), flexion/extension, lateral bending, and axial rotation.

The tissue is predominantly aneural and the disc is considered the largest avascular structure in the body, with some parts of the disc up to 8mm away from the closest blood supply (Benneker et al., 2005). Like vertebrae, the size and shape of intervertebral discs varies according to the spinal region: the cross-sectional area generally increases caudally and the shape of the disc changes in line with the functional requirements of each region. The transverse cross section of cervical and lumbar discs is generally elliptical, whilst thoracic discs tend to be more circular (Pooni et al., 1986). Despite regional differences, all intervertebral discs have three constituents: the gel-like nucleus pulposus, which is surrounded by the annulus fibrosus, and cartilaginous endplates sandwiching the nucleus and annulus as illustrated in Figure 1.4. The area between the nucleus and annulus is not a solid distinctive line, instead there is a “transition zone” where the nucleus blends into the inner annulus as shown in Figure 1.5.

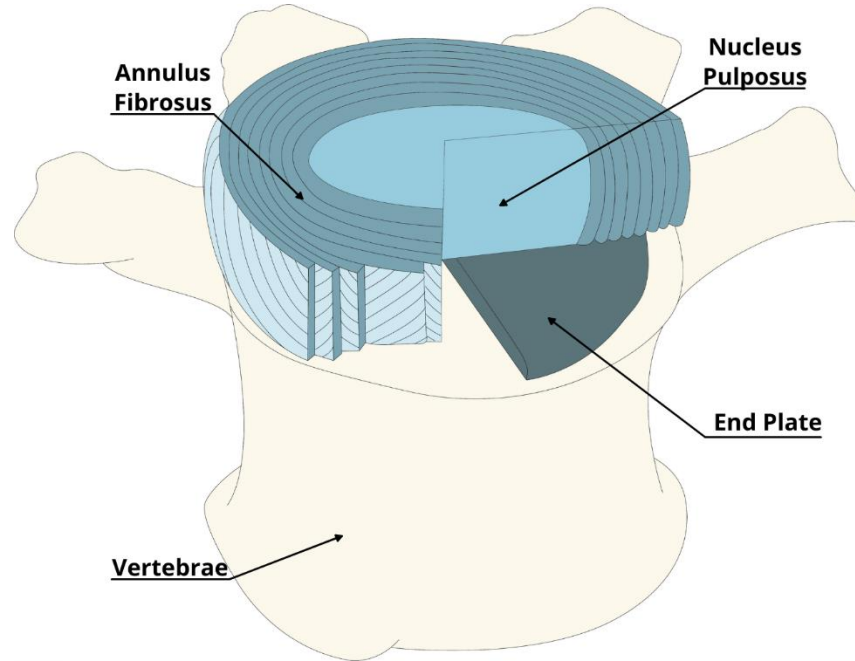


Figure 1.4 - Illustration of the general structures in an intervertebral disc (Adapted from Dixon et al., 2021)

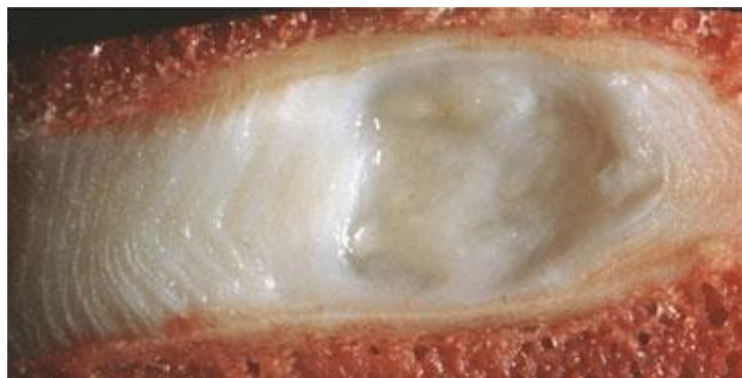


Figure 1.5 - Sagittal cross section of health young adult disc (Reproduced from Adams et al., 2000)

1.2.2 Nucleus Pulposus

The nucleus pulposus is an oval-shaped, gel-like, highly hydrated core of the intervertebral disc, which distributes compressive loading across the disc. Water is the main constituent of the nucleus pulposus making up approximately 80-90% of the volume. The dry weight nucleus pulposus comprises collagen (~20%), proteoglycans (~50%), and other non-collagenous proteins (~30%) (Eyre, 1979). At the centre of the nucleus pulposus, the collagen content is approximately 85% type II collagen which reduces towards the transition zone and into the annulus fibrosus (Eyre and Muir, 1977). Aggrecan is the main proteoglycan present in the disc and is largely responsible for the water content of the disc. Aggrecan has a fixed charge density from its high anionic glycosaminoglycan (GAG) content which creates an osmotic pressure attracting water to balance the ion density. If left unconstrained the nucleus pulposus can swell up to

200% of its volume (Kurtz and Edidin, 2006). The distribution of GAG is not constant throughout the disc. There is a decreasing gradient of GAG content from the centre of the nucleus pulposus outwards (Antoniou et al., 1996).

1.2.3 Annulus Fibrosus

The annulus fibrosus is a series of fibrocartilaginous layers encircling the nucleus pulposus and is the main load-bearing structure of the disc. Like the nucleus, the annulus fibrosus consists of water, proteoglycans (15 to 20% of dry weight), collagen (50-60% of dry weight), and other proteins (remainder of dry weight) (Eyre, 1979). The annulus fibrosus comprises approximately 20 concentric layers of collagen fibres, called lamellae. The fibres in the lamellae are angled between approximately 25° and 45° from the transverse plane and alternate in their direction as shown in Figure 1.6 (Cassidy et al., 1989; Marchand and Ahmed, 1990). The alternating angled layers align the length of the fibres in a plywood-like manner to improve the load distribution of the annulus across multiple directions. The thickness and constituents of the lamellae vary radially. There is a decrease in water content from approximately 80% to 60% in the outer annulus fibrosus (Antoniou et al., 1996). The radial change in water content is accompanied by an increasing gradient of type I collagen, and a decreasing gradient of type II collagen, where the outer most layer is almost entirely type I collagen (Eyre and Muir, 1977). The laminae were initially thought to be single complete layers (Inoue, 1981; Cassidy et al., 1989), however, it is now accepted that the fibres terminate and originate across a single lamina (Marchand and Ahmed, 1990). The outermost fibres of the annulus fibrosus are anchored deep in the adjacent vertebrae, whereas the inner fibres encircle the nucleus pulposus and merge into the endplates (Inoue, 1981).

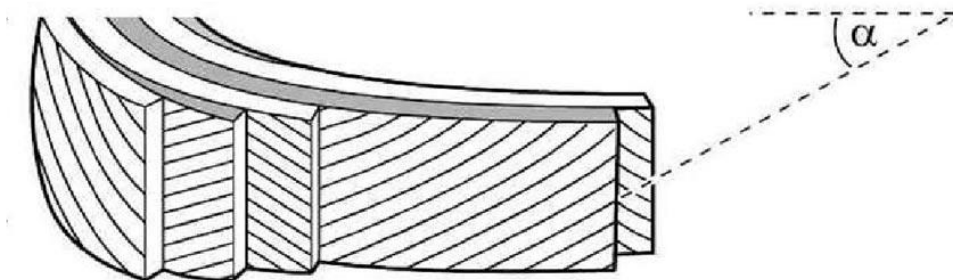


Figure 1.6 - Angled lamellae of the annulus fibrosus, $\alpha = 25^\circ$ to 45° (Adapted from Adams and Roughley, 2006)

1.2.4 Endplates

The endplates are layers of cartilage on either side of the disc, and act as layers on the end of the vertebral body securing the nucleus and the annulus. There are broadly two layers to the endplates, a hyaline layer followed by an osseous layer. The hyaline

cartilage layer predominately consists of collagen type II and merges into a calcified osseous layer that attaches to the vertebral bone (Roberts et al., 1989; Moore, 2000). The endplates are ~1 mm thick and the thickness varies in the transverse plane with the vertebrae, nucleus, and annulus (Roberts et al., 1989). The endplates are thought to enable diffusion of nutrients or metabolic waste to and from the blood in the vertebrae through penetrating capillary buds and bone marrow channels. The vascular channels have presented direction dependent flow which retains fluid in the disc and maintains mechanical properties of the nucleus and annulus (Ayotte et al., 2001). Although a largely avascular structure, the endplates are thought to play an important role in cellular activity in the disc (Malandrino et al., 2014).

1.2.5 Hydration and Cellular behaviour

In general, water flow in and out of the disc is based on the osmotic pressure generated by aggrecan contrasted with hydrostatic pressure generated by loading through the intervertebral disc. As hydrostatic pressure within a disc increases, the disc will lose water, resulting in an increase in the osmotic pressure as the disc aims to achieve equilibrium. Consequently, fluid flow in the disc has a daily cycle, in which the net flow during the day is out (during high loading) and the net flow during the night is in (during low loading). The disc loses can lose approximately 20% of its water each day from general daily activities (Botsford et al., 1994).

The intervertebral disc is considered to have a low cell density (nucleus pulposus: 4×10^6 cells/cm³, annulus fibrosus: 9×10^6 cells/cm³ (Kurtz and Edidin, 2006)). A nutrient supply is necessary to maintain cell metabolism. While there is regular water flow in and out of the disc, it has been shown that water flow has little effect on nutrient supply (Urban et al., 2004). Instead, diffusion is considered the main method of nutrient transport, where concentration gradients enable diffusion of oxygen, glucose, and lactic acid to and from the disc (Urban et al., 2004). There are thought to be two potential diffusion pathways through the vascular channels of the endplate (Ayotte et al., 2001), or through the annulus fibrosus from surrounding tissues (Urban et al., 1982).

There is evidence to suggest that both pathways are viable. The capillary density of the vertebrae is greatest at the centre of the disc and decreasing radially becoming impermeable at the outer edges (Nachemson et al., 1970). This may imply that the centre of the disc receives its nutrient exchange from the vertebrae whilst the outer sections may find nutrient supply from surrounding tissue. The endplates demonstrate direction dependent flow resistance, where inflow is favoured over outflow. (Ayotte et al., 2001). It has been shown that the outer annulus can be vascularised with blood vessels

(Maroudas et al., 1975) and that the annulus is more permeable than the endplates (Cortes et al., 2014), providing a feasible water and nutrient pathway through the annulus. It is currently unclear to what degree the outer annulus, and other tissues, can supply the remainder of the disc as a pathway for solutes and hydration. The hydration and nutrition of the intervertebral disc is multifactorial, and the relative importance of the different routes is currently unclear.

1.2.6 Mechanical behaviour

The mechanical behaviour of the disc is influenced by the mechanical properties of and the interaction between the nucleus, annulus, and endplates. The high water content of the nucleus pulposus enables it to behave with fluid and solid-like behaviour exhibiting viscoelastic mechanical properties (Iatridis et al., 1996; Leahy and Hukins, 2001). The hydrostatic pressure and viscoelastic properties of the nucleus pulposus are highly dependent on its hydration level, for example: as water leaves the disc, the nucleus pulposus will become stiffer and less fluid-like. The type II collagen fibres of the nucleus pulposus are randomly organised, which results in isotropic mechanical behaviour. Basic mechanical properties of the nucleus pulposus are shown in Table 1-1.

*Table 1-1 - Mechanical properties of the nucleus pulposus. *Biphasic-swelling model*

Property	Value	Reference
Young's Modulus (kPa)	6 to 65	(Umehara et al., 1996; Cortes et al., 2014)
Shear Modulus (kPa)	6 to 20	(Iatridis et al., 1997)
Poisson's ratio *	0.24	(Cortes et al., 2014)

The mechanical properties of the annulus fibrosis vary spatially with the bulk mechanical behaviour of the annulus affected by the fibre composition, fibre orientation, the inter-lamellar matrix, and the inter-lamellar spacing. When sections of the annulus have been dissected and tested, the tissue has been found to be nonlinear and viscoelastic (Best et al., 1994; Elliott and Setton, 2001). The viscoelasticity of the annulus arises from fluid flow within the tissue, resulting in a strain and frequency dependant response (Sen et al., 2009). Like in other connecting tissues (tendons, ligaments), the annular fibres have a zig-zag or crimped structure. This structure creates a non-linear toe region at the start of a tension stress-strain plot as the collagen fibres uncrimp resulting in a large strain with a low stress. The toe region is then followed by a linear elastic and a failure region which eventually leads to a catastrophic break. (Elliott and Setton, 2001) assessed spatial variation of the annulus by taking samples at different orientations from the inner and outer annulus. They found no difference in the axial elastic modulus or axial Poisson's ratio between inner and outer annulus. However, when assessing the circumferential elastic modulus and circumferential Poisson's ratio, a significant

difference was found between inner and outer annulus (inner circumferential elastic modulus: 5.6 ± 4.7 MPa, outer circumferential elastic modulus: 17.4 ± 14.3 MPa, inner circumferential Poisson's ratio: 1.6 ± 0.7 , outer circumferential Poisson's ratio: 0.67 ± 0.22). The differences in the circumferential mechanical properties were attributed to the radially changing matrix composition and structure in the annulus. The extrafibrillar matrix, the ion density and the fluid content are also thought to contribute to the bulk mechanical properties of the disc. Two studies from the same group have attempted to assess these factors by using confined loading protocols whilst controlling the osmotic swelling of the tissue (Cortes and Elliott, 2012; Cortes et al., 2013). These studies identified that the extrafibrillar matrix mechanical properties are dependent on the location of the tissue, the load applied, and the age of the specimen.

The specific mechanical properties of the endplates are challenging to evaluate as endplates are so thin and difficult to isolate. One method that has been successful in the past is through indentation testing. An indentation test is useful as it allows *in situ* evaluation, however, results will vary depending on indenter geometry. Indenter testing has shown that the mechanical properties of the endplate vary significantly with location with the stiffest regions at the posterior lateral region of the endplate (Grant et al., 2001).

In general, the typical loading on the disc is a form of dynamic compression which varies based on activity. In simple uniaxial compression, the gel-like nucleus becomes pressurised and pushes out against the annulus, causing the disc to bulge. The nucleus creates a hoop stress which redistributes the load and puts the annulus in tension as shown in Figure 1.7.

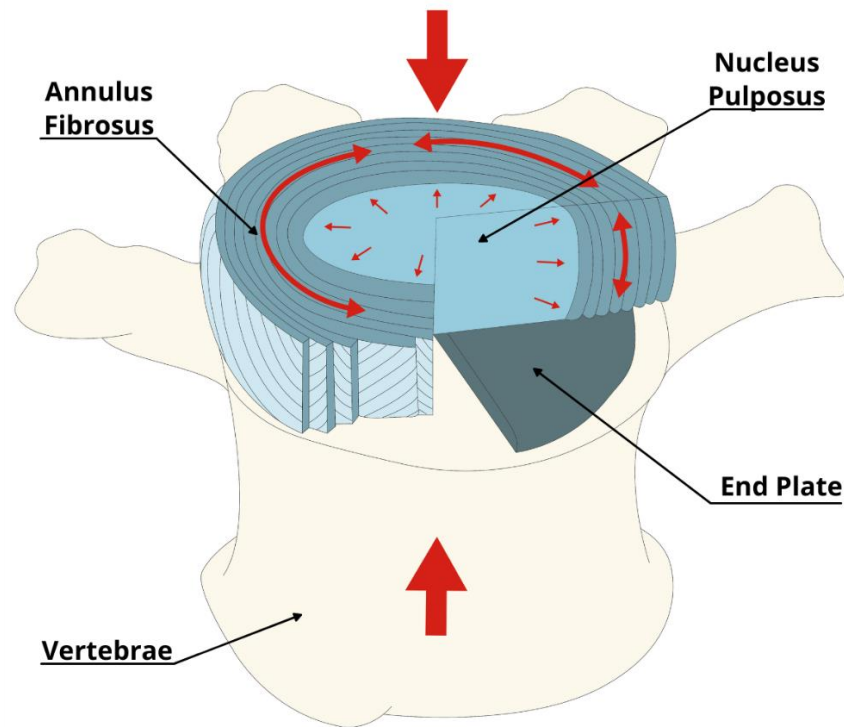


Figure 1.7 - Single axis compression of intervertebral disc (Reproduced from Dixon et al., 2021)

As the spine moves through its range of motion, the nucleus will shift within the disc to best distribute the load. For example, during flexion and extension, the nucleus will move anteriorly or posteriorly (Zou et al., 2009). As the nucleus moves to accommodate these motions, there will be an area of increased localised tension in sections of the annulus. When the disc is loaded, the endplates have been shown to deform up to 1 mm into the vertebral body, which causes a subsequent increase in the volume available to the nucleus pulposus causing a minor decrease in pressure (Brinckmann et al., 1983). This decrease in pressure assists with load distribution through the vertebrae by promoting load sharing through the neural arch and facet joints (Brinckmann et al., 1983).

Under a simple static compressive load for an extended time, the disc will reduce in height. The height loss occurs due to the continuous hydrostatic pressure in the nucleus causing fluid to be expelled. When the load is reduced or removed, height recovery occurs from water returning to the disc due to the change in osmotic equilibrium. This leads to a day and night cycle where, during the day, the disc reduces in height, and during the night, the disc recovers the height loss. Cyclically loading the intervertebral disc results in non-linear non-symmetrical loading and unloading paths. These paths indicate a form of viscoelasticity for the overall behaviour of the disc. Cyclic loading over time results in fluid loss which in turn will reduce the disc height and change the mechanical behaviour of the disc.

In line with the viscoelastic behaviour observed, the disc properties also show rate dependency, where, in general, the faster a disc is loaded the stiffer it becomes (Race et al., 2000; Nicolas Newell et al., 2017; Newell et al., 2020). The intervertebral disc exhibits time-dependent behaviour which has been attributed to the fluid flow. The exact behaviour of fluid flow in the disc is unknown, however, rheological models have shown two responses, a fast response and a slow response (O'Connell, Vresilovic, et al., 2011; Paul et al., 2013; Vergroesen et al., 2015). As the name suggests the fast response occurs quickly (usually within the first few minutes), whilst the slow response occurs over a longer duration (+1hr). In general, the fast response has been attributed to the viscoelasticity of the tissue, whilst the slow response has been associated with poro-elastic fluid flow. Mathematical models have been fitted to experimental data of change in disc height with respect to time. Two commonly cited models are: the stretched exponential model (Paul et al., 2013; Vergroesen et al., 2016), and the double Voight model (Johannessen et al., 2006; O'Connell, Jacobs, et al., 2011; Van der Veen et al., 2013). However, it has been found that the stretched exponential model over-estimated deformation while the double Voight model under-estimated deformation (Van der Veen et al., 2013). Other work by Riches et al. (2002) resulted in a model based around poro-elastic theory in which they generated a one-dimensional model using tissue permeability and osmotic potential functions that was successfully fitted to data. Although it is a simplified model, the main advantage of the one-dimensional permeability model is that was able to provide mechanical properties for dynamic loading situations.

Other contributors to load bearing through the spine include vertebral facet joints, the muscles, and spinal ligaments. The exact load sharing capability of these components with the intervertebral disc is difficult to quantify and varies depending on the motion of the spine. Asano et al., (1992) found the posterior elements contributed to the compressive stiffness, tensile stiffness, and torsional stiffness of a functional spinal unit (vertebrae-disc-vertebrae) by approximately 25%, 23% and 48% respectively. Similar results were found by Yang and King, (1984) where the posterior elements in a healthy spine took approximately 20% of the compressive load at 2° extension. The contribution from ligaments and musculature is highly dependent on the individual. As a result, when attempting to assess only the intervertebral disc *in vitro*, removal of soft tissues and posterior elements has been recommended (Newell et al., 2017).

1.3 Disc degeneration

Disc degeneration is a complex process which is thought to be cyclic where a series of changes to the mechanical and cellular environments occur throughout life. These

factors are inter-related where the cellular environment affects the disc's mechanical properties and the mechanical loading affects the cellular behaviour (Paul et al., 2013), thus creating a cycle of degeneration. It has been proposed that the cycle can be entered at any point due to mechanical response, biological response, or a combination of the two (Vergroesen et al., 2015). Early degeneration is generally asymptomatic while advanced degeneration has been linked with severe consequences including lower back pain, sciatica, and disc herniation. Disc degeneration can begin in early life but typically begins in early middle age, and will generally become more severe with ageing (Boos et al., 2002). There are several different levels of degeneration, starting with a healthy disc which has a clear annulus layers and gelatinous nucleus, to an extreme degenerated disc where there is little demarcation between the annulus and nucleus and inward annulus bulging, are shown in Figure 1.8.

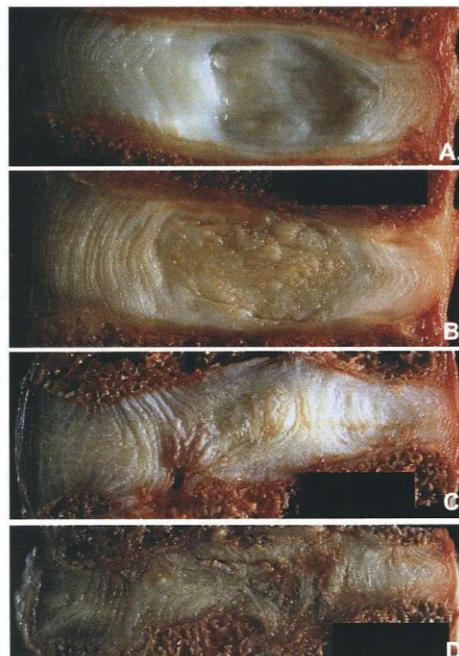


Figure 1.8 - Progression of disc degeneration (A) non-degenerated disc (B) moderately degenerated disc (C) Severe degeneration (D) extreme degeneration (Reproduced from Kurtz and Edidin, 2006)

Degeneration of the intervertebral disc is most common in the lumbar region of the spine (Adams and Dolan, 2012), and is associated with: a loss of proteoglycans, disorganisation of the extracellular matrix, tears in the annulus fibrosus, and loss of disc height. These changes subsequently alter the loading through the spine, and can cause facet joint osteoarthritis due to increased loading on the joint (Adams and Hutton, 1980).

The loss of proteoglycans and consequently in a reduction of GAG content results in a decrease in the osmotic pressure across the disc. This can lead to a reduction in hydration and overall height of the disc. Generally, as the nucleus pulposus contains the most water it also loses the most water compared to the other tissues. The amount of

water loss has been related to age, current loading, and degeneration status (Gower and Pedrini, 1969). However, a non-linear relationship has been observed between disc height and proteoglycan content (Urban and McMullin, 1988; Vergroesen et al., 2016). As degeneration progresses, collagen denaturing and protein modifications in the annulus and the nucleus have been observed, and can cause a change in colour of the tissue from white to yellow/brown (Hormel and Eyre, 1991; Antoniou et al., 1996).

In the nucleus, the collagen content changes with degeneration, where the amount of type II collagen decreases, and the amount of type I increases (Antoniou et al., 1996). This shift in collagen results in a more fibrous nucleus, where in severe cases, the collagen fibres can become denatured (Antoniou et al., 1996). Alongside the shift in collagen in the nucleus, the amount of cross-linking collagen fibres increases, further contributing to a stiffer nucleus. The increase in cross linking is thought to be due to tissue remodelling and increased matrix turnover (Duance et al., 1998). As degeneration progresses, the annulus collagen cross-linking also increases and an increase in nerve ingrowth and blood vessels in the annular outer layers. This increase in nerves has been associated with back pain resulting from degeneration (Roberts et al., 1995). In early adulthood, the cartilage of the endplate calcifies, and is considered a part of disc degeneration. The calcification of endplates essentially restricts the vascular channels, which will reduce fluid and nutrient flow in and out of the disc (Bernick and Cailliet, 1982; Urban et al., 2004). Specifically, the restriction of the nutrient and fluid pathways can result in a decrease in oxygen content which causes the cells to undergo anaerobic respiration and produce lactic acid. The lactic acid will remain in the disc making a low pH environment, which has been shown to reduce proteoglycan synthesis (Ohshima and Urban, 1992).

The exact cause of disc degeneration is unknown, however, it is thought to have multiple contributing factors including: genetics, systematic disorders, and as previously discussed, nutrient supply to the disc. Twin studies have shown that genetics appears to have a large impact on disc degeneration, and that mechanical loading may play a minor role in degeneration (Videman et al., 1995; Livshits et al., 2011). However, it has been found that other environmental factors such as smoking (Battié et al., 1991) and obesity (Livshits et al., 2011) also contribute to disc degeneration.

Degeneration directly affects the mechanical behaviour of the disc, where the ability of the disc to imbibe water decreases, the poro-elastic response of the disc will reduce causing the disc to behave in a more solid-like manner. In general, as degeneration progresses the height loss and recovery behaviour of the disc becomes compromised, meaning that the disc will reduce in height less during the day (as there is less water to

expel), and recover less during the night (as there is a reduction in the fixed charged density and therefore osmotic pressure) (Showalter et al., 2014).

The mechanical behaviour of intervertebral discs have been shown to be dependent on nucleus GAG content (Boxberger et al., 2006). As the degenerate nucleus has reduced fluid content, its internal pressure and stiffness will decrease. The bulk material behaviour of the nucleus pulposus will shift away from the gel-like flow to a more solid-like material (Costi et al., 2002; Boxberger et al., 2009). As the nucleus becomes less hydrated it will not flow as readily, reducing its ability to distribute loads onto the annulus. With the reduction in nucleus hydrostatic pressure, the normally tensioned annulus begins to bulge inwards at the innermost fibres. In early degeneration, some hypermobility has been observed from the reduced tensioning of the annulus (Brown et al., 2002). As degeneration progresses, fibres of the annulus become more disorganised, resulting in a change in their mechanical response. In severe degeneration cases, the main loading through annulus can become compressive (from the loading) rather than tension (from the nucleus) (Smith and Fazzalari, 2009). As the degeneration continues over time. the annulus shows an increase in defects such as cracks, fissures, and delamination. The mechanical effects of degeneration on the end plates are difficult to quantify accurately. However, increased endplate lesions have been associated with degeneration (Wang et al., 2012) which could contribute to further endplate damage.

The load sharing through the disc, ligaments, muscles, and posterior elements will shift disc reduces in height and the joint space becomes narrower. Specifically, the facet joints will come into contact taking a large proportion of the loading. (Pollintine et al., 2004) suggesting up to 50% of the load may be transferred through the facet joints. As the joint space narrows with degeneration the soft tissue biomechanics will also change. Initially, ligaments will become lax resulting in muscles changing their behaviour to maintain spinal stability. As time goes on, the ligaments can tighten or calcify further changing the biomechanics with time.

1.3.1 Diagnosis

Diagnosis of intervertebral disc degeneration in patients is performed by specialist physicians who use patient history, physical exams, and imaging techniques to determine the severity of the degeneration. Early stage degeneration is often asymptomatic, and pain is generally only seen with later stage degeneration alongside structure deformation (McNally et al., 1996) or neural ingrowth (Freemont et al., 1997). A patient with degenerative discs is considered to have degenerative disc disease when the degenerative disc is also painful (Adams and Roughley, 2006). The patient pathway

generally begins with a patient presenting lower back pain with or without sciatica. In accordance with the NICE guidelines, the patient is then referred for specialist opinion (NICE NG59, 2016). Imaging is currently recommended only for specialist settings primarily because it does not affect immediate choice of treatment. Reducing hospital burden and potential patient radiation doses also influences this recommendation. In chronic or cases with additional pathology, imaging can be important as it can inform treatment by indicating the severity or stage of degeneration. X-rays, Computed Tomography (CT), and Magnetic Resonance Imaging (MRI) are all imaging techniques that can be used in the diagnosis of disc degeneration. Discography is a technique used to diagnose disc degeneration where contrast agent is injected into the disc while using X-ray fluoroscopy.

X-rays are used to assess bone structure, rather than directly diagnose disc degeneration. They can also be used to identify other influencing factors which can be an indication of disc degeneration, for example scoliosis, fractures, major instability, osteophytes, and facet joint osteoarthritis. With a history of x-rays over time early-stage degeneration may be implied using x-rays by assessing reduction in disc height. The use of x-rays can help to identify factors associated with disc degeneration.

CT scanning is a series of x-rays taken at different projection angles. By reconstructing the x-ray data taken during the CT scanning process, a 3D image of the joint can be generated. For diagnosis, CT scanning has similar limitations to x-rays and is generally performed under non-weight bearing positions. As it provides a 3D view, CT can be more effective than traditional x-rays in identifying features relating to disc degeneration such as osteophytes, endplate calcification, and facet joint damage.

Like CT scanning, MRI provides a 3D image and visibility of overall bony structures, neural arches, and facet joints. MRI uses magnetic fields and radio frequency disruptions to measure excitement of hydrogen ions. MRI assesses the repetition times and time to echo with different disruption sequences, then measures time for the hydrogen ions to either return to equilibrium (T1 weighted scan) or go out of phase with each other (T2 weighted scan). MRI provides a method to view the hydration levels of tissue and in doing so, it is possible to gain an indication of the level of degeneration.

The final common technique for diagnosis of disc degeneration is discography where radiopaque contrast dye is injected into the intervertebral disc under fluoroscopy guidance. When the disc is injected four factors are assessed: patient pain response, the volume of injected fluid, the morphology of the disc, and the no pain response in a healthy adjacent disc. By comparing the pain response with the suspected symptomatic

disc with adjacent discs, an indication of degeneration can be gained by the clinician. During the surgery, abnormal movement of the fluid (such as leakage from an annular fissure) can be noted then, after discography whilst the radiopaque fluid remains in the disc, CT scans have been used for further confirmation. A concern around discography is its use of an large gauge needles, often as large as 18-gauge (Walker et al., 2008). Previous work has shown needle puncture causes an increased risk of further degeneration (Carragee et al., 2009) and that a smaller gauge needle will reduce the risk of puncture damage (Kang, 2010). The use of discography is generally surgeon dependent, and current NICE guidelines recommend imaging rather than discography.

Currently, there is no universally accepted single standardised grading system for assessing intervertebral disc degeneration. Thompson et al., (1990) developed a commonly used classification scheme based on histological analysis using cadaver specimens. The proposed grading was a five grade scheme based around midsagittal sections of the lumbar specimens, a summary transcribed from the paper is shown in Table 1-2.

Table 1-2 - Grading system proposed by Thompson et al., 1990

Grade	Nucleus	Annulus	Endplate	Vertebral body
I	Bulging gel	Discrete fibrous lamellas	Hyaline, uniformly thick	Margins rounded
II	White fibrous tissue peripherally	Mucinous material between lamellas	Thickness irregular	Margins pointed
III	consolidated fibrous tissue	Extensive mucinous infiltration; loss of annular-nuclear demarcation	Focal defects in cartilage	Early chondrophytes or osteophytes at margins
IV	horizontal clefts parallel to end-plate	Focal disruptions	Fibrocartilage extending from subchondral bone; irregularity and focal sclerosis in subchondral bone	osteophytes less than 2mm
V	Clefts extend through nucleus and annulus		Diffuse sclerosis	osteophytes greater than 2mm

Pfarrmann et al., (2001) developed a validated algorithm that translated Thompson's five grade system to the clinic using T2 weighted MRI. The Pfarrmann grading system is widely used for diagnosis and classification of the disc for scientific studies (Costi et al., 2002; O'Connell, Vresilovic, et al., 2011; Detiger et al., 2016). A summary table reproduced from (Pfarrmann et al., 2001) is shown in Table 1-3.

Table 1-3 - Grading system proposed by Pfarrmann et al., 2001

Grade	Structure	Distinction of Nucleus and Annulus	Signal Intensity	Height of Intervertebral Disc
I	Homogeneous, bright white	Clear	Hyperintense	Normal

II	Inhomogeneous with or without horizontal bands	Clear	Hyperintense	Normal
III	Inhomogeneous, grey	Unclear	Intermediate	Normal to slightly decrease
IV	Inhomogeneous, grey or black	Lost	Immediate to hypointense	Normal to moderately decrease
V	Inhomogeneous, black	Lost	Hypointense	Collapsed disc space

1.3.2 Treatment

Initial treatment of disc degeneration is conservative and surgical intervention is only considered when a patient does not respond to these conservative treatments. The management of lower back pain in the UK begins with self-management and, if the condition persists, is followed by conservative treatments including exercise, education, manual therapy treatment packages (manipulation of soft tissue), pharmacological options, and radiofrequency denervation. If these treatments are unsuccessful surgical options are considered, where fusion is only offered as part of a clinical trial (NICE NG59, 2016). The available surgical options for disc degeneration focus firstly on conservative treatment options to manage pain, such as discectomy. In general, other more invasive surgical options are not recommended for pain from disc degeneration alone. Pfirrmann grades three to five disc degeneration can often present in clinic or can contribute towards the progression other spinal pathologies such as spondylolisthesis or nerve impingement. Where other spinal pathologies are present, more invasive surgeries are used for treatment including spinal fusion and intervertebral disc replacement.

Discectomy is a surgical intervention where the intervertebral disc is partially or fully removed. This surgery is often used to relieve pain caused by a herniated nucleus impinging on the nervous system. A large study comparing non-operative treatment to discectomy in an eight year follow-up study showed the surgical option was better for pain relief and function than non-operative treatments (Lurie et al., 2014).

Fusion, also called spinal arthrodesis, is a treatment which immobilises the joint. There are several different fusion implants including wedges/spacers, fusion cages, and spinal rods. Wedges and spacers are implanted onto the vertebral processes sitting across a disc and aim to increase joint space. Fusion cages are small, meshed implants which are placed into the disc after nucleotomy and use materials that encourage osteointegration to fuse the cranial and caudal vertebrae. Spinal rods are metal rods held in place using pedicle screws which can span over several discs. Disc fusion is widely

practised in clinic partially due to its long clinical history (Fritzell et al., 2001). There is some controversy regarding fusion and the surgery has been criticised for inconsistent outcomes (Harris et al., 2018). An example of this, is a study reviewing between 1966 to 1991 which found 32% of patients reported complications such as chronic pain (Turner et al., 1992). One possible contributing factor towards these poor outcomes is that fusion alters the natural biomechanics which can impact adjacent tissues. A study completed by Ghiselli et al., (2004) predicted that ~35% of patients will develop adjacent level degeneration that requires further surgical intervention within 10 years. As a result, there have been calls for better treatments that relieve pain and maintain function.

Total disc replacements were developed as an alternative treatment to fusion, which aim to maintain mobility. A typical total disc replacement includes two metal components interspaced by a polymer component, as shown in Figure 1.9. One to five year studies showing disc replacement is at least equal in outcomes to fusion (Van Den Eerenbeemt et al., 2010; Jacobs et al., 2012; Ding et al., 2017). Longer term studies (5 to 10 years) have been completed for in the cervical region of the spine and showed similar outcomes to the shorter length lumbar studies (Mehren et al., 2017; MacDowall et al., 2019). Clinical trials for total disc replacements are still ongoing with data expected in the future (MAVERICK™ Total Disc Replacement; CerPass; ISRCTN - ISRCTN83445469)



Figure 1.9 - The Charité intervertebral disc replacement (reproduced from Hall et al., 2006)

1.3.3 Nucleus replacement and nucleus augmentation

Due to the varying outcomes and late-stage nature of currently available clinical treatments for disc degeneration, there has been interest in developing early intervention minimally invasive procedures. These novel treatments aim to either restore the disc to its native healthy state or prevent/slow the degenerative cascade. They are often injectable biomaterials which can be used in two similar proposed procedures: nucleus

replacement and nucleus augmentation. Nucleus replacement is completed after a nucleotomy, where the replacement device is inserted into the vacant space. Nucleus augmentation is a proposed treatment which injects a biomaterial directly into the disc without removing any nucleus pulposus tissue.

Nucleus replacement devices can be in the form of solid mechanical replacements or using an injectable biomaterial. Solid mechanical nucleus replacement devices are commercially available, some example materials are pyrolytic carbon, and PEEK (Coric and Mummaneni, 2008). Nucleus replacement technologies appear promising, with success during pilot clinical studies (Bertagnoli and Schönmayr, 2002; Jin et al., 2003; Ahrens et al., 2009), and evidence of the devices able to readily mimic the material properties of the natural nucleus (Bertagnoli et al., 2005; Tsantrizos et al., 2008; Wan et al., 2016; Hu et al., 2017). However, due to the novelty of the devices, pain relief, mobility restoration, long term performance, and *in vivo* recovery remain unclear. Current literature has highlighted some adverse outcomes from nucleus replacement devices including herniation, device expulsion, and mechanical subsidence (Lindley et al., 2010; JC et al., 2013; Akgun et al., 2014).

There are a range of injectable biomaterials proposed for use in replacement and augmentation from stem cell injections to acellular biomaterials. Several materials are currently being researched injection during nucleus replacement or nucleus augmentation, however, the pathway to clinic use for these materials is unclear. Recent analysis has identified requirements and potential routes to market for these materials highlighting the need for biological and mechanical testing (Schmitz et al., 2020; Culbert et al., 2022). Specific requirements for translation have been identified by Culbert et al., (2022) where considerations must be given to the delivery, biology, and mechanics of the proposed material.

On top of these highlighted material requirements, there are other clinical translation requirements. Specifically, when and how much of a given material should be administered. Providing treatment to a healthy disc may introduce damage to the natural tissue and instigate further degeneration or increase the risk of herniation. Alternatively, if the treatment is provided too late, it may be unsuccessful or unable to restore the disc. The amount of the material injected is yet to be evaluated and will likely be dependent on the patient and the level of degeneration. Other technical considerations with regards to nucleus augmentation include material migration, needle damage, and material longevity.

The University of Leeds has a patented self-assembling peptide:GAG hydrogel that was developed for nucleus augmentation (Miles et al., 2016; Warren et al., 2021). The hydrogel is an acellular two-part system, consisting of a self-assembling peptide and a GAG solution which instantaneously gelate upon contact. Individually the two components have a low viscosity compared to the hydrogel, therefore the needle diameter size can be minimised which will minimise damage to the annulus upon delivery. The self-assembling peptide has been tuned to closely mimic the mechanical properties of the native nucleus pulposus. The concentration of the GAG component is similar to the native nucleus and aims to restore the osmotic gradient in the degenerate disc. This hydrogel shall be used for testing throughout this project.

1.4 Load estimation of intervertebral discs

To ensure appropriate mechanical *in vitro* testing, it is vital that appropriate loading is applied to the disc. Direct measurement of the load transmitted through the intervertebral disc is not yet possible. Instead, estimates and predictions can be generated by combining basic mechanical calculations, limited *in vivo* measurements, and models.

An initial estimate can be found with the crude free body diagram in a standing upright position. Using static mechanics where moments from bodyweight and muscle forces are balanced around the centre of a disc load estimates can be calculated. Assuming a weight of 80 kg and using estimates from literature for anatomy (Schultz and Andersson, 1981; Potvin, 1997) a compressive force of 0.9 kN on the disc can be calculated for a simple standing position. Loading from other activities may be calculated in a similar manner, where the loading through the disc will increase during bending or lifting due to an increase in the weight bearing moment. Although estimates of loading on a given intervertebral discs can be useful, such calculations are crude because of the large number of assumptions around the geometry of the spine. More complex three dimensional analysis was completed by Schultz and Andersson, (1981) who performed a series of calculations for the internal compressive and shear forces. These calculations encompassed multiple muscle forces and separate moment arms for the bodyweight for the torso, head and arms. Cappozzo, (1983) used free body diagrams to assess the loading on lumbar discs during normal walking. Unsurprisingly, this study found loading was dependant on walking speed where the load ranged from as low as 0.2 times bodyweight to as high as 2.5 times body weight at frequencies between 1.3 and 2.5Hz.

More sophisticated models than the previously discussed basic free body diagrams have been generated and in general, are either regression based models (Potvin, 1997; Stokes and Gardner-Morse, 2001; Merryweather et al., 2009), multibody linked segment

models (de Looze et al., 1992; Kingma et al., 1996; Ayoub, 1998; Hajihosseinali et al., 2015) or finite element models (Wang et al., 1998; Schmidt et al., 2007; Stokes et al., 2010; Dreischarf et al., 2013; Castro et al., 2014; Yang and O'Connell, 2017). Models can offer a prediction of the overall force on the disc through a range of different activities quickly. These models, generally require experimental validation and often make assumptions about muscle groups (Schultz and Andersson, 1981; Schultz et al., 1982; Potvin, 1997; Merryweather et al., 2009) or apply optimisation programs to determine material properties and forces (Stokes and Gardner-Morse, 2001; Hajihosseinali et al., 2015).

1.4.1 Direct measurements of the disc for load estimation

Direct measurement of loading at the disc *in vivo* is not yet possible, instead, scientists utilise three techniques to provide insight into the loading including: intradiscal pressure measurement, deep electromyography, and instrumented implants. These measurements can then be translated to loads which are used for *in vitro* testing and biomechanical models.

1.4.1.1 Intradiscal pressure

Intradiscal pressure is measured by inserting a needle with a pressure transducer on the end into the centre of the nucleus pulposus. This needle can then be rotated or moved around the disc to find the hydrostatic pressure in a given area. Intradiscal pressure measurement of lumbar intervertebral discs using a transducer needle has been completed both *in vivo* (Nachemson, 1981; Sato et al., 1999; Wilke et al., 1999; Takahashi et al., 2006) and *in vitro* (Nachemson, 1963; Panjabi et al., 1988; McNally and Adams, 1992).

Intradiscal pressure changes has been demonstrated to change depending on the activity. For example, whilst standing upright a pressure of approximately 0.8 MPa has been observed in comparison to approximately 0.2 MPa when lying prone. (Dreischarf et al., 2016) completed a review paper collecting data from several *in vivo* studies, Figure 1.10 has been reproduced from this study and shows the intradiscal pressure from several studies during standing.

Standing

Measured intradiscal pressure

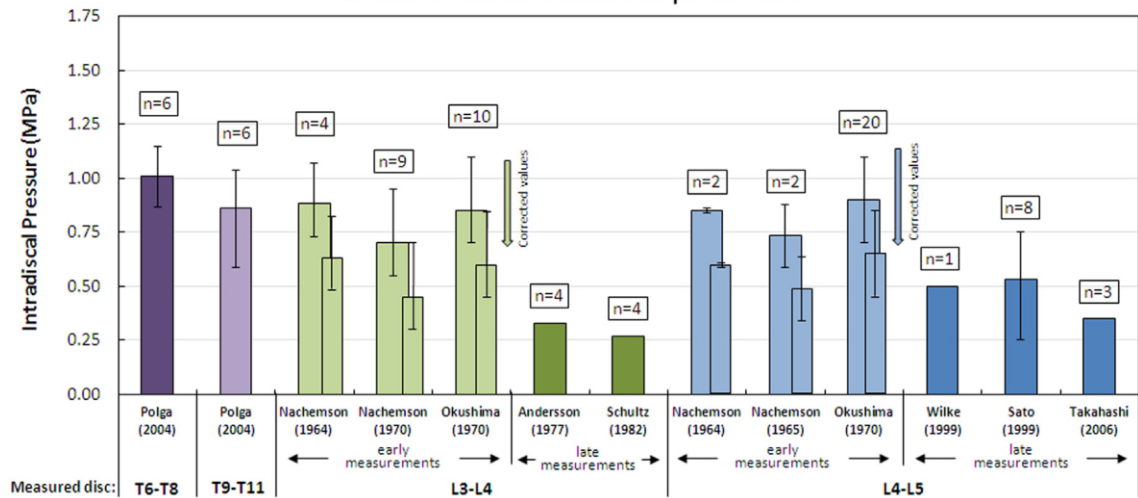


Figure 1.10 - Comparison of intradiscal pressure during standing, note: Corrected values are due to pressure transducer heating. (Reproduced from Dreischarf et al., 2016)

Although the intradiscal pressure can be used to generate physiological loading profiles, there are several limitations to the technique. Firstly, the method measures fluid pressure and has limited ability to capture the full nucleus behaviour and any annular activity. Secondly, to complete the technique a needle puncture is required which may affect the pressure as well as damage the annulus. When performed *in vivo* on healthy subjects, this would be regarded as unethical. Finally, there is difficulty translating a pressure measurement to a load directly.

To calculate a force from an intradiscal pressure, a set of converting equations have been developed based on *in vitro* measurements by Nachemson, 1965. A more common alternative is to multiply the measured intradiscal pressure by the cross sectional area of the disc (Sato et al., 1999; Takahashi et al., 2006). This method involves assuming the measured intradiscal pressure is equivalent to the stress on the whole disc, that the disc has a homogeneous material composition, and that there is a single compressive force acting uniformly across the disc. The method usually takes a single cross section and in so doing not accounting for any disc bulging or collapsing. To address the assumptions associated with converting between intradiscal pressure to a compressive force, a subject specific factor between 0.55 and 0.77 has been proposed (Dreischarf et al., 2016). In doing so, the estimated loading will be reduced and has been suggested to accommodate the non-uniform loading of the disc and its heterogeneous material composition.

1.4.1.2 Electromyography

Whilst not measuring the disc directly, electromyography measures muscle activity which can be used as input data when faced with an indeterminate model (Schultz et al., 1982; Dolan et al., 1994; Ning et al., 2014; Hajihosseinali et al., 2015). It is a non-invasive process involving placement of electrodes on the subject's skin. As it is non-invasive it is possible to readily measure a wide range of activity without risk of conservative motion from the subject. The signals of electrical activity of the muscles can be translated into a force. Difficulty has been highlighted with electromyography measurements due to crosstalk, signal attenuation, and signal processing (Charles and Souayah, 2013). Due to these issues, it is not possible to assess deep muscle groups limiting the use of this technique.

Schultz et al., (1982) generated a statically indeterminate free body diagram of a cross section of the lumbar spine. They used electromyography alongside an intradiscal pressure measurement to predict the load on the L3-L4 joint, and found forces from 380N in relaxed sitting to 2.3 kN when standing while holding an 8 kg weight. Marras and Granata, (1997) developed a more complex model that included ten muscle groups as force vectors around the trunk and the lumbar. This model was used by Ning et al., (2014) to find the compressive force at the L5-S1 joint during a range of symmetric and asymmetric dynamic lifting tasks. Loads up to 2.6 kN were calculated in this study during the most extreme activity which is close to the 2.3 kN found by Schultz et al., (1982). These are relatively simple models as they encompass a limited number of muscles, assume static equilibrium, and use assumptions around muscle actuation, however, they provide useful insight with regards to expected loads during daily activities. More sophisticated hybrid models have been developed which generally combine electromyography data with optimisation modelling to generate a more accurate load estimation (Cholewicki and McGill, 1994; Gagnon et al., 2001; Hajihosseinali et al., 2015). Muscular electrography is useful as an input to a model, however, the process is dependent on the sophistication and assumptions of the model.

1.4.1.3 Instrumented implants

Another method adopted to measure the load on the lumbar spine is using instrumented implants. Two types of implant have been researched: vertebral body replacement, and rod fixators as shown in Figure 1.11. In both cases, the devices were powered by induction which allowed measurement of loads through strain gauges, and data was transferred from the implant via telemetry (Rohlmann et al., 1994; Rohlmann et al., 2007). The vertebral body replacement measured load in six axes (compression, lateral

shear, anterior/posterior shear, and moments about each of these axes). The spinal fixator rods only measured the compressive force along the axis of the rod (Z axis in Figure 1.11) and the bending moment on the rod.

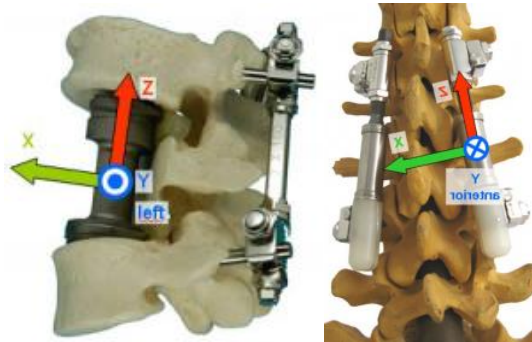


Figure 1.11 - Load axes for vertebral body replacement (left) and spinal fixator rods (right). (Adapted from Orthoload.com accessed 18th Dec 2021)

Studies using the vertebral body replacement found resultant forces between 20N to 1000N (Rohlmann et al., 2012; Rohlmann et al., 2014; Dreischarf et al., 2015), and studies using the spinal fixator rod found compressive forces between 0N and 300N (Rohlmann et al., 1999; Rohlmann, Graichen, et al., 2000; Rohlmann, Bergmann, et al., 2000). The difference between these two measurement methods has been attributed to their relative location and the load sharing across each individual implant. Early work utilising the spinal rods compared data pre and post anterior inter vertebral body fusion (Rohlmann, Graichen, et al., 2000; Rohlmann, Bergmann, et al., 2000). This work showed varying results which were dependant on the anterior intervertebral body fusion surgery. In some patients, traction was observed on the device, whilst in others a large compressive load was observed.

Although these measurements are useful, however, they do not readily transfer to an *in vitro* test methodology for intervertebral discs. Firstly, these devices cover multiple discs (e.g.: T12 to L2) and therefore the load distribution for any kind of test will need to be different. Secondly, fusion of the disc is known to alter the basic biomechanics of the spine, so any direct translation of the reported forces is not possible. Finally, the work was completed on a small number of patients (N<10), and the inter-subject variability was large (Rohlmann et al., 2013). The instrumented implant measurements are important for future implant design, however, their relevance diminishes when assessing load on intervertebral discs.

1.4.1.4 Direct measurement of the disc for load estimation summary

Intradiscal pressure measurement, electromyography, and instrumented implants have been used to generate estimates for the loading on the intervertebral disc. These

methods have been used across a wide variety of loading activities ranging from standing (~100 N) to bending over and lift weights (up to ~5000 N). A summary table containing load estimates on the lumbar spine from *in vivo* studies is shown in Table 1-4. Each of these methods have specific assumptions and limitations, however only one method, intradiscal pressure, directly measures the disc. Based on this, intradiscal pressure measurements are generally the best representation of loading profiles.

Table 1-4 - Summary of load estimates from literature

Reference	Method	Details	Load estimate technique	Compressive load estimate			
				Min	Activity	Max	Activity
Nachemson, 1981	Intradiscal Pressure	L3-L4 disc, 70 kg person	Experimental equations	100 N	Supine, semi-fowler position	2100 N	Flexion 20° and rotated 20° with 10 kg weight
Sato et al., 1999	Intradiscal Pressure	L4-L5 disc, mean weight 73 kg	Disc cross sectional area	800 N	Standing upright	2000 N	Flexion, standing
Takahashi et al., 2006	Intradiscal Pressure	L4-L5 disc, mean weight 72 kg	Disc cross sectional area	645 N	Standing upright	2776 N	Flexion 30° with 10 kg weight
Schultz et al., 1982	EMG	L3-L4 disc, mean weight 62.8 kg	Free body diagram	340 N	Relaxed sitting	2350 N	Flexion 30°, arms out, holding 8 kg
Ning et al., 2014	EMG	L5-S1 disc, mean weight 71.2 kg	Multi-segment model	2100 N	Standing upright with 6.8kg weight	2500 N	Standing upright with 6.8 kg weight held above head
Hajihosseinali et al., 2015	EMG	L5-S1 disc, various weights	Multi-segment model	400 N	Standing upright	5000 N	Flexion 80° lifting 180 N weight
Dreischarf et al., 2015	Vertebral Body Replacement	Multiple discs, mean weight 65.4 kg	Telemetered implant	200 N	Relaxed sitting	565 N	Return to standing
Rohlmann et al 2000	Spinal fixation	Multiple discs, mean weight 74.2 kg	Telemetered implant	5 N	Walking	350 N	Walking post anterior inter-body fusion

1.5 *In vitro* testing

The following section will cover the key areas regarding *in vitro* mechanical testing of intervertebral discs, including information from a recent publication jointly authored by the PhD candidate (Dixon et al., 2021). *In vitro* mechanical testing is an essential aspect for clinical translation of nucleus augmentation materials. There have been several recent reviews assessing *in vivo* and *in vitro* loading in the disc (Newell et al., 2017), *in vitro* testing methods (Dixon et al., 2021), and other preclinical assessments (Schmitz et al., 2020; Culbert et al., 2022). There are several factors that affect *in vitro* testing of intervertebral discs including the loading, the specimen preparation, the test environment, selected tissue models, artificial degeneration, and freeze thaw cycling. Each of these factors are reviewed and discussed in this section. The influence of these factors on nucleus augmentation alongside additional requirements for nucleus augmentation are also assessed.

1.5.1 Mechanical loading

The loading regime used during *in vitro* testing of discs for the evaluation of injectable treatments were extensively reviewed by the author (Dixon et al., 2021). This section evaluates different loading protocols by presenting sections of the published work alongside some additional detail where relevant.

Researchers have used various loading profiles to translate the *in vivo* load estimations to meaningful *in vitro* loads. There are two broad forms of mechanical testing: constant/ramped loading and cyclic loading.

Constant/ramped loading includes testing where a load is either increased at a given rate or applied for a duration of time. A summary table containing maximum loads, rates (if applicable), and if disc mechanical failure occurred is shown in Table 1-5. The maximum and minimum loads applied were 18.6 kN (16.9 MPa) (Hom et al., 2019) and 0.09 kN (0.1 MPa) (Malonzo et al., 2015) respectively.

Table 1-5 - Constant load review table, *Value reported as a force and converted to MPa using data from Beckstein et al., 2008, ** Value reported in MPa and converted to a force using data from Beckstein et al., 2008; Paul et al., 2012; Dreischarf et al., 2016, all converted values are italicised (Reproduced from Dixon et al., 2021)

Publication	Tissue	Max Compressive Load (MPa / kN)	Rate	To failure?
Chan et al., 2010	Bovine	0.60 / 0.66*	-	N
Cruz et al., 2018	Bovine	-	2 mm/min	Y
Freemont and Saunders, 2008	Bovine	0.60** / 1.00	-	N
Hom et al., 2019	Bovine	12.5 0/ 13.70*	2 mm/min	Y
Likhitpanichkul et al., 2014	Bovine	0.20 / 0.20*	-	N
Lin et al., 2019	Bovine	16.90 / 18.60*	2 mm/min	Y
Malonzo et al., 2015	Bovine	0.10 / 0.09*	-	N
Miles et al., 2016	Bovine	5.40** / 9.00	1 mm/min	Y
Teixeira et al., 2016	Bovine	0.46 / 0.50*	-	N
Varma et al., 2018	Bovine	1.00** / 0.17	1 N/s	N
Gullbrand et al., 2017	Caprine	3.80** / 0.23	-	N
Boyd and Carter, 2006	Human	1.20** / 3.50	-	Y
Tsantrizos et al., 2008	Human	0.41** / 1.20	-	N
Borde et al., 2015	Murine	20% initial disc height	-	N
Sloan et al., 2017	Murine	40% strain	-	Y
Balkovec et al., 2016b	Porcine	10.75** / 14.20	-	Y
Khalaf et al., 2015	Porcine	0.80 / 0.70*	60 seconds	N
Zhou et al., 2014	Porcine	1.70** / 0.15	90 N/s	N

The table highlights the wide range in load applied which is a consequence of differing test goals. Tests applying a load increasing at a given rate aimed to instigate failure, whereas constant load tests were used to determine viscoelastic material properties of the disc. For the failure testing, failure was consistently defined as either nucleus herniation or endplate fracture which reflects the clinical risks associated with injectable treatments. Although consistent failure points were used, a wide range of failure forces were found as shown in Table 1-5. Several factors can directly affect a load to failure test such as: loading rate, degeneration state, and non-uniaxial loading. Rate of loading is known to affect the mechanics of the disc (Newell et al., 2019), however, as shown in Table 1-5, no widely accepted rate was identified. Studies that provided a loading rate generally had limited justification or referred to another biomechanical testing investigation. In general, a lower failure load was identified for degenerated and treated specimens when compared to native state controls (Sloan et al., 2017; Hom et al., 2019; Lin et al., 2019). However, one key factor affecting this was that these studies applied a trans-annular nucleotomy which increased failure risk through the created annular damage. The studies which applied 5° bending did not show a reduced load to failure compared to others. This bending was used to better mimic physiological loading and to

create a more consistent location for failure. In general, studies that applied constant loading not resulting in disc failure were used to supplement other forms of testing, for example, simulate diurnal cycles in cell cultures (influencing mechanotransduction effects) or act as a preload to establish an osmotic equilibrium prior to a further loading. To better represent the physiological state of the disc, compressive cyclic protocols have been used. Cyclic loading is broadly represented by two categories, uniaxial compression and range of motion testing. The testing protocol can be described by the magnitude of the loading (max/min force/displacement), the rate/frequency the loads are applied, and the duration of test (number of cycles). A summary of the uniaxial compressive loading is shown in Table 1-6. The loading range varied from study to study, with the highest maximum being 1.85 kN (0.96 MPa) (Smith et al., 2014) and the lowest minimum being a tension of 0.275 kN (0.28 MPa) (Varma et al., 2018; Hom et al., 2019). The frequency applied was between 10 Hz (Peroglio et al., 2017) and 0.1 Hz (Cannella et al., 2014; Peroglio et al., 2017; Varma et al., 2018; Hom et al., 2019), and the number of cycles applied ranged from three (Dupré et al., 2016) to 100,800 cycles (Chan et al., 2010) .

Table 1-6 -Uniaxial cyclic loading table. *Values reported in MPa and converted to a force using data from Beckstein et al., 2008, ** Values reported as a force have been converted to MPa using data from Beckstein et al., 2008; Paul et al., 2012; Dreischarf et al., 2016, all converted values are italicised. One study applied uniaxial cyclic loading to failure of the disc whilst applying a 6 Nm flexion throughout (Lin et al., 2019). (Adapted from Dixon et al., 2021)

Publication	Tissue	Max compressive load (MPa / kN)	Min compressive load (MPa / kN)	Frequency (Hz)	Max number of cycles/test stage
Chan et al., 2010	Bovine	0.20 / 0.22*	-0.20 / -0.22*	1	100,800
Chan et al., 2013	Bovine	10 % strain	0 / 0	0.5 to 2	10
Hom et al., 2019	Bovine	0.50 / 0.55*	- 0.25 / -0.28*	0.1	20
Kalaf et al., 2014	Bovine	0.09** / 0.15	0.03** / 0.05	2	30,000
Kalaf et al., 2017	Bovine	0.09** / 0.15	0.03** / 0.05	2	10,000
Likhitpanichkul et al., 2014	Bovine	0.40 / 0.44*	0 / 0	0.1	~14,000
Lin et al., 2019	Bovine	0.18 ** / 0.30	0.03** / 0.05	1	To failure (max: 21,000)
Milani et al., 2012	Bovine	30% strain	0 / 0	0.167	5
Murab et al., 2015	Bovine	0.3% strain	0 / 0	0.167	5
Peroglio et al., 2017	Bovine	0.08 / 0.08*	0.02 / 0.02*	0.1 to 10	756,000
Saunders et al., 2007	Bovine	0.60** / 1.00	0 / 0	1mm/min	5
Schmocker et al., 2016	Bovine	0.20 / 0.22*	0.05 / 0.06*	0.2 to 1	500,000
Thorpe et al., 2016	Bovine	0.65 / 0.72*	0.53 / 0.58*	2	200
Varma et al., 2018	Bovine	0.50 / 0.55*	- 0.25 / -0.28*	0.1	25
Gullbrand et al., 2017	Caprine	0.38** / 0.23	-0.19** / -0.12	0.5	20
Arthur et al., 2010	Human	0.34** / 1.00	-0.05** / -0.15	0.1 to 1	50
Cannella et al., 2014	Human	0.51** / 1.50	-0.05** / -0.15	0.1	5
Dupré et al., 2016	Human	0.09** / 0.25	0 / 0	-	3
Showalter et al., 2015	Human	0.96 / 1.85*	0.12 / 0.23*	2	10,000
Smith et al., 2014	Human	0.96 / 1.85*	0.12 / 0.23*	2	10,000
Malhotra et al., 2012	Ovine	0.39** / 0.30	-0.39** / -0.30	1	20
Pelletier et al., 2016	Ovine	1.29** / 1.00	-0.13** / -0.1	100 N/s	4
Tsujimoto et al., 2018	Ovine	0.30** / 0.3	-0.39** / -0.30	1	1,000
Balkovec, et al., 2016)b	Porcine	30% estimated strength	0 / 0	0.5	1,000
Leckie et al., 2012	Porcine	0.30** / 0.40	0 / 0	60 mm/min	5
Zhou et al., 2014	Porcine	0.15** / 0.20	0.08** / 0.10	0.5 to 5.5	2,640

The loads used in these studies were calculated from intradiscal pressures based around previously highlighted historic work (Nachemson and Morris, 1963; Wilke et al., 1999; Sato et al., 1999). The variation in loading is explained by research groups selecting different representative activities. The variability in loads is further compounded by variability in measurement of cross-sectional area used for the calculation. Uniaxial

compression loading provides a simplified form of physiologically which has the ability indicate mechanical properties of intervertebral discs.

In studies where a range of motion loading was applied, flexion/extension, axial rotation and/or lateral bending were used. The type and magnitude of loading is summarised in Table 1-7. Loading was applied as a torque or an angular displacement where the maximum and minimum values were 7.5 Nm (Tsantrizos et al., 2008) or $\pm 4^\circ$ (Hom et al., 2019), and -7.5 Nm (Arthur et al., 2010). Similar to the uniaxial loading, the maximum and minimum frequencies were 2 Hz (Chan et al., 2013) and 0.1 Hz (Hom et al., 2019) respectively. The number of cycles ranged from three (Dupré et al., 2016) to 8,000 (Balkovec et al., 2013) .

Table 1-7 -Range of motion cyclic loading summary

Publication	Tissue	Flexion/ extension	Axial rotation	Lateral bending	Loading	Frequency	Max number of cycles/test stage
Chan et al., 2013	Bovine	N	Y	N		$\pm 2^\circ$ 0.5, 1, 2 Hz	10
Hom et al., 2019	Bovine	N	Y	N		$\pm 4^\circ$ 0.1 Hz	20
Arthur et al., 2010	Human	Y	Y	Y		± 7.5 Nm 0.1 Hz	-
Dupré et al., 2016	Human	Y	Y	Y		± 5 Nm -	3
Tsantrizos et al., 2008	Human	Y	Y	Y		0 to 7.5 Nm -	5
Pelletier et al., 2016	Ovine	Y	Y	Y		± 5 Nm 1 Nm/s	4
Tsujimoto et al., 2018	Ovine	Y	Y	Y		± 6 Nm -	1
Balkovec et al., 2013	Porcine	Y	N	N		- -	8,000
Balkovec, et al., 2016a	Porcine	Y	N	N	Unique/specimen	-	10
Balkovec et al., 2016b	Porcine	Y	N	N		- -	10
Leckie et al., 2012	Porcine	Y	Y	Y		± 5 Nm 2°/s	5

During range of motion testing, for ease of testing and analysis, the protocols generally applied each direction of loading independently to another. As with the uniaxial loading, these values were based on historic data and recommendations (Panjabi et al., 1986; Wilke et al., 1998) to represent a medium to high range of motion for the disc (White and Panjabi, 1978). Alongside the bending, the majority of studies applied a form of axial compression (50 to 300 N) as a preload either before or throughout the test. By applying this type of loading the experiment set up is more complex, however, it better simulates physiological loading.

The mechanical behaviour of the disc has been shown to be affected by loading rate (Costi et al., 2008; Sen et al., 2009; Newell et al., 2019), and was reflected by studies in this review which found changes in behaviour across different frequencies (Chan et al., 2013; Zhou et al., 2014). As shown in Table 1-6 and Table 1-7, the most common frequencies were 0.1, 1, and 2 Hz. These frequencies represent standard activities such as small motions during rest or sleep (0.1 Hz) or walking (2 Hz). Whilst there is not a widely accepted set frequency to run tests, there is a range of frequencies that best represent general activities and are widely used.

The final key parameter considered is the duration of the test or the number of cycles. This is as an important factor for intervertebral disc testing, where studies have found that the mechanical properties of the disc change over time (Brinckmann et al., 1987; Périé et al., 2006; Showalter et al., 2014; Alsup et al., 2017). As shown in Table 1-6 and Table 1-7, the number of cycles for various tests spanned over a large range (as low as three to over 100,000). Tissue survivability over longer duration of tests will influence the mechanical response of the disc during loading. Tests which loaded the disc above 10,000 cycles all completed testing under cell culture and were assessing mechanotransduction effects rather than mechanical properties (Peroglio et al., 2017). Hydration of the tissue will change the mechanical behaviour of the disc with loading over the duration of a test. Options for tissue hydration are discussed later in this *in vitro* testing section. Overall, there is no clear ideal number of cycles. Applying too few cycles presents the risk of not fully capturing the mechanical behaviour of the disc, as initial levels of hydration, which are influenced by the tissue preparation and handling, will dominate. Alternatively, too many cycles risk causing mechanical deterioration of the disc resulting in skewed data.

The behaviour of the disc is directly affected by what is known as 'preloading'. Preloading is application of load before the start of the test. The objective of preloading is to allow all discs in a study to start a test from the same point therefore ensuring reproducibility.

This is accomplished by applying loading to the disc so osmotic equilibrium is reached. A preload can be applied through uniaxial compressive loading (Hutton and Adams, 1982; Izambert et al., 2003; Marini et al., 2015; Dhara B. Amin et al., 2016), cyclic compression (Izambert et al., 2003; Cannella et al., 2014; Showalter et al., 2014), or in other more complex forms (Tencer et al., 1982; Patwardhan et al., 1999; Patwardhan et al., 2003; Stanley et al., 2004; Renner et al., 2007; Zirbel et al., 2013). Of the 38 studies discussed in this section, 17 applied preloading in order to affect the osmotic equilibrium of the disc. A summary of the preloading applied during testing from the studies identified earlier in this section is shown in Table 1-8.

Table 1-8 – Summary of the preloading applied from the previously discussed studies.

Publication	Tissue	Preload Applied?	Load type	Max Load	Length
Chan et al., 2010	Bovine	N	-	-	-
Chan et al., 2013	Bovine	N	-	-	-
Cruz et al., 2018	Bovine	Y	Constant load	25 N	-
Freemont and Saunders, 2008	Bovine	N	-	-	-
Hom et al., 2019	Bovine	Y	Constant load Uniaxial cyclic	0.1 Mpa 0.5 MPa	5 min 20 cycles
Kalaf et al., 2014	Bovine	N	-	-	-
Kalaf et al., 2017	Bovine	Y	Constant load	50 N	"Overnight"
Likhitpanichkul et al., 2014	Bovine	N	-	-	-
Lin et al., 2019	Bovine	Y	Constant load	20 N	Not reported
Malonzo et al., 2015	Bovine	N	-	-	-
Milani et al., 2012	Bovine	Y	Uniaxial cyclic	30% strain	1 cycle
Miles et al., 2016	Bovine	N	-	-	-
Murab et al., 2015	Bovine	N	-	-	-
Peroglio et al., 2017	Bovine	N	-	-	-
Saunders et al., 2007	Bovine	N	-	-	-
Schmocker et al., 2016	Bovine	N	-	-	-
Teixeira et al., 2016	Bovine	N	-	-	-
Thorpe et al., 2016	Bovine	N	-	-	-
Varma et al., 2018	Bovine	Y	Constant load	30 N	1 min
Gullbrand et al., 2017	Caprine	Y	Uniaxial cyclic	230 N	19 cycles
Arthur et al., 2010	Human	Y	Uniaxial cyclic	150 N	50 cycles
Boyd and Carter, 2006	Human	Y	Constant load	250 N	-
Cannella et al., 2014	Human	N	-	-	-
Dupré et al., 2016	Human	Y	Range of motion	5 Nm	2 cycles
Showalter et al., 2015	Human	Y	Uniaxial cyclic		10,000 cycles
Smith et al., 2014	Human	N	-	-	-
Tsantrizos et al., 2008	Human	Y	Constant load	500 N	-
Borde et al., 2015	Murine	N	-	-	-
Sloan et al., 2017	Murine	N	-	-	-

Malhotra et al., 2012	Ovine	Y	Uniaxial cyclic	300 N	19 cycles
Pelletier et al., 2016	Ovine	N	-	-	-
Balkovec et al., 2013	Porcine	Y	Constant load	300 N	15 mins
Balkovec, et al., 2016a	Porcine	Y	Constant load	300 N	15 mins
Balkovec et al., 2016b	Porcine	Y	Constant load	300 N	15 mins
Khalaf et al., 2015	Porcine	N	-	-	-
Leckie et al., 2012	Porcine	Y	Constant load	100 N	5 mins
Zhou et al., 2014	Porcine	N	-	-	-

In general, studies apply a preload that aligns to a specific activity, for example Izambert et al., (2003) used 400N to represent the bodyweight whilst standing for a spinal segment. The magnitude of preload is usually below the loading applied during the test protocol. Studies have been completed that compare the effect of different preloads, and show that the stiffness of the disc is dependent on the magnitude of preload (Janevic et al., 1991; Kasra et al., 1992; Gardner-Morse and Stokes, 2004). The duration of a preload is applied varies greatly from as low as 5 minutes (O’Connell et al., 2011), to greater than 16 hours (Costi et al., 2008). Preload duration presents the material deterioration issue highlighted earlier when using a high number of cycles. A study applying a static load of 2 kN over long periods found the disc reaches 99% its equilibrium in approximately 14 hours (O’Connell, Jacobs, et al., 2011). Currently no consensus has been reached on the ideal preload, however, in a recent consensus review the spinal community acknowledge a preload was necessary in order to maintain consistency of test outputs (Costi et al., 2021).

1.5.2 Specimen preparation

Specimen preparation refers to removal of soft tissue and bone, as well as other pretest preparations such as fixation methods or cleaning of the disc. Removing muscle tissue and ligaments is common across intervertebral disc studies (Newell et al., 2017). These soft tissues directly affect the mechanics of the spine during testing. By maintaining these tissues *in vitro*, the complexity of the testing protocol and the analysis of results would increase greatly. By removing these tissues the researcher is able to isolate the disc and identify its mechanical behaviour.

Preparation of the vertebral bone, on the other hand is far more diverse. Firstly, how many disc levels to incorporate into a test needs to be discerned. To simplify analysis, most testing is completed on a single disc (Newell et al., 2017), however, there are examples of multilevel testing which allow analysis of adjacent level effects (Patwardhan et al., 2003; Stanley et al., 2004; Renner et al., 2007). When completing single disc testing, the amount of bone left on either side of the disc directly effects the mechanical

behaviour during test (Sikora et al., 2018). Full vertebrae can be left on both sides of the disc creating a functional spine unit which provides a physiological base and allows testing of posterior elements (Adams and Hutton, 1980; Brinckmann and Horst, 1985; Smeathers and Joanes, 1988; Asano et al., 1992; Cannella et al., 2014; D. B. Amin et al., 2016). However, this restricts the number of discs that can be harvested from a single spine. When trying to evaluate the disc, the retention of the posterior processes is not always beneficial, as they can increase the complexity of analysis due to load sharing. Another common option is to use parallel transverse cuts on each adjacent vertebrae to form bone-disc-bone units (Virgin, 1951; Markolf and Morris, 1974; Moroney et al., 1988; Holmes et al., 1993). This preparation would allow all discs in a spine to be utilised in a test. Using parallel cuts at a set distance from the disc introduces additional controls for the disc and can result in more consistent data (Sikora et al., 2018). Transverse sectioning, however, does not allow the researcher to retain the posterior elements, which can restrict the scope of the test.

An important contributor to the mechanical performance of the disc is its hydration state. A review paper comparing fluid flow *in vivo* and *in vitro*, found a discrepancy between the two where larger loads and longer periods of recovery time are required *in vitro* to replicate the *in vivo* behaviour (Schmidt et al., 2016). One contributing factor that was highlighted is blockage of endplates by coagulated blood and bone debris. Whilst the effect removing coagulated blood and cleaning the disc has not been studied directly, doing so may enable *in vitro* testing to better replicate the *in vivo* state.

A common method of fixation is to mount the disc in bone cement (Berkson et al., 1979; Kasra et al., 1992; Costi et al., 2008; Zirbel et al., 2013; Cannella et al., 2014). Whilst this method can allow consistent positioning and accommodate the application of complex loads, the hydration of the disc will likely be affected. By cementing an end of the disc, the endplate essentially become sealed blocking a potential hydration pathway.

Specimen preparation directly affects the mechanical behaviour of the disc and is a limitation of *in vitro* testing. Although specimen preparation is a limitation to a study, it can enable better consistency across specimens and allows the application of high or complex loads. The chosen test environment will have a direct impact on the hydration of the disc *in vitro*. There are two major considerations regarding test environment, first the method of hydration and second the temperature of the environment.

1.5.3 Test environment

As the actual hydration pathway for the disc is currently unclear, it is not possible to directly replicate the natural environment of the disc *in vitro*. There are several common

hydration regimes used in studies, including performing the test in air whilst spraying with water or saline (Nachemson, 1981; Brinckmann and Horst, 1985; Hansson et al., 1987; lencean, 2000; Cannella et al., 2014), wrapping the disc in saline soaked gauze (Hansson et al., 1987; O'Connell et al., 2007; O'Connell et al., 2011; Marini et al., 2015), placing the disc in a humidity chamber (Koeller et al., 1984; Panjabi et al., 1988; Moroney et al., 1988; Adams et al., 1996), and immersing the disc in a saline bath (Virgin, 1951; Smeathers and Joanes, 1988; Izambert et al., 2003; Costi et al., 2008; O'Connell, Vresilovic, et al., 2011). A study found that air exposure with saline spray and wrapping the disc do not have an effect on the hydration of the disc (Pflaster et al., 1997). To add to this, the use of a bath or a humidity chamber runs the risk of over-swelling the disc, however, this can be prevented with suitable axial compression (Pflaster et al., 1997).

The temperature of the test environment used in studies, unsurprisingly, is either room temperature (18°C to 22°C) or body temperature (37°C). Whilst the exact mechanical effects of the temperature change is unclear, Koeller et al., (1986) found that axial creep at 37°C was approximately 10% greater than at room temperature. This was attributed to a shift in the viscoelastic behaviour towards more elastic behaviour. Consistency in test environment temperature is vital for any set of testing as it enables meaningful comparison across test groups within a study.

1.5.4 Tissue models

Animal tissue is often used in place of human tissue for *in vitro* testing. Animal tissue used for testing is acquired from the food chain, making it more readily available and, generally, gives a consistent model as animals are slaughtered at a similar age. The overall structure of animal discs, like human discs, contains the nucleus, the annulus, and adjacent endplates alongside spatially dependent mechanical properties. Geometrically, however, the majority of animal discs are smaller and are shaped differently to human discs (O'Connell et al., 2007; Beckstein et al., 2008; Monaco et al., 2016). For example, the major dimensions of bovine tail discs are smaller than human tissue and are more circular than human tissue (Monaco et al., 2016). Although the size of the disc will directly affect its behaviour, testing protocols can be adapted to accommodate such differences for example, by altering the magnitude of applied loads. A summary of major tissue geometries for animal models commonly used in spinal biomechanics studies can be found in Table 1-9.

Table 1-9 - Comparison of large animal intervertebral disc dimensions adapted from Monaco et al., 2016 and human tissue dimensions adapted from Pooni et al., 1986

Species	IVD height (mm)	ML width (mm)	AP width (mm)	Vertebral body height (mm)
Human lumbar (n=5)	17	55	38	-28
Bovine tail (n=5)	12	23	24	38
Ovine lumbar (n=4)	4	25	18	37
Porcine lumbar (n=5)	8	38	25	37

Biomechanically there are several differences between species, one obvious example is the difference between bipedal species and quadrupeds. Although this causes altered biomechanics, the majority of the load is along the length of the muscles resulting in the predominant load to be compressive loading along the axis of the spine. It is only the bodyweight component that acts in a different direction in quadruped spines compared to human spines. One consequence of the altered biomechanics is that animal discs will demonstrate slightly different spatial mechanical properties to human disc. Whilst this can be mitigated by using animal tissue with similar anatomy to human discs, the difference in the spatial mechanical properties of animal discs is a limitation of their use for *in vitro* testing.

The spatial variability extends to the extracellular matrix, where proteoglycan content and collagen content will vary depending on spine level and position on the disc (Alini et al., 2008). When comparing the biological composition of human and animal intervertebral discs a key difference is the presence of notochordal cells. In humans these cells are present in the disc at an early age and by adulthood are no longer found in the disc. Many species (mouse, cat, pig, and rabbit) maintain notochordal cells throughout their life. Cows, sheep and some breeds of dog are similar to human discs and do not retain their notochord cells in adulthood (Alini et al., 2008). The importance of these cells is that they act as contributors to the metabolism and cellular constituents of the disc, therefore, are thought to be contributor to prevention of degeneration (McCann and Séguin, 2016). This highlights another limitation of animal tissue, modelling tissue degeneration. This limitation is furthered by the fact animals used for *in vitro* testing are normally sourced from the food chain, meaning the age and skeletal maturity of a given species is approximately the same. Whilst useful for inter-specimen comparison, this limitation generates difficulty when comparing the variety of degenerative status possible for human tissue. Despite their limitations, the reduced cost and greater availability of animal models means provide a pragmatic basis for demonstrating the mechanical efficacy of a biomaterial prior to use of human tissue.

1.5.5 Artificial degeneration

Artificial degeneration is a common method used *in vitro* to simulate *in vivo* conditions. This is particularly relevant for animal tissue models which may not present any form of natural degeneration. Two broad categories of artificial degeneration have been employed: biochemical and mechanical degeneration. A summary of these methods is outlined in Table 1-10 showing enzyme, incubation time, annular damage, and an overview of nucleotomy techniques.

Table 1-10 - Artificial degeneration techniques applied across different studies, highlighting incubation times, annular damage, and nucleotomy details (Adapted from Dixon et al., 2021).

Publication	Tissue	Artificial degeneration				
		Biochemical			Mechanical	
		Collagenase	Chondroitinase	Papain/ Trypsin	Annular damage	Nucleotomy
Chan et al., 2013	Bovine	-	-	10 days	25G	-
Cruz et al., 2018	Bovine	-	-	-	4mm biopsy punch	up to 0.12 g removed with rongeur
Freemont and Saunders, 2008	Bovine	18 hrs	-	-	-	-
Hom et al., 2019	Bovine	-	-	-	4mm biopsy punch	0.188±0.025 g removed with rongeur
Kalaf et al., 2014	Bovine	20 hrs	-	-	100 x 22G punctures	-
Kalaf et al., 2017	Bovine	18 hrs	-	-	21G	-
Likhitpanichkul et al., 2014	Bovine	-	-	-	Box cut 4.5mm by 4.5mm	-
Lin et al., 2019	Bovine	-	-	-	Cruciate incision	up to 0.2 g removed with rongeur
Malonzo et al., 2015	Bovine	-	-	7 days	22G	-
Milani et al., 2012	Bovine	18 hrs	-	-	-	-
Murab et al., 2015	Bovine	18 hrs	-	-	-	-
Peroglio et al., 2017	Bovine	-	-	-	-	Transpedicular nucleotomy
Saunders et al., 2007	Bovine	18 hrs	-	-	-	-
Schmocker et al., 2016	Bovine	-	-	6 days	-	-
Teixeira et al., 2016	Bovine	-	-	-	21G needle	-
Thorpe et al., 2016	Bovine	2 hrs	-	-	-	-
Varma et al., 2018	Bovine	-	-	-	Cruciate incision	up to 0.2 g removed with rongeur
Gullbrand et al., 2017	Caprine	-	12 weeks	-	-	-
Arthur et al., 2010	Human	-	-	-	3.25mm hole	Tissue removed with nucleotome for 20 mins

Publication	Tissue	Artificial degeneration				
		Biochemical			Mechanical	
		Collagenase	Chondroitinase	Papain/ Trypsin	Annular damage	Nucleotomy
Boyd and Carter, 2006	Human	-	-	-	-	Nucleotomy completed - no data
Cannella et al., 2014	Human	-	-	-	-	up to 0.24 g removed with nucleotome for 20 mins
Showalter et al., 2014	Human	-	-	-	4x4mm incision	up to 2.06 g removed with rongeur
Smith et al., 2014	Human	-	-	-	4mm incision	up to 2.17 g removed with rongeur
Tsantrizos et al., 2008	Human	-	-	-	-	Nucleotomy completed - no data
Borde et al., 2015	Murine	-	-	-	21G	-
Sloan et al., 2017	Murine	-	-	-	1mm window	Compression to herniation
Malhotra et al., 2012	Ovine	-	-	-	2.5mm incision	up to 0.02 g removed with rongeur
Pelletier et al., 2016	Ovine	-	-	-	18G	-
Tsujimoto et al., 2018	Ovine	-	-	-	5x3 mm window	0.2 g removed
Balkovec, et al., 2016a	Porcine	-	-	-	12G	-
Balkovec et al., 2016b	Porcine	-	-	-	-	Compressive fracture
Khalaf et al., 2015	Porcine	-	-	7 days	-	-
Leckie et al., 2012	Porcine	-	4 weeks (in vivo)	-	100 x 22G punctures	-
Zhou et al., 2014	Porcine	-	-	-	-	Trans end plate nucleotomy

Two families of enzyme were utilised: proteases (papain, collagenase), which break down the amide bonds within protein structures and carbohydrases (chondroitinase ABC), which break down the glycosidic bonds within polysaccharide structures. Papain and trypsin are non-selective proteases which break down various amino-acid linkages in the proteins (Amri and Mamboya, 2012; Rawlings and Salvesen, 2013), while collagenase selectively causes the breakdown of collagen (Nagase, 2001). Chondroitinase ABC results in the breakdown of the proteoglycan and glycosaminoglycans in the disc (Prabhakar et al., 2005). Both families of enzymes cause the degeneration of the disc to occur by destabilising the connective tissue. This then causes measurable mechanical changes in the disc that aim to represent natural tissue degeneration. Based on the studies shown, no major benefit from one type of enzyme over another has been identified.

It is important to note that to actually deliver the enzymes a needle puncture is required. This is a form of mechanical degeneration and depending on the bore size may contribute towards observed degeneration (Elliott et al., 2008). When looking to only introduce biochemical degeneration, use of small gauge size needles would be required which is reflected in Table 1-10 where needle sizes between 21G and 25G were used to deliver enzymes. Another important aspect of using this method of degeneration, which is under-reported, is in controlling the level of degeneration. The level of degeneration is related to many variables (such as incubation time, incubation temperature, and enzyme concentration) and must be controlled to ensure that the degeneration methodology is reproducible, and the achieved degeneration level is similar between samples. Most enzymes are only denatured either through high temperatures or by chemically altering the enzyme structure, consequently at physiological temperatures, tissues will continue to degenerate *in vitro*. Without control measures, such as the use of an inhibitor, continued degeneration would add further variability to samples (Nikawa et al., 1994).

Mechanical degeneration disrupts how the disc distributes loads, by either directly damaging the annulus or by undertaking a nucleotomy. Five studies were identified as using a method of directly damaging the annulus only. Four studies needle punctures were used (12 to 21 gauge needle size), and in one study a 4.5 mm² box cut was completed. In both techniques, the annular fibres are torn, compromising its ability to distribute loads and creating a potential increased risk of herniation. The more common method of mechanical degeneration, used by 16 studies, was a full or partial nucleotomy. By removing the nucleus, the mechanics of the disc change drastically, as the nucleus has reduced ability to tension the annulus. Twelve of the 16 studies completed the nucleotomy through the annulus, which again would also cause annular damage

degeneration effects. Whilst a trans-annular approach may represent a clinical setting for the use of these identified biomaterials (e.g.: disc restoration post herniation), the influence of annular damage on the disc may compromise restorative effects. The nucleus was accessed with two tools to remove nuclear material, a rongeur or a nucleotome. In using these tools either a set mass (for the rongeur) or a set time (for nucleotome) was employed to control the level of degeneration. An alternative trans-annular method was used in two studies where compressive overload was also used to generate a form of nucleotomy. This technique is promising, however, it required prior annular damage to ensure herniation rather than end plate fracture. Two alternative techniques identified were nucleotomy via endplates (Zhou et al., 2014) or through the pedicles (Peroglio et al., 2017). These approaches maintain the annulus and may reduce overall disruption to the disc compared to a trans-annular approach. However, the trans-endplate or trans-pedicular approaches are more complex to implement as repair of the bone may be required. The trans-endplate approach is completed *in vitro* and accesses the disc in the cranial-caudal axis, going through the superior end of the prepared bone-disc-bone unit. The trans-pedicular approach is completed *in vivo* and access to the disc is accomplished via a posterior lateral approach through the pedicles. Both techniques access the nuclear material via a hole in the endplate, which was smaller using the transpedicular approach. Overall, trans-annular nucleotomy with rongeurs is the most prevalent mechanical method for inducing artificial degeneration and may be a suitable *in vitro* representation of a herniated disc patient undergoing surgery.

While biochemical and mechanical methods have advantages and disadvantages, an important consideration for early stage degeneration models is the level of annular damage caused by the approach. For example, in studies where the effect of the treatment injection is of interest, methods that preserve an intact annulus would be necessary because any pre-existing damage due to the simulated degeneration could mask the outcomes of interest. Both categories of degeneration are relative to the scale of the intended measurement and observation. In the biochemical degenerate models, the changes are caused to the microstructure of the disc tissue. In contrast, mechanical models cause changes on the bulk or macrostructure. Due to the differences in the scales of these respective changes, the suite of experimental methods that can be employed to investigate and evaluate the changes are broad.

1.5.6 Freeze-thaw cycling

There have been several studies investigating the effects of freeze-thaw cycles on the mechanical performance of the disc. In studies that have assessed the effects of freezing duration (up to 232 days) on the mechanical performance of the disc (Panjabi et al.,

1986; Smeathers and Joanes, 1988; Riches et al., 2002), no statistically significant difference was identified as a result of duration. To the author's knowledge the effects of multiple freeze-thaw cycles has not been investigated on human intervertebral discs. Sunni et al., (2014) assessed the effect of up to five freeze-thaw cycles on calf thoracic discs. The study found differences in the mechanical performance of the disc after five freeze-thaw cycles in axial rotation (decrease of 6%) and lateral bending (increase of 30%). The effect of freezing temperature has not directly been studied, and could be a contributing factor to the performance of the disc.

1.5.7 Nucleus augmentation

There are several mechanical clinical considerations for nucleus augmentation. Based on evidence from nucleus replacement devices, two specific concerns are subsidence or device integration and device expulsion or herniation (Bertagnoli and Schönmayr, 2002; Lindley et al., 2010; Iatridis et al., 2013; Akgun et al., 2014). These can be assessed *in vitro* by using and building on the previously highlighted testing.

Mechanical loading has a large influence on how these concerns can be addressed. Firstly, ramped load to failure may directly assess the likelihood of disc herniation. However, ramp to failure tests which compare between the native, degenerate, and treated states of a disc currently do not have a consistent test methodology. One potential representation of clinical herniation can be achieved by applying extreme ranges of motion (flexion/extension, lateral bending axial rotation) in combination with each other and the ramped force to failure. Cyclic loading may also be able to evaluate device migration and subsidence risk. It is likely that a small number of cycles (three hundred) would not be sufficient to detect changes due to alterations in the biomaterial behaviour and hydration. On the other hand tests lasting days risk natural deterioration the disc unrelated to the injected biomaterial. Since it is not feasible to test to millions of cycles *in vitro* due to tissue degradation, some form of accelerated simulation is required. One potential avenue is to exacerbate and accelerate potential issues from biomaterial injection using higher loads to generate extremes of physiologically relevant disc pressure (above 1 MPa) over a lower number of cycles (thousands rather than millions). A testing approach where fewer cycles are used to predict the longer-term behaviour may also be possible. In both cases, further work is necessary to build evidence of appropriate loads and durations.

1.5.8 Biomaterial delivery

An important influencing factor on the performance of injectable nucleus augmentation biomaterials is the how much should be injected. Currently no studies actively investigate

by varying volume injected, however, across literature there is variation in delivery methods. Currently there are two main methods used to control delivery injecting to a set volume or based on haptic feedback. Other methods are also used but uncommon for example, Arthur et al., (2010) controlled the injection based on pressure of an implanted balloon and Cannella et al., (2014) used change in disc height to control the injection. A summary of methods used in studies and the maximum volume injected is shown in Table 1-11. The maximum and minimum volumes injected were 2.3 mL (Dupré et al., 2016) and 0.1 mL (Chan et al., 2010; Chan et al., 2013; Borde et al., 2015) respectively.

Table 1-11 – Methods used to deliver augmentation material and maximum volumes injected (Adapted from Dixon et al., 2021)

Publication	Tissue	Delivery Method		
		By volume	By haptic feedback	Max volume injected (mL)
Chan et al., 2010	Bovine	Y	N	0.1
Chan et al., 2013	Bovine	Y	N	0.1
Freemont and Saunders, 2008	Bovine	Y	N	0.5
Hom et al., 2019	Bovine	N	Y	-
Kalaf et al., 2014	Bovine	Y	N	1
Malonzo et al., 2015	Bovine	N	Y	0.15
Miles et al., 2016	Bovine	Y	N	0.125
Peroglio et al., 2017	Bovine	Y	N	0.15
Saunders et al., 2007	Bovine	Y	N	0.5
Schmocker et al., 2016	Bovine	N	Y	0.2
Teixeira et al., 2016)	Bovine	Y	N	0.5
Thorpe et al., 2016)	Bovine	N	Y	0.2
Varma et al., 2018)	Bovine	N	Y	0.75
Gullbrand et al., 2017)	Caprine	N	Y	-
Cannella et al., 2014)	Human	N	N	-
Dupré et al., 2016)	Human	N	Y	2.3
Showalter et al., 2014)	Human	Y	N	0.5
Smith et al., 2014)	Human	Y	N	0.5
Borde et al., 2015)	Murine	N	Y	0.1
Malhotra et al., 2012)	Ovine	N	Y	0.35
Pelletier et al., 2016)	Ovine	N	Y	-
Tsujimoto et al., 2018)	Ovine	N	Y	0.25
Balkovec et al., 2013	Porcine	N	Y	1.4
Balkovec et al., 2016a	Porcine	N	Y	-
Khalaf et al., 2015	Porcine	Y	N	1
Leckie et al., 2012	Porcine	Y	N	0.25
Zhou et al., 2014	Porcine	Y	N	1

Haptic feedback has a history of being used in clinics for procedures such as discography (Kapural and Goyle, 2007) or enzyme induced nucleotomy (Fraser, 1984). This type of method is difficult to practically transfer to *in vitro* testing as there is a host of variables

that will affect the feedback. Firstly, it is a qualitative measure that will be dependent on the user. This user specific feedback while injecting will be further impacted by the variation in natural properties of the disc (e.g. size, degeneration level). On top of this, the properties of the chosen biomaterial (e.g. viscosity) and the delivery needle (e.g. needle bore size, needle length) are experimental factors that will further compound to distort the user's response of the injection. Alternatively, using a set volume, can be readily reproducible within and across studies, but does not as effectively reflect historical clinical practice. As with haptic feedback, the individual specimen size will heavily influence any mechanical outcomes observed from using a set volume method. Whilst set volume is more readily reproduced *in vitro*, when transferring to clinic it would likely require specific information on the properties of the disc being treated. To reduce this inherent variation that will occur from injection, some level of normalisation to disc size could be adopted. This may allow better comparison between specimens and evaluation of the most suitable volumes to inject.

The main objective of analysing the delivery should be to optimise the restorative effects of a treatment, by preventing under- or over-filling of the disc. In doing so, surgical risk can be further mitigated preventing unnecessary surgery (under-filling) or increasing herniation risk (over-filling). In one study injection was based on relative increase in disc height rather than haptic feedback or set volume. This change was then compared to the restorative effects from injection (Cannella et al., 2014). Although this study used a different technique for controlling injection compared to other work, it demonstrates an option for performing analysis to enable treatment optimisation. This analysis could readily be applied to other injection control techniques. An understanding of the restorative effects based on the injection variables is likely vital for the development of injectable biomaterials. On top of this, it will be necessary to provide evidence for guidelines for eventual use in clinical trials.

An experimental set up factor that may also influence injection is whether loading is applied whilst injecting. Loading on the disc during injection will affect the intradiscal pressure and annular tensioning, which will in turn affect the quantity of biomaterial that can be injected into the disc. (Arthur et al., 2010; Cannella et al., 2014) applied a low compressive load during injection, aiming to represent lying supine reflecting potential surgical practice. Importantly, compressive loading during injection will directly affect studies with injection control based on haptic feedback. The inclusion of an applied load during injection is likely to affect the volume and distribution of the biomaterial, so a representation of physiological loading in clinic is important to include.

1.6 Summary and Conclusions

Disc degeneration is a major cause of back pain worldwide and can result in severe disability. The cause of disc degeneration is thought to be a result of mechanical or biological damage that contribute to a degenerative cycle.

Current treatments are invasive and have resulted in mixed clinical outcomes due to altered biomechanics leading to adjacent disc degeneration. There is a necessity for new treatments to be developed that prevent or delay the onset of intervertebral disc degeneration. One promising alternative minimally invasive option is nucleus augmentation in which a biomaterial is injected into a degenerated disc with the aim of restoring biological and mechanical function.

One limiting factor to the introduction and development of new minimally invasive techniques is difficulty in proving the mechanical efficacy of the treatments *in vitro*. This is due to the complex mechanical interactions between the tissue of the disc and an injected biomaterial. In the literature there is a wide range of testing methods to investigate disc biomechanics which report varying results. To provide more robust testing during preclinical tests, the development of a protocol which is able to consistently evaluate the mechanical properties of the disc and enable assessment of different clinical variables is required.

A peptide:GAG hydrogel for treatment of disc degeneration has been developed at the University of Leeds. This hydrogel is thought to be well-suited to a clinical application as it is possible to inject the through fine gauge needle, can gel instantaneous, and has mechanical properties that mimic natural nucleus. The peptide:GAG hydrogel developed shall be used throughout this project, allowing evaluation of both the gel and any methods developed.

By generating new *in vitro* methodologies to assess delivery and mechanical efficacy of biomaterials, these novel treatments can be thoroughly evaluated and optimised prior transitioning to *in vivo* studies.

1.7 Aims and Objectives

The overarching aim of this work was to develop and utilise test methods to evaluate the mechanical effects of injectable treatments on the intervertebral disc. Specifically, the project utilised *in vitro* models as a tool to assess mechanical properties of the intervertebral disc in different states. A further goal of this project was to examine the surgical delivery of the augmentation material was also considered. There were four main objectives to this work:

- 1) To develop an *in vitro* animal model to assess the change mechanical behaviour over test duration of intervertebral discs and the effects of injectable biomaterials for nucleus augmentation.
- 2) To use the developed animal model to evaluate potential surgical parameters relating to biomaterial delivery.
- 3) To adapt and apply the *in vitro* model to human spinal tissue.
- 4) To specify, design, and evaluate a prototype delivery device for a self-assembling peptide hydrogel.

1.8 Thesis structure

In Chapter 2, the general materials and methods used in the other chapters are outlined. Objective 1 is addressed by the work performed in Chapter 3. This study involved the application of cyclic loading to bovine tails using a protocol that enabled assessment of the discs in different states: native, artificially degenerated, and treated. Further analysis was then performed on the data to assess whether the use of a shorter testing protocol was suitable.

Chapter 4 reports the application of the developed methodology to accomplish Objective 2. In this chapter parameters relevant to the delivery of the hydrogel were evaluated against the mechanical restoration of the disc.

For Objective 3, Chapter 5 applied the testing knowledge gained in Chapters 3 and 4 to transfer the develop methodology to human tissue. A set of preliminary tests were completed where the method was directly transferred to human tissue without the artificial degeneration step. Due to failure of the preliminary testing, the method was then adapted to account for the identified issues and a small sample size was completed with the adapted method.

Objective 4 is addressed by the work described in Chapter 6. In this chapter the design of a novel hydrogel delivery system for nucleus augmentation is described. The design

work is reported alongside *in vitro* testing, rheological analysis, and an *ex vivo* study to evaluate the device.

The final chapter, Chapter 7, provides an overall discussion of the impact of the project, an outline of main conclusions of the research, and recommendations for future investigations.

2 Materials and Methods

2.1 Introduction

This chapter outlines the test methods used and built upon throughout this project. The preparation of stock solutions used throughout this project is described. A detailed description of shared methods used in the bovine tissue *in vitro* testing chapters (Chapters 3, 4, and 6) is outlined.

2.2 Methods

2.2.1 General stock solution preparation

A detailed description for the preparation of sodium citrate, phosphate buffered saline (PBS), papain, ebselen, and the peptide hydrogel used in this project can be found in Appendix 1.

2.2.2 General *in vitro* testing approach

Testing of intervertebral discs in this project was completed using a sequential state testing procedure. After specimen preparation, discs were subjected to cyclic mechanical loading, artificial degeneration, needle puncture, or treatment, and finally mechanical loading again. A sequential state method was chosen because it allows each disc to act as its own control between states which can reduce variation in analysis (Dixon et al., 2021). A typical flowchart of the sequential state testing is shown in Figure 2.1.

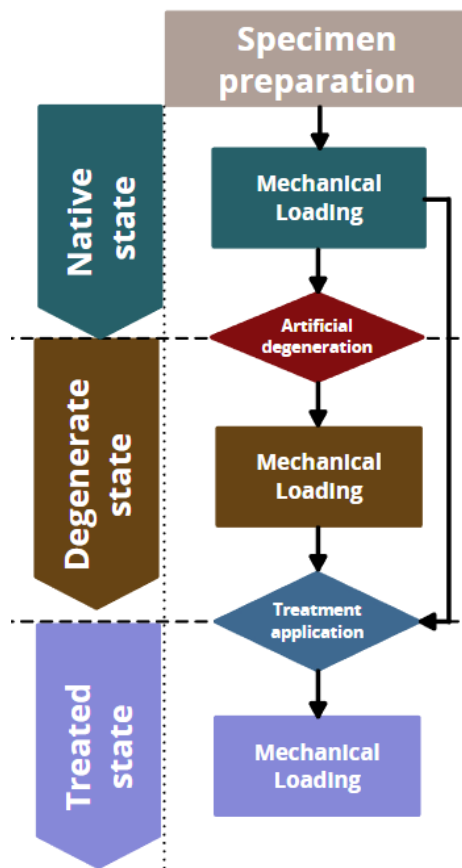


Figure 2.1 – Flow chart of testing completed including artificial degeneration and treatment. The bypassing arrows indicate testing where the native state can be treated directly, for example *in vivo* degenerate discs treated without any prior intervention. (Adapted from Dixon et al., 2021)

2.2.3 Bovine tail dissection methodology

Bovine tails were procured with the skin removed from a local abattoir on the day of kill (John Penny & Sons, Leeds, UK). The tails used by this abattoir were from animals under 30 months and two different breeds: British Blue or Limousin cattle. The exact age and breed of the animal was not known for this work. Tails were dissected in accordance with the method previously outlined by Sikora et al., (2018). A transverse cut was made through fifth disc of the tail (Figure 2.2 A and B). Next, the surrounding soft tissue was carefully removed, preserving the intervertebral discs (Figure 2.2). After dissection, the tissue was sealed in a plastic bag and stored in a -80°C freezer.

To aid in sectioning, on the day of preparation, whilst frozen, the cranial end of the bovine tail was cemented (two component polymethyl methacrylate cement (WHW Plastics, UK)) into a mantle approximately 20mm deep. The tails were placed in a custom-made rig with radio-opaque guides (Sikora et al., 2018) and imaged using a CT scanner (XtremeCT, Scanco Medical AG, Switzerland) at a voxel size of 82 μm . The CT scans were used to identify the cranio-caudal axis and the locations for sectioning (Figure 2.2 D and E). Individual bone-disc-bone units were then extracted by making two cuts

parallel to the cranio-caudal axis approximately 15 mm from the start of each endplate. The quantity of bone on either side of the disc has previously been shown to affect the mechanical properties; therefore, a 15 mm length was selected to ensure consistency in test output (Sikora et al., 2018).

Once the intervertebral discs were isolated to bone-disc-bone units, the endplates were cleaned using a surgical wound debridement system (Pulsavac Plus, Zimmer Biomet, USA). After cleaning (Figure 2.2F and G) the discs were placed into containers filled with sodium citrate for 24 hours to remove any coagulated blood (See Section 2.2.1 for sodium citrate preparation details). These two steps were performed to reduce any potential hampering of the fluid inflow to the discs (Schmidt et al., 2016). The specimens were taken out of the sodium citrate, rinsed with PBS and then frozen at -80°C until the day of testing.

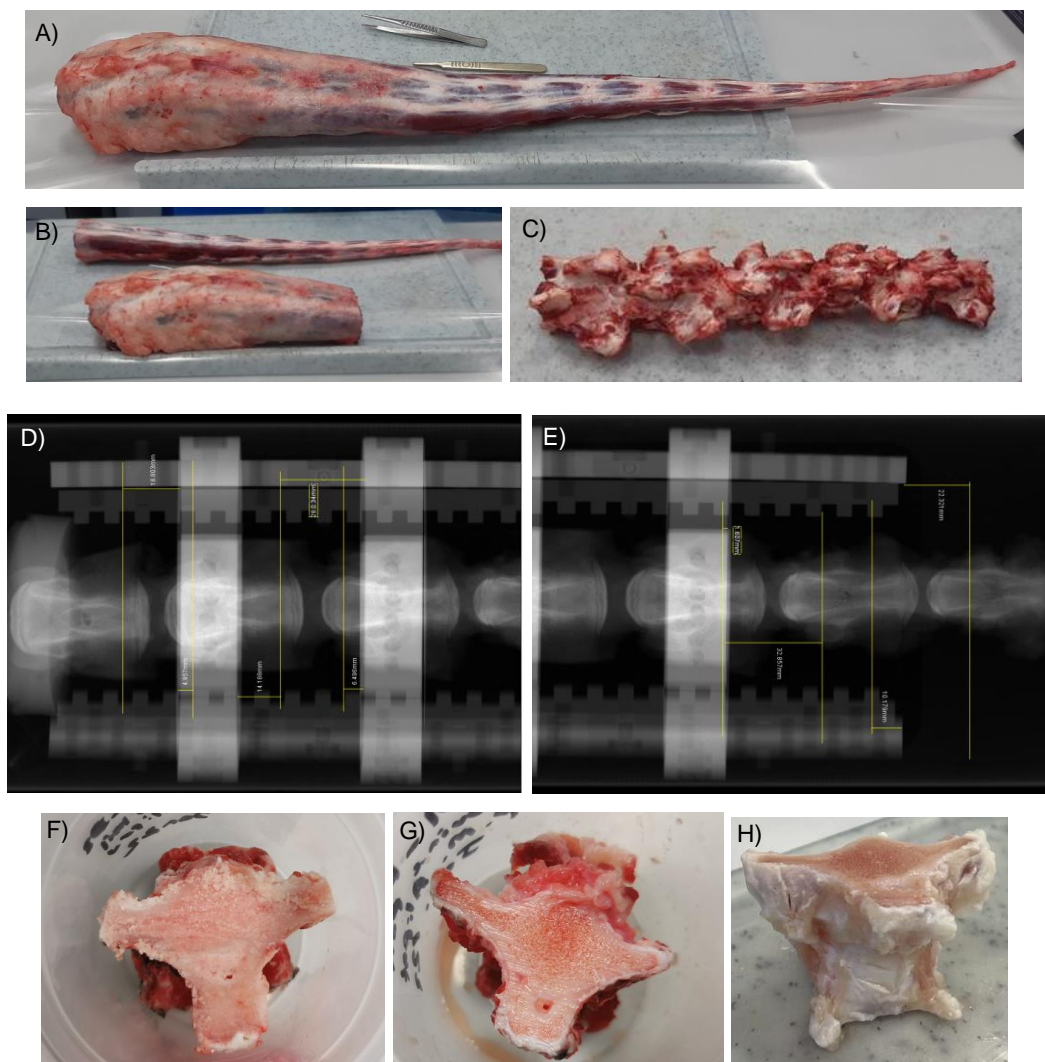


Figure 2.2 – Preparation of bovine bone-disc-bone units A) Full tail, B) Tail cut down from transverse cut along fifth disc, C) Tail with soft tissue removed, D & E) CT scans of cranial and caudal ends of the tail with bone-disc-bone unit measurements, F) Separated bone-disc-bone unit pre water piking, G) Separated bone-disc-bone unit post water piking, H) Isometric view of bone-disc-bone unit

2.2.4 Bovine bone-disc-bone unit biomechanical testing

Prior to mechanical testing, the bone-disc-bone units were placed in a PBS bath treated with antibiotics, antifungals, and aprotinin (See Appendix 1 for preparation of PBS) at 37°C for a 24-hour hold period. The 24-hour hold period was selected based on a combination of historic testing at the University of Leeds (Sikora et al., 2018) and a set of preliminary testing completed by Dr. Ruth Coe and Dr. James Warren (University of Leeds, UK) prior to this project (unpublished data shared through private communication). In this small study, three native state discs were subjected to a load of 40 N for 24 hours. The change in bone-disc-bone unit height over the 24 hours was found to be less than 0.2% between 10 and 15 hours as shown in Figure 2.3.

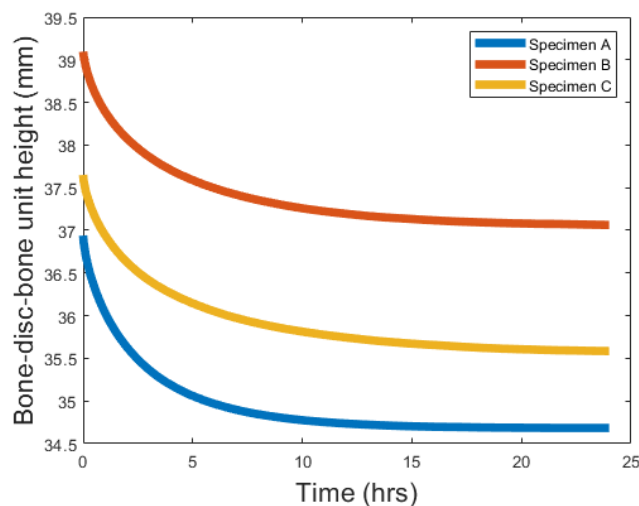


Figure 2.3 - Preliminary testing which captured the full 24-hour data and was used as the basis for the length of the osmotic equilibrium portion of the main testing (Data from Dr. Ruth Coe and Dr. James Warren University of Leeds, UK), unpublished data shared through private communication)

After the hold period, a cyclic compression test was carried out in a PBS bath at 37°C with an electromechanical linear-torsion instrument (ElectroPuls E10000, Instron, USA), fitted with a 10 kN load cell (2527 series 10 kN biaxial dynacell, Instron, USA). The load cell was calibrated annually and has an accuracy of $\pm 0.5\%$ of indicated load or $\pm 0.005\%$ of load cell capacity (whichever is greater) and 0.01 mm displacement respectively (Instron, 2015). The test protocol began with a 30-minute hold period to compensate for any shifts in hydration during transfer to the testing machine. After the hold period, compressive sinusoidal cycles were applied to the sample at 1 Hz varying between a predetermined maximum and minimum load. A frequency of 1 Hz was selected as it is used in the current ISO standard (ISO 18192-2:2010) and acts as a compromise to best represent the various activities reflected by the loading. The number of cycles differed across the studies and is reported in detail in Chapters 3, 4, and 6. The loads were calculated by using the mean cross-sectional area of discs determined from historical

testing (Sikora et al., 2018), a correction factor (Dreischarf et al., 2015) and intradiscal pressure load cases. For the bovine tissue, load cases were selected from literature for the hold period, the lower compressive cyclic limit, and the upper compressive cyclic limit (Nachemson et al., 1970; Wilke et al., 1999; Dreischarf et al., 2016). As discussed in Chapter 1, these values were based on intradiscal pressure studies and high load values were selected to exacerbate and accelerate potential issues, such as herniation, from biomaterial injection. A summary of the loads applied alongside the representative intradiscal pressure, and the activity upon which they were based, is shown in Table 2-1. The biomechanical testing protocol is also depicted in Figure 2.4.

After each cyclic compression test, specimens were imaged in an unloaded state using μ CT (μ CT100, Scanco Medical AG, Switzerland) at a voxel size of 73.4 μ m. Details of the scan are as follows, current: 114 μ A, integration time: 300 ms, and voltage peak: 70 kV. All CT images were examined using ImageJ software (Fiji ImageJ, USA).

Table 2-1 – Summary of loads applied during testing with the intradiscal pressure/activities the load represents. References for intradiscal pressure activities A – Wilke et al., 1999, B – Sato et al., 1999, and C – Nachemson and Morris, 1963. Bovine loads calculated using a correction factor of 0.66 as recommended by Dreischarf et al., 2016.

Protocol stage	Representative Activity	Intradiscal pressure (MPa)	Bovine Load (N)
Hold period	lying in supine position ^{A,B}	0.1	40N
Lower limit	unsupported sitting, standing flexing forwards, holding a 20 kg weight close to the body ^{A,B}	1.1	356N
Upper limit	weighted 50ighting with different techniques ^{A,C}	2.3	744N

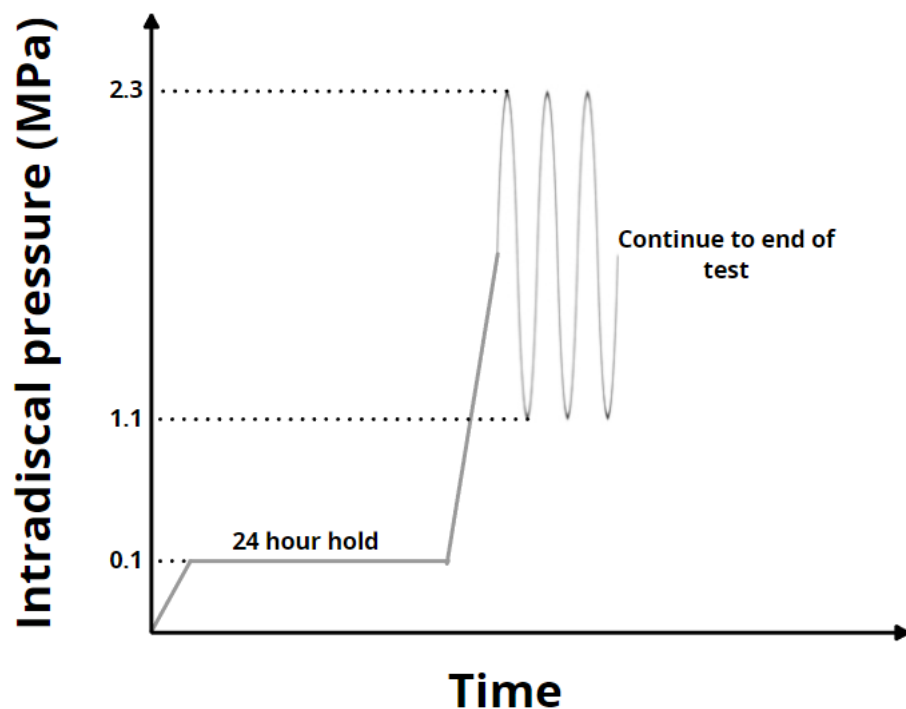


Figure 2.4 – Visual depiction of mechanical loading protocol for bovine bone-disc-bone units.

2.2.5 Bovine bone-disc-bone unit artificial degeneration

To allow in vitro testing of the augmented disc, it was important to have a consistent degenerate model which allowed for sequential testing of a disc in native, degenerate, and treated states. In theory, the ideal time to apply a nucleus augmentation procedure is at early stage degeneration. Therefore, a degeneration model should aim to replicate early stage (Pfirrmann grades 2 to 3) degeneration. An enzymatic degeneration protocol for bovine tissue was developed by Dr. James Warren at the University of Leeds and was used on the bovine tissue throughout this project. Artificial degeneration was performed after the initial native state mechanical testing (see Figure 2.1). The bone-disc-bone units were injected with 0.3 mL of papain using a 30G needle. Next, the discs were replaced in the treated PBS bath (See Section 2.2.1 for preparation of PBS), used for the native mechanical testing, under the hold period load at a temperature of 42°C for 24 hours. Papain was chosen because it indiscriminately degenerates tissue through non-specific protein degradation therefore replicating disc degeneration better than other artificial degeneration methodologies (See Appendix 1 for preparation of papain) (Roberts et al., 2008; Chan et al., 2013). The higher temperature was selected as a compromise between increasing enzymatic activity and preventing thermal tissue degradation (< 43°C Yarmolenko et al., 2011). After the higher temperature hold period, the discs were injected using a 30G needle with 0.3 ml of ebselen, an organo-selenium inhibitor to prevent further degeneration (See Appendix 1 for preparation of ebselen). Once injected with the inhibitor, the discs were returned to the PBS bath under the hold period load at 37.5°C for 24 hours. The bone-disc-bone unit continued through the testing as shown in Figure 2.1

2.2.6 Statistical testing

Statistical testing was used to analyse the experimental data and was conducted in this project using the Math, Statistics, and Optimization package in MATLAB (R2020a, Mathworks, USA). Preclinical research is often conducted with small sample sizes due to important ethical, time, and financial constraints. The anticipated data was a set of repeated measurements for the same sample at different time point, continuous repeated measures sampling, with sample sizes between three to eight. Based on the type of data anticipated, the parametric tests repeated measures ANOVA with post hoc paired t-testing or the non-parametric tests Friedmann test with post hoc Wilcoxon sign rank testing were the most appropriate statistical tests. These tests have assumptions regarding the data distribution and equal variances. Even at small sample sizes the Shapiro-Wilk test is able to test for data normality. Where the assumption of normality is

invalid, the non-parametric tests should be used. Assessing for equal variances with low sample sizes is generally less reliable and the assumption is ignored for this statistical testing. For sample sizes of six and below in a two tailed test, the critical value for the Wilcoxon sign rank test is zero. Therefore, for sample sizes of six or below the repeated measures ANOVA and paired t-test will be used, even where the normality assumption is violated. To summarize, a Shapiro-Wilk test was used to assess for a normal distribution. Where a normal distribution was present a repeated measures ANOVA with post hoc paired t-tests was completed. Where the data was not normally distributed and the sample size was above six, a Friedmann test with post hoc Wilcoxon sign rank tests was completed. If the sample size was six or less the repeated measures ANOVA and paired t-tests were completed instead. A summary flow chart of the statistical testing methods is shown in Figure 2.5. Where multiple comparisons were made a Bonferroni correction was applied to the data. All statistical testing was carried out at a significance level of 0.05.

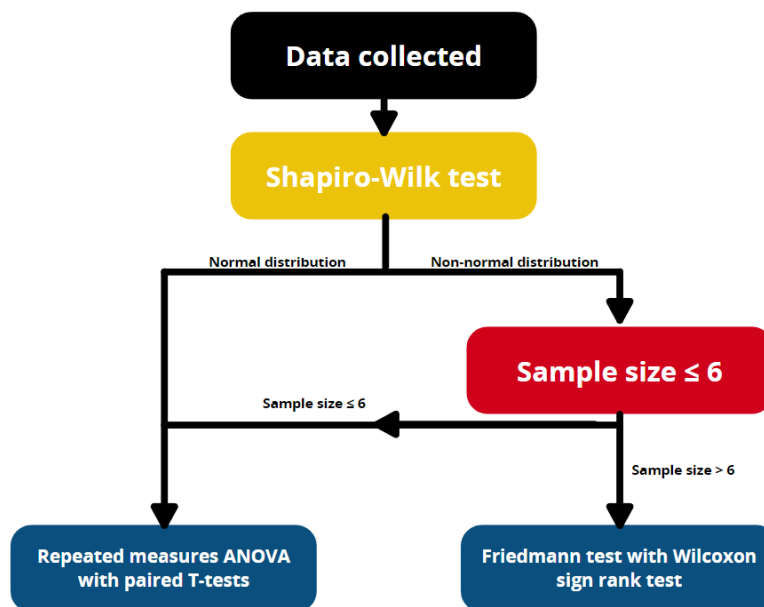


Figure 2.5 - Summary flow chart of the statistical testing.

3 High cycle loading of bovine tail intervertebral discs

3.1 Introduction

As discussed in Chapter 1, in current international standards for evaluation of disc replacements, it is recommended to apply high loads to ten million cycles (ISO, 2011). These standards are not intended for soft tissue tests and do not consider *in vitro* tissue degradation. To assess viability of novel injectable treatments for the intervertebral disc, an *in vitro* method is required that can consistently determine the mechanical behaviour of the disc. One useful method to initially screen treatments is *in vitro* testing with animal tissue from the food chain. Animal tissue sourced from the food chain does not exhibit natural degeneration; therefore, as part of the screening methodology, a rapid, consistent, and effective degeneration model needs to be developed. Specifically, to evaluate the effects of a treatment, a degenerate model is required that consistently demonstrates detectable mechanical differences between the native and degenerate states. Previous degeneration models either take several weeks to reach a level of significant degeneration (Chan et al., 2013; Malonzo et al., 2015; Gullbrand et al., 2017) or rely on damaging the disc directly (Pelletier et al., 2016; Varma et al., 2018; Lin et al., 2019). Neither method is ideal, the first may lead to more general tissue degradation due to timescales while the other can cause tissue damage that is not representative of natural disc degeneration. As a result of this there is no current methodology that quickly assesses the mechanical properties of a disc or the efficacy of an injectable treatment. The work in this chapter addresses Objective 1 by developing an *in vitro* model to assess the mechanical performance of injectable biomaterials. Specifically, the aim was to investigate the number of cycles required to minimise the total test duration and prevent tissue deterioration during the process.

3.2 Methods

3.2.1 Overview

This section builds on the methods described in Section 2.2.2 providing additional details specific to this study. A total of 48 bone-disc-bone units were prepared as per Section 2.2.3. The units were then subjected to the previously outlined sequence, where the discs were mechanically tested in the native state, artificially degenerated, mechanically tested in the degenerated state, treated with a nucleus augmentation procedure, and finally mechanically tested in the treated state. A summary flow chart of the testing is shown in Figure 3.1.

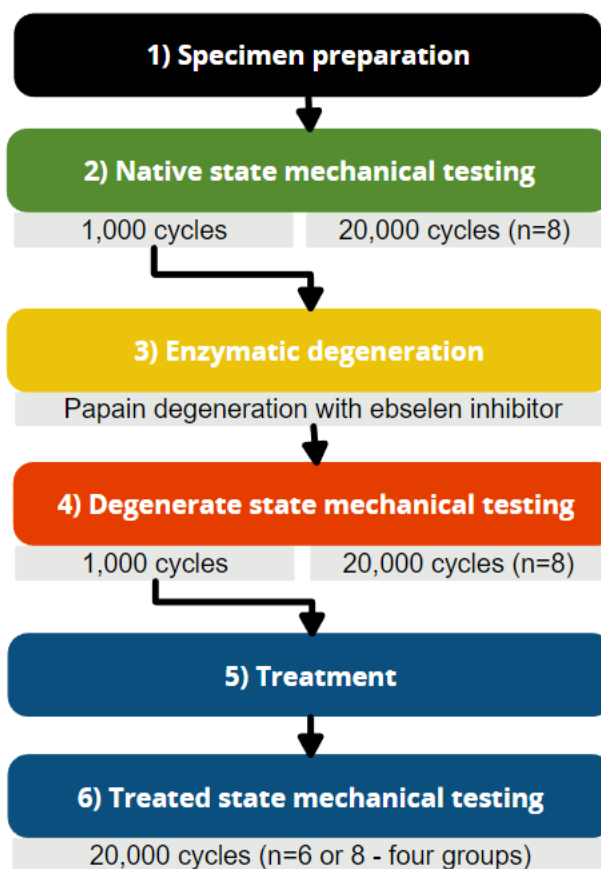


Figure 3.1 - Summary flow chart of testing protocol

Prior to testing, specimens were sorted into groups and were then tested to different final stages in the testing protocol. When a specimen reached its final state, 20,000 cycles of mechanical load were applied to the disc (steps 2, 4 or 6). Where specimens continued to the next state, only 1,000 cycles were applied. The 48 bone-disc-bone units were divided into seven groups: four test groups and three control groups. The four test groups included a native only group, a degenerate group, and two treatment groups where different volumes of hydrogel were injected. The biomaterial used for the

treatment was a two-part peptide:glycosaminoglycan (PEP:GAG) hydrogel . The three control groups consisted of a ‘sham’ degenerate procedure, and two treatment groups where a set volume of saline:glycosaminoglycan (SAL:GAG) or saline:saline (SAL:SAL) was injected. The groups, sizes, and ending stage are outlined in Table 3-1.

*Table 3-1 – Groups, respective size, and end stage for different specimens. See Figure 3.1 for details on end stage or 20,000-cycle step. *two of the specimens in these groups were completed in a previous study by Dr. Ruth Coe and Dr. James Warren.*

Group	Group size	20,000-cycle test stage
Native	8*	2
Degenerate	8*	4
0.3 mL PEP:GAG (treatment)	8*	6
1 mL PEP:GAG (treatment)	6	6
Sham degenerate (control)	6	4
1 mL SAL:GAG (control)	6	6
1 mL SAL:SAL (control)	6	6

3.2.2 Sham degenerate group

The sham control group was a modified form of the degenerate procedure as outlined in Section 2.2.1, where the papain and ebselen solutions were substituted with a PBS solution. No other changes were made to the degenerate procedure.

3.2.3 Treatment

In step 5, four different injection groups were made by hand using two 25G needles. Two groups underwent peptide injections of a two part hydrogel treatment of PEP:GAG mixture (Miles et al., 2016; Warren et al., 2021) to a set volume of 0.3 mL or 1 mL. The two remaining groups acted as control groups where injections of 1 mL SAL:GAG or 1 mL SAL:SAL were carried out. After injection, the specimens were then subjected to the 20,000-cycle compression protocol.

3.2.4 Data Analysis

3.2.4.1 Disc Mechanical Properties

The data collected by the materials testing machine was the specimen displacement and the load during each cycle. From this, three mechanical properties of the disc were evaluated for each individual cycle: the bone-disc-bone unit height, hysteresis, and stiffness. The bone-disc-bone unit height was calculated by using the fixturing to set a known zero position for the cranial and caudal ends of the unit then using the displacement output from the electromechanical machine. For a given cycle the disc height was defined as the height at the end of the cycle. The change in height from the start (cycle 1) to the end of the test (cycle 1,000) was then determined. The hysteresis over each cycle was analysed by subtracting the integral of the unloading cycle from the integral of the loading cycle to produce the area described by the force-displacement

plot. The stiffness of each individual testing cycle was extracted from a linear fit of the force-displacement data during the loading half of the cycle, excluding 5 datapoints from the extreme values (~10% of loading cycle). This value was selected based on preliminary testing to ensure the best fit through the data. An example of this analysis is shown in Figure 3.2.

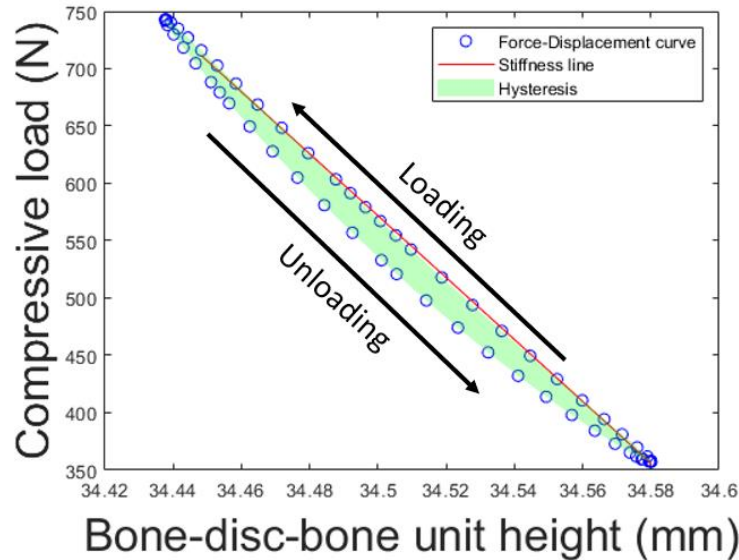


Figure 3.2 - Example curve for a single cycle with stiffness analysis

As discussed in Chapter 1, different material properties can be used to define the mechanical behaviour of the disc. Stiffness was selected for analysis in this project as initial data processing showed that differences between specimens were not changed through normalisation based on disc cross sectional area or disc height. This has also been shown previous literature using finite element modelling to review material properties (Sikora et al., 2018).

To examine the change of specimens over the length of the test, statistical testing was applied to the data comparing the stiffness after 1,000 cycles and 20,000 cycles. The statistical testing was performed within a single state and group i.e. comparison of the 1,000 cycle stiffness and the 20,000 cycle stiffness for the treated state of 0.3 ml PEP:GAG group.

3.2.4.2 Stiffness comparison across states

Two methods were applied to the data to compare the stiffness across different disc states: a direct comparison at 1,000 cycles, and a set of extrapolation models which enable comparison at 20,000 cycles. The direct comparison utilised the data at 1,000 cycles and only uses the raw data from the tests.

The extrapolation analysis started by identifying suitable predictive models, which enabled the stiffness at 20,000 cycles to be predicted based on the 1,000-cycle native and degenerate tests applied to the treated specimens. Once the best model was identified a comparison was made between the predicted 20,000-cycle native and degenerate properties were compared to the actual 20,000-cycle treated state test data. A summary of these two comparisons is shown in Figure 3.3.

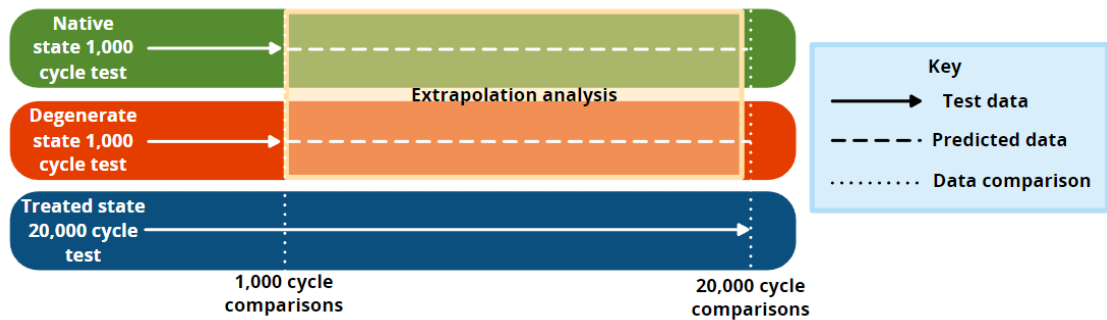


Figure 3.3 - Data comparison points for stiffness comparison at 1,000 cycles and using extrapolation analysis to compare at 20,000 cycles

3.2.4.3 Direct stiffness comparison (1,000 cycles)

Individual specimen stiffness variation with cycles was evaluated across the length of the test. To reduce the effect of experimental noise, the stiffness values were smoothed by defining the stiffness of a disc as the mean stiffness from the last 10 cycles (for example the stiffness quoted at cycle 1,000 was calculated as the mean stiffness between cycles 990 and 1,000). The degenerate and treated state stiffness values of each specimen were expressed as a proportion of the native state stiffness to enable direct comparison. Statistical testing was applied to the data as described in Section 2.2.6.

3.2.4.4 Extrapolation modelling to 20,000 cycles

Extrapolation was applied to the data to assess whether tests could be shortened with minimal compromise to the data. Two sets of analysis were performed: linear regression and function curve fitting. The linear regression compared the stiffness at 20,000 cycles to the stiffness at lower cycle numbers (100, 1,000, 2,500, 5,000, 7,500, and 10,000 cycles).

An exponential function, a natural log function, and a power law function were defined and a variable search, using an in built Matlab optimising function, was used to find the variables for each function. The process provided a three unique functions for each 20,000 cycle specimen test. The variable search was conducted using different amount of input data, data up to 100, 1,000, 2,500, 5,000, 7,500, and 10,000 cycles. The functions were then extrapolated up to 20,000 cycles. The root mean squared error was

calculated comparing the experimental to the predicted stiffness values at 20,000 cycles for each method and the coefficient of determination (R-squared) was calculated for the linear regression. To verify the suitability of the extrapolation models, leave one out analysis was completed where one specimen was left out of the calculation and the model was run again. This was repeated within groups for each specimen and the percentage error (between actual and predicted values) of the left out specimen as calculated.

3.2.4.5 Application of extrapolation models

Once a suitable extrapolation model was identified it can be used to enable within specimen comparison of native, degenerate, and treated states (rather than across the groups). The model with the lowest root mean squared error selected for subsequent analysis. It was used to predict the stiffness at 20,000 cycles and 95% confidence intervals from the native and degenerate data at 1,000 cycles for the four treated state groups. The native and degenerate state stiffness predictions at 20,000 cycles with 95% confidence intervals were compared to the treated state stiffness at 20,000 cycles.

This made two ranges, the native and degenerate state confidence intervals, which could intersect or remain separate and a single point, the treated state stiffness at 20,000 cycles. The treated state stiffness point were then assessed and allocated one of six statuses: over restored, unknown restoration, damaged, restored, partially restored, and not restored. An example graph showing the generated raw data with the extrapolated confidence intervals for a restored specimen is shown in Figure 3.4. A summary of the categorisation and grouping is shown in Figure 3.5.

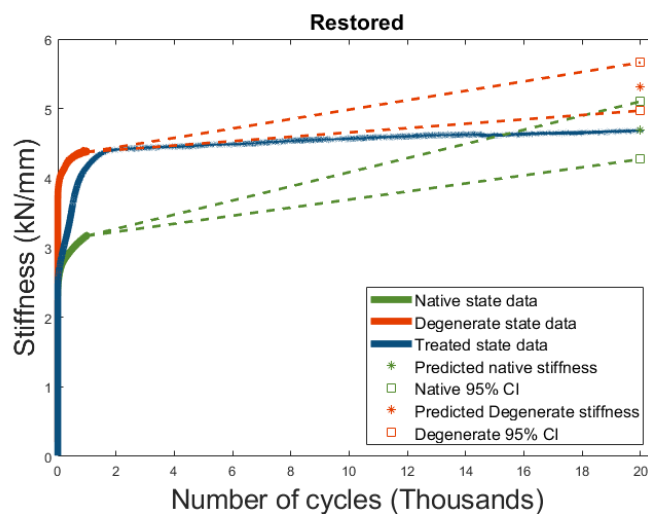


Figure 3.4– Example plot showing the actual data with the extrapolated confidence intervals for a restored specimen

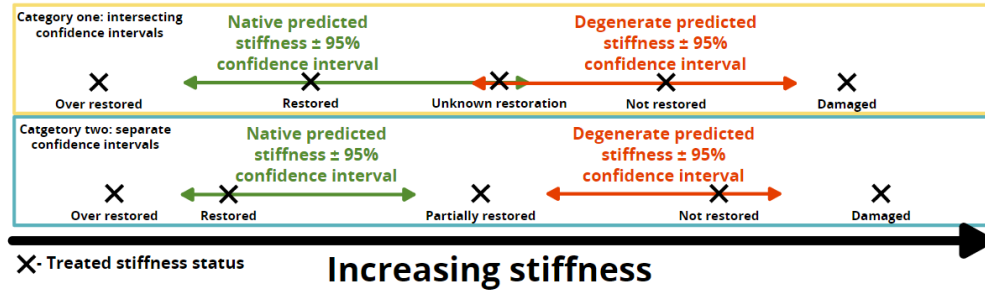


Figure 3.5 - Categorisation and status of treated state stiffness based on native and degenerate state predictions, note: over-restored, damaged, restored and not restored occur in both categories.

3.3 Results

3.3.1 Disc Mechanical Properties.

The bone-disc-bone unit height was found to reduce throughout the duration of the test, regardless of specimen state. An example of the height reduction seen through the cycles in each state for a single treated specimen is shown in Figure 3.6.

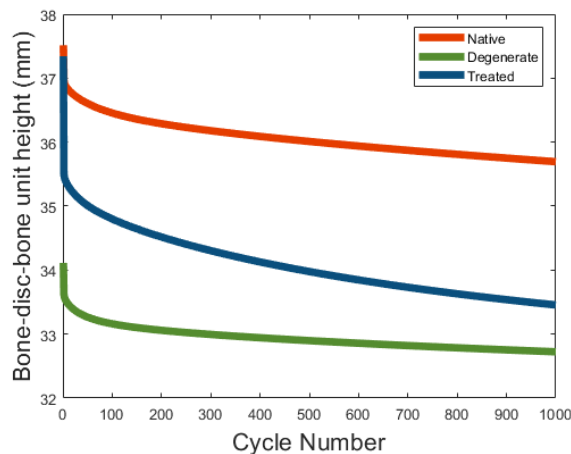


Figure 3.6 - Example of decreasing specimen height throughout duration of test (up to 1,000 cycles), data taken from specimen in 1 ml GAG:PEP group

The change in height over the duration of the test was dependent on the state. A summary of the change in height for each specimen is shown in Figure 3.7. Specifically, the degenerate state discs consistently showed the smallest change in height across the 1,000 cycle tests. The greatest change in bone-disc-bone unit height was inconsistent, where the greatest overall change was 2.26 mm in one specimen in the 1 ml SAL:SAL group.

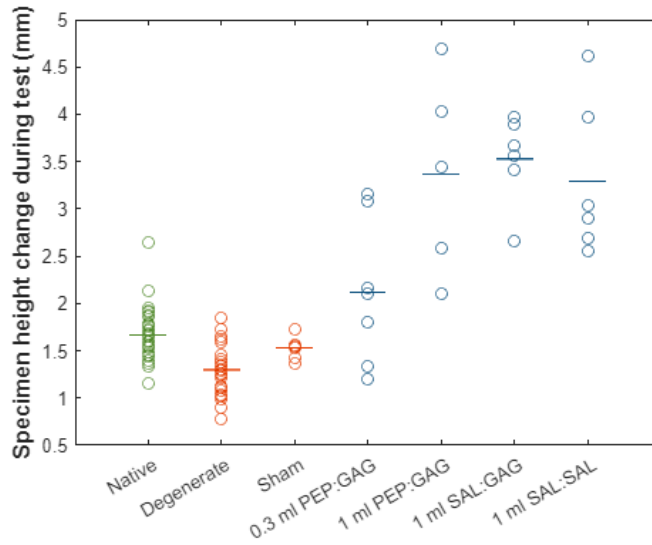


Figure 3.7 - Change in specimen height from the cycle 1 to cycle 1000 for each specimen

The hysteresis loops were assessed for each specimen in each state, and it was found that the hysteresis decreased throughout the cyclic compression test as shown in Figure 3.8A and B.

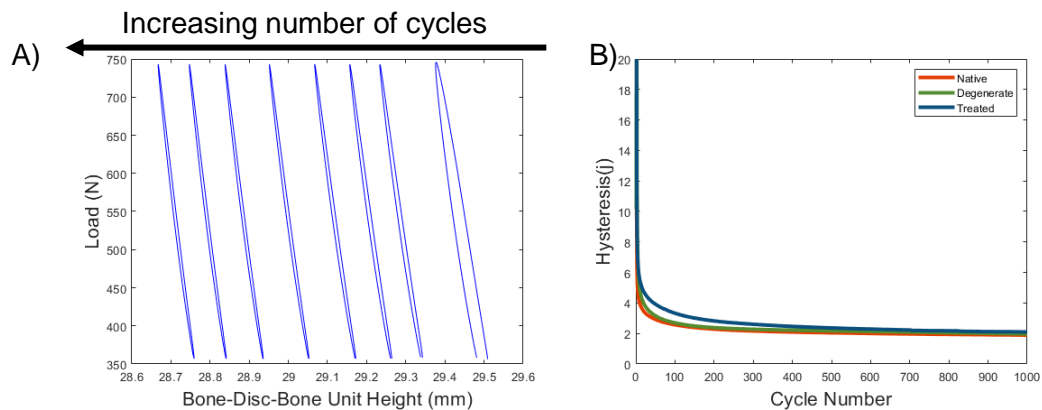


Figure 3.8 - Decreasing size of hysteresis loop throughout length of test, A) example full hysteresis loops from different cycles, B) Example plot of hysteresis change over 1,000 cycles across multiple states

The stiffness was analysed for each state of each specimen and in general showed a smooth increase in stiffness throughout the duration of the test (Figure 3.9 A & B). No clear plateau was reached for all the samples. In 13 out of the 122 individual state stiffness plots, disruptions to the smooth increase were observed on the plot. Two broad categories of stiffness disruption were observed, 1) a large change in stiffness (< 2 kN/mm) in treated specimens within the first 1,000 cycles, and 2) a small change in stiffness (>2 kN/mm) in any disc state across less than 50 cycles. The observed shift in stiffness, number of specimens, and group details are shown in Table 3-2 and graphical examples are shown in Figure 3.9 C, and D.

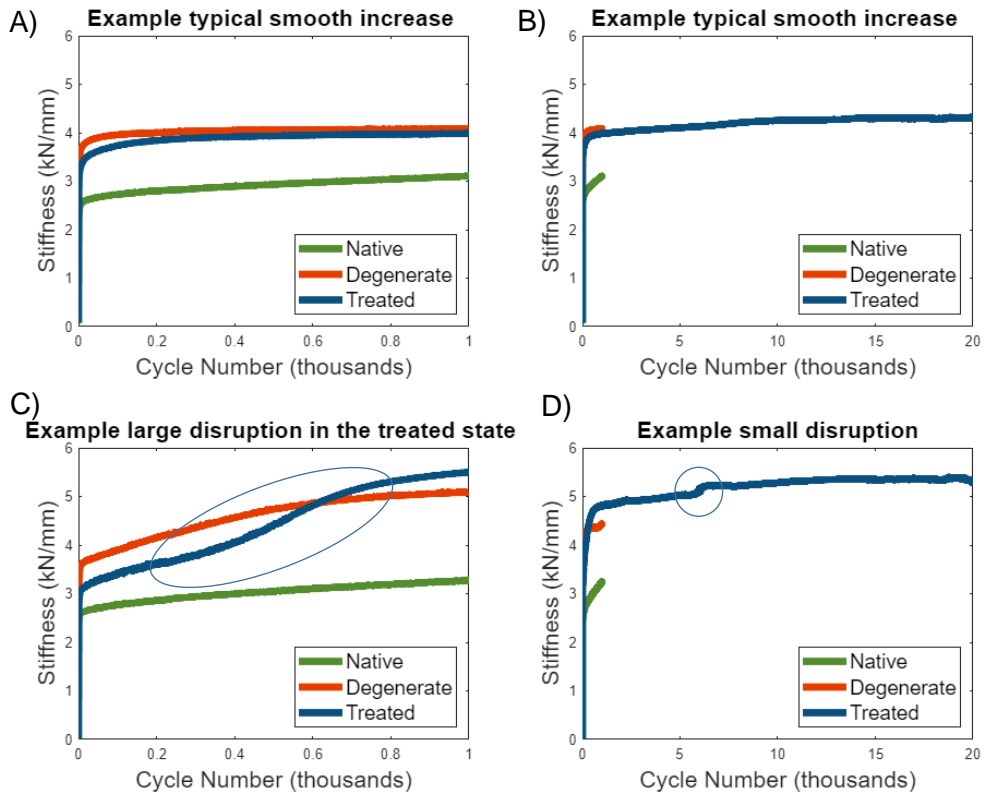


Figure 3.9 - A&B) Example plot of same specimen from 0.3 mL PEP:GAG group showing smooth increase throughout test: A) sample to 1,000 cycles, B) sample to 20,000 cycles, C) Example from 0.3 mL PEP:GAG group showing observed large shift exhibited by treated state specimens, D) Example from 0.3 mL PEP:GAG group showing small change in stiffness observed.

Table 3-2 - Observed disruptions to smooth stiffness data alongside the group and number of specimens

Observed stiffness behaviour	Group				
	Degenerate	0.3 mL PEP:GAG	1 mL PEP:GAG	1 mL SAL:GAG	1 mL SAL:SAL
1) Large change	0	2	2	1	3
2) Small change	1	2	2	0	0

During radiographic analysis two specimens within the small change category were identified as exhibiting transverse plane motion, one from the degenerate group and the other from the 1 mL PEP:GAG group. An example of the transverse plane motion from a sagittal view of a CT is shown in Figure 3.10.

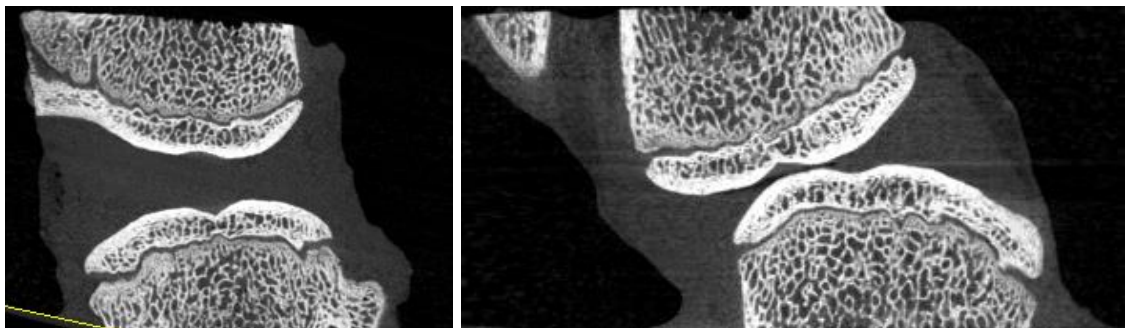


Figure 3.10 - Example of lateral transverse plane motion from post test CT scan, left) Post native test CT scan, right) Post degenerate test CT scan

Throughout the testing, no extrusion of material through the annulus was observed for any samples.

A summary of the statistical testing conducted to compare the stiffness after 1,000 cycles and the stiffness at 20,000 cycles for each group is shown in Table 3-3. Statistically significant differences were found between cycle 1,000 and cycle 20,000 for each group.

*Table 3-3 - Statistical testing comparing the stiffness at 1,000 cycles and the stiffness at 20,000 cycles within groups. The table contains data for the Shapiro-Wilk test p values, type of test used, and test outcomes. All statistically significant results are highlighted in blue. *Specimens did not have normal distribution in all data but had an sample size of six meaning t-tests were chosen over Wilcoxon sign rank tests*

Group	Shapiro-wilk test p values		Test used for comparison	Statistical test p-values
	1,000 cycles	20,000 cycles		
Native (n=8)	0.072	0.749	paired t-test	4.37E-03
Degenerate (n=8)	0.901	0.442	paired t-test	2.09E-02
Sham degenerate (n=6)	0.951	0.912	paired t-test	7.63E-05
0.3ml PEP:GAG (n=8)	0.9552	0.405	paired t-test	4.80E-03
1 ml PEP:GAG (n=6)	0.0089	0.1842	paired t-test*	4.20E-02
1 ml SAL:GAG (n=6)	0.846	0.756	paired t-test	2.70E-06
1 ml SAL:SAL (n=6)	0.4503	0.6907	paired t-test	6.50E-03

3.3.2 Stiffness comparison across states

3.3.2.1 Direct stiffness comparison (1,000 cycles) – Degenerate model

The stiffness at 1,000 cycles for each disc in its degenerate state was expressed as a proportion of the native state. The mean increase in stiffness from the native and enzymatically degenerate was 40%. The mean increase in stiffness from the native and ‘sham’ degenerate state was 6%. The data of the discs in the degenerate state and the ‘sham’ degenerate discs are presented in Figure 3.11. A summary of the statistical testing is shown in Table 3-4. The paired t-tests showed a significant difference for the specimens subjected to the enzymatic procedure ($p < 0.05$) and no significant difference for the ‘sham’ degenerate procedure group ($p > 0.05$).

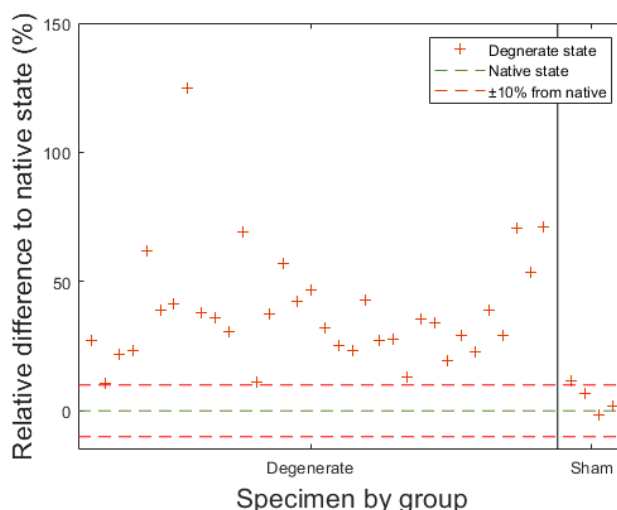


Figure 3.11 – Degenerate state stiffness normalised to the native state stiffness for Individual discs, n=34 for degenerate state, n=6 for 'sham' degenerate state. Dashed lines are at 0, the native state and ±10% from the native.

Table 3-4 - Statistical testing for the degenerate and 'sham' groups. The table contains data for the Shapiro-Wilk test p values, type of test used, and test outcomes. All statistically significant results are highlighted in blue.

Group	Shapiro-wilk test p values		Test used for comparison	Statistical test p values
	Native state	Degenerate state		
Enzymatic degenerated	0.05	0.45	paired t-test	6.22e-12
Sham' procedure	0.95	0.56	paired t-test	0.08

3.3.2.2 Direct stiffness comparison (1,000 cycles) – Treated discs

The degenerate and treated state stiffness values were calculated as a proportion of the native state to allow comparison, as shown in Figure 3.12. It was found that in most treatment groups that the stiffness was reduced from the degenerate state. The mean decrease in stiffness from the degenerate state to the treated state was 3%, 17%, 15%, and 8% for the 0.3 mL PEP:GAG, 1 mL PEP:GAG group, 1 mL SAL:GAG group, and 1 mL SAL:SAL group respectively. In two cases in the 0.3 mL PEP:GAG group, the treated state resulted in an increase in stiffness indicating the disc became more degenerate after treatment.

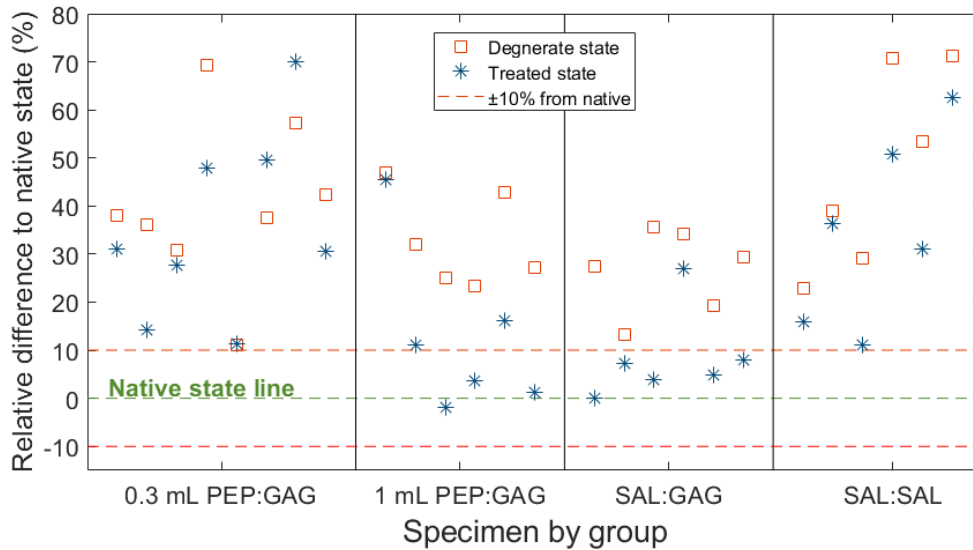


Figure 3.12 – Degenerate and treated state stiffnesses normalised to the native state stiffness for individual discs, split by group. Dashed lines are at 0, the native state and $\pm 10\%$ from the native.

A biomechanically successful treatment would show significant differences between the degenerate and treated states and no significant difference between native and treated states. The p value results of the Shapiro-Wilk normality test and the selected test for comparison for the different treatment groups is shown in Table 3-5.

Table 3-5 – Shapiro-Wilk normality test p values and selected test for statistical comparison. All statistically significant results are highlighted in blue. *Specimens did not have normal distribution in all data but had a sample size of six meaning t-tests were chosen over Wilcoxon sign rank tests.

Group	Shapiro-Wilk test p values			Test used for comparison
	Native state	Degenerate state	Treated state	
0.3 ml PEP:GAG	0.49	0.27	0.96	Repeated measures ANOVA with paired t-test
1 ml PEP:GAG	0.87	0.85	0.01	Repeated measures ANOVA with paired t-test*
1 ml SAL:GAG	0.09	0.07	0.96	Repeated measures ANOVA with paired t-test
1 ml SAL:SAL	0.96	0.80	0.45	Repeated measures ANOVA with paired t-test

The results of the statistical comparison for the different treatment groups is shown in Table 3-6

Table 3-6 – p values for the repeated measures ANOVA and follow up paired t-tests for the different treatment groups. All statistically significant results are highlighted in blue.

Group	Repeated measures ANOVA	States compared	
		Native to Treated	Degenerate to Treated
0.3 ml PEP:GAG	1.60E-05	1.40E-03	0.32
1 ml PEP:GAG	3.14E-04	0.13	3.80E-03
1 ml SAL:GAG	1.55E-04	0.08	0.01
1 ml SAL:SAL	1.31E-04	7.70E-03	0.01

3.3.3 Extrapolation modelling to 20,000 cycles

A strong relationship was found between the stiffness at 20,000 and the stiffness at 10,000 cycles across all groups. An example plot showing the linear regression for all the data is shown in Figure 3.13. A strong relationship was identified for all groups at 10,000 cycles. The relationship between the stiffness at 20,000 cycles and the stiffness at 100 cycles was found to be strong for the native state, degenerate state, and 1 ml SAL:GAG groups with a R-squared value at or above 0.8. Across all the data a root mean squared error below 10% was observed by 2,500 cycles with diminishing returns on reducing error with increasing number of cycles. The R-squared and root mean squared error are presented in Table 3-7 and Table 3-8 respectively.

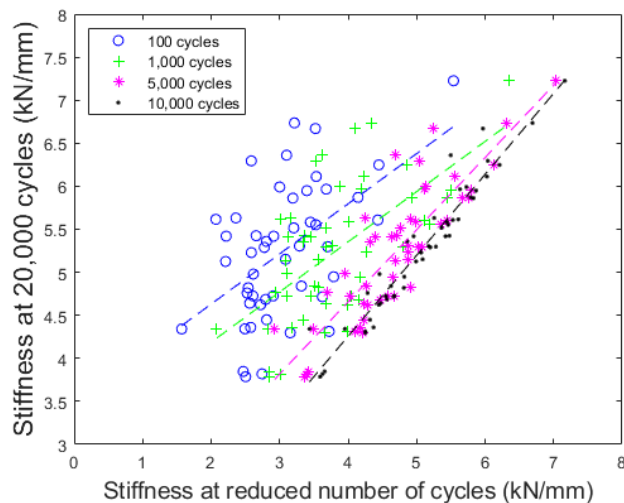


Figure 3.13 - Linear regression for all data comparing the low cycle stiffness to the stiffness at 20,000 cycles

Table 3-7 –R squared values of the linear regression analysis between the actual 20,000-cycle data and reduced cycle numbers. Values above 0.8 have been highlighted in green to show strong relationships.

Group	R-squared values for the stiffness at reduced number of cycle to the 20,000-cycle stiffness					
	100	1,000	2,500	5,000	7,500	10,000
All data (n=48)	0.27	0.38	0.52	0.74	0.86	0.93
Native (n=8)	0.80	0.84	0.89	0.92	0.95	0.97
Degenerate (n=8)	0.87	0.86	0.93	0.99	1.00	1.00
Sham degenerate (n=6)	0.71	0.73	0.74	0.74	0.79	0.86
0.3ml PEP:GAG (n=8)	0.16	0.48	0.73	0.92	0.97	0.99
1 ml PEP:GAG (n=6)	0.00	0.14	0.03	0.04	0.42	0.89
1 ml SAL:GAG (n=6)	0.80	0.91	0.93	0.92	0.86	0.93
1 ml SAL:SAL (n=6)	0.26	0.60	0.74	0.96	0.97	0.98

Table 3-8 - Root mean squared error of the linear regression analysis between the actual 20-000 cycle data and reduced cycle numbers. Values with an error of 10% or lower have been highlighted in green to show low errors

Group	Root mean squared values for the stiffness at reduced number of cycle to the 20,000-cycle stiffness					
	100	1,000	2,500	5,000	7,500	10,000
All data (n=48)	13.5%	12.0%	10.4%	7.6%	5.6%	4.0%
Native (n=8)	8.7%	7.5%	6.1%	4.9%	3.8%	2.8%
Degenerate (n=8)	6.6%	6.5%	4.7%	2.0%	1.1%	0.7%
Sham degenerate (n=6)	6.4%	5.9%	5.7%	5.7%	5.2%	4.1%
0.3ml PEP:GAG (n=8)	14.8%	10.7%	7.2%	3.7%	2.2%	1.4%
1 ml PEP:GAG (n=6)	7.1%	6.5%	7.0%	6.9%	5.2%	2.3%
1 ml SAL:GAG (n=6)	6.1%	3.9%	3.4%	3.5%	4.8%	3.5%
1 ml SAL:SAL (n=6)	8.8%	6.5%	5.2%	2.1%	2.0%	1.5%

Three mathematical functions were fitted to the stiffness data to a reduced number of cycles. An example of the function curves is shown in Figure 13. The root mean squared error between an extrapolated 20,000-cycle stiffness for each mathematical model and the data actual 20,000 stiffness value. For all models, it was found that none had a root mean squared error below 10% across all groups when the first 10,000 cycles of data was used to derive the function. The root mean squared error values for the exponential function, natural log function, and power law function are shown in Table 8, Table 9, and Table 10 respectively

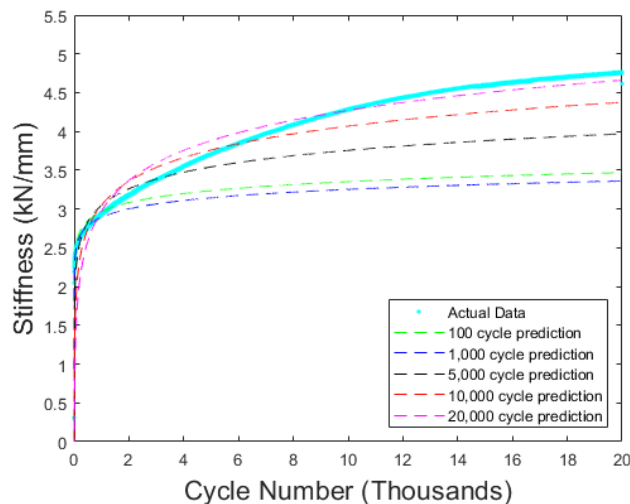


Figure 3.14 – Example plot of function used to predict high cycle behaviour using a small dataset

Table 3-9 – Root mean squared error comparing outputs from the exponential function fitting with reduced cycle numbers to the actual stiffness. Values with an error of 10% or lower have been highlighted in green to show low errors

Exponential - Ae^{Bx}	Root mean squared values for the extrapolated stiffness from reduced number of cycles to the 20,000-cycle stiffness					
	100	1,000	2,500	5,000	7,500	10,000
All data (n=48)	44.6%	33.6%	28.9%	12.15	13.4%	8.0%
Native (n=8)	42.3%	30.4%	20.5%	13.2%	12.9%	13.5%
Degenerate (n=8)	20.0%	22.4%	4.12%	2.4%	2.0%	0.0%
Sham degenerate (n=6)	47.1%	34.6%	22.9%	13.1%	8.3%	5.2%
0.3ml PEP:GAG (n=8)	38.0%	48.1%	12.6%	8.6%	4.5%	2.5%
1 ml PEP:GAG (n=6)	46.6%	27.4%	61.3%	15.4%	5.0%	2.6%
1 ml SAL:GAG (n=6)	60.1%	39.2%	28.5%	21.0%	32.5%	13.9%
1 ml SAL:SAL (n=6)	49.3%	26.7%	12.2%	7.0%	5.8%	4.0%

Table 3-10 - Root mean squared error comparing outputs from the natural log function fitting with reduced cycle numbers to the actual stiffness. Values with an error of 10% or lower have been highlighted in green to show low errors

Natural log - $A\ln(x) + B$	Root mean squared values for the extrapolated stiffness from reduced number of cycles to the 20,000-cycle stiffness					
	100	1,000	2,500	5,000	7,500	10,000
All data (n=48)	25.7%	21.2%	15.2%	10.5%	8.3%	7.2%
Native (n=8)	23.0%	23.4%	16.8%	10.2%	6.5%	4.4%
Degenerate (n=8)	13.7%	11.7%	6.2%	6.2%	5.4%	4.4%
Sham degenerate (n=6)	27.7%	27.5%	20.0%	12.9%	9.3%	7.1%
0.3ml PEP:GAG (n=8)	19.4%	16.8%	13.7%	7.8%	5.7%	4.5%
1 ml PEP:GAG (n=6)	22.3%	21.4%	14.2%	14.2%	11.2%	8.1%
1 ml SAL:GAG (n=6)	41.4%	30.1%	20.8%	12.6%	10.2%	10.6%
1 ml SAL:SAL (n=6)	29.0%	14.2%	12.0%	9.0%	10.1%	10.1%

Table 3-11 - Root mean squared error comparing outputs from the power law function fitting with reduced cycle numbers to the actual stiffness. Values with an error of 10% or lower have been highlighted in green to show low errors

Power law - Ax^B	Root mean squared values for the extrapolated stiffness from reduced number of cycles to the 20,000-cycle stiffness					
	100	1,000	2,500	5,000	7,500	10,000
All data (n=48)	23.0%	26.7%	17.6%	13.0%	11.6%	9.7%
Native (n=8)	19.4%	20.9%	13.3%	6.4%	3.9%	3.4%
Degenerate (n=8)	19.2%	10.8%	9.6%	9.9%	8.0%	6.0%
Sham degenerate (n=6)	24.1%	24.9%	16.0%	9.1%	7.1%	6.0%
0.3ml PEP:GAG (n=8)	21.4%	32.0%	20.6%	10.7%	8.2%	6.5%
1 ml PEP:GAG (n=6)	17.0%	24.7%	20.3%	22.5%	15.0%	10.3%
1 ml SAL:GAG (n=6)	36.5%	21.7%	13.6%	14.0%	20.3%	19.4%
1 ml SAL:SAL (n=6)	20.8%	43.4%	26.2%	15.5%	13.9%	10.6%

Leave one out analysis was completed for the different predictive model. In all cases the linear regression model had the lowest error. A summary of the mean error from the predicted values using 1,000 cycles for prediction is shown in Table 3-12.

Table 3-12 -Mean error from predictions generated by different models using data from 1,000 cycles

Group	Mean error when using 1,000 cycles to predict			
	Linear regression	Exponential	Natural log	Power law
All data (n=48)	9.0%	24.0%	18.0%	20.0%
Native (n=8)	8.0%	27.1%	22.7%	21.8%
Degenerate (n=8)	7.0%	17.3%	14.7%	15.1%
Sham degenerate (n=6)	7.0%	34.6%	27.2%	24.7%
0.3ml PEP:GAG (n=8)	12.0%	18.5%	15.8%	20.2%
1 ml PEP:GAG (n=6)	14.0%	24.9%	9.6%	9.0%
1 ml SAL:GAG (n=6)	5.0%	37.3%	26.7%	21.9%
1 ml SAL:SAL (n=6)	9.0%	11.6%	8.9%	28.3%

3.3.4 Application of extrapolation models

The linear regression method was found to have a lower root mean squared error. Linear regression was taken forward to generate predicted 20,000 cycle native and degenerate stiffness values for the treated discs, where the native and degenerate state tests only went to 1,000 cycles. The predicted stiffness at 20,000 cycles for the native and degenerate groups was calculated and compared to the true values at 20,000 cycles for these groups and are present with 95% confidence intervals in Figure 3.15 A and B.

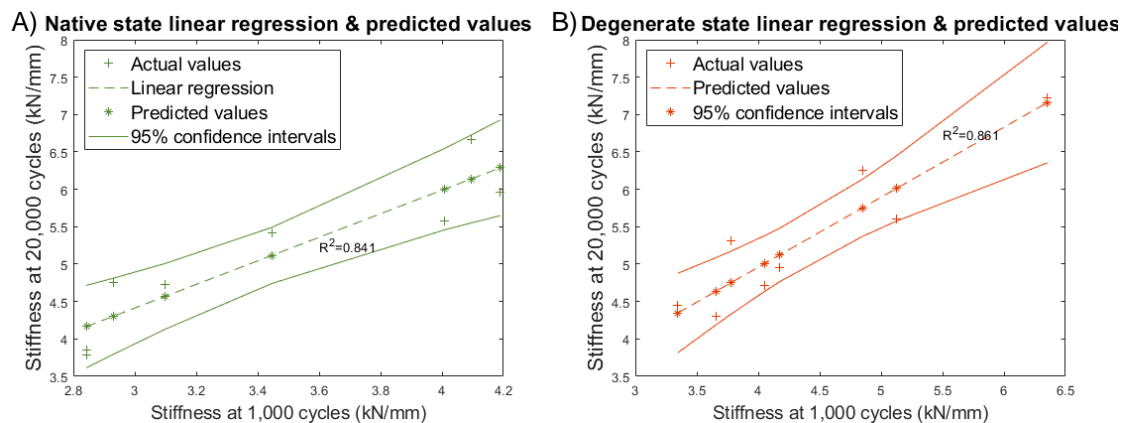


Figure 3.15 – Actual value at 20,000 cycles, predicted values based on 1,000 cycle test, and 95% confidence intervals for the A) native and B) degenerate groups.

The predicted stiffness values at 20,000 cycles for the native and degenerate states of individual specimens in treatment groups, and their respective confidence intervals, were calculated and categorised in accordance with statuses in Figure 3.5. Two examples of the predictive analysis within the stiffness plots are shown in Figure 3.15. The 1 ml PAP:GAG appeared to provide the best restoration, where three discs were restored and

one was over-restored. The other treatments had reduced effects and the 1 ml SAL:GAG group damaged five of the six discs. The full results are shown in Table 3-13.

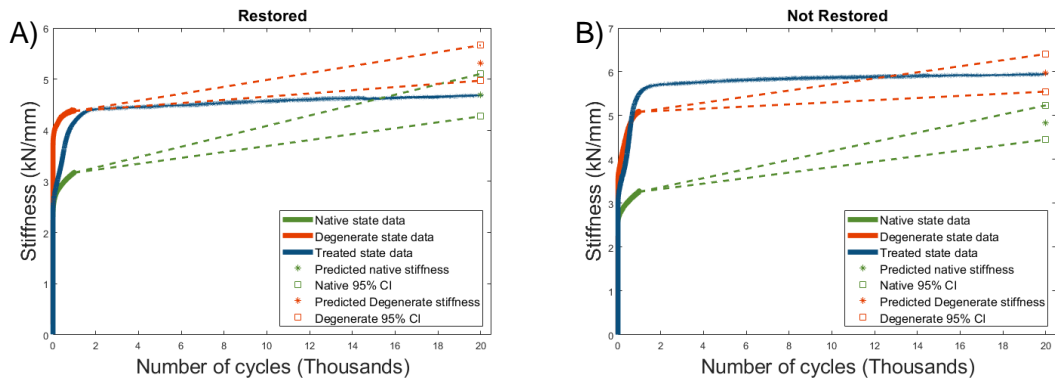


Figure 3.16 – Two examples of predictive analysis, both plots from 0.3 mL PEP:GAG group, showing A) Stiffness restored, and B) Stiffness not restored

Table 3-13 – Status of treated specimens broken down by group.

Status	Group				
	0.3mL PEP:GAG	1 mL PEP:GAG	1 mL SAL:GAG	1 mL SAL:SAL	
Damaged		1	2	5	1
Not restored		3	0	1	1
Unknown restoration		1	0	0	1
Partially restored		1	0	0	1
Restored		2	3	0	2
Over restored		0	1	0	0

3.4 Discussion

3.4.1 Disc Mechanical Properties

Throughout the study, a large change in all mechanical properties (bone-disc-bone unit height, hysteresis, and stiffness) was observed within the first 10 cycles of mechanical loading. The shift during the initial cycles is caused by the increased loading expelling water from the nucleus with minimal recovery time. After this initial shift, small changes in the mechanical properties continued throughout the length of the test. Specifically, the bone-disc-bone unit height decreased, hysteresis remained low, and the stiffness increased. As with the initial shift, the volume of the disc continued to reduce due to the high loading and minimal recovery time. A pictorial representation of the fluid inflow and outflow throughout one set of testing is shown in Figure 3.17.

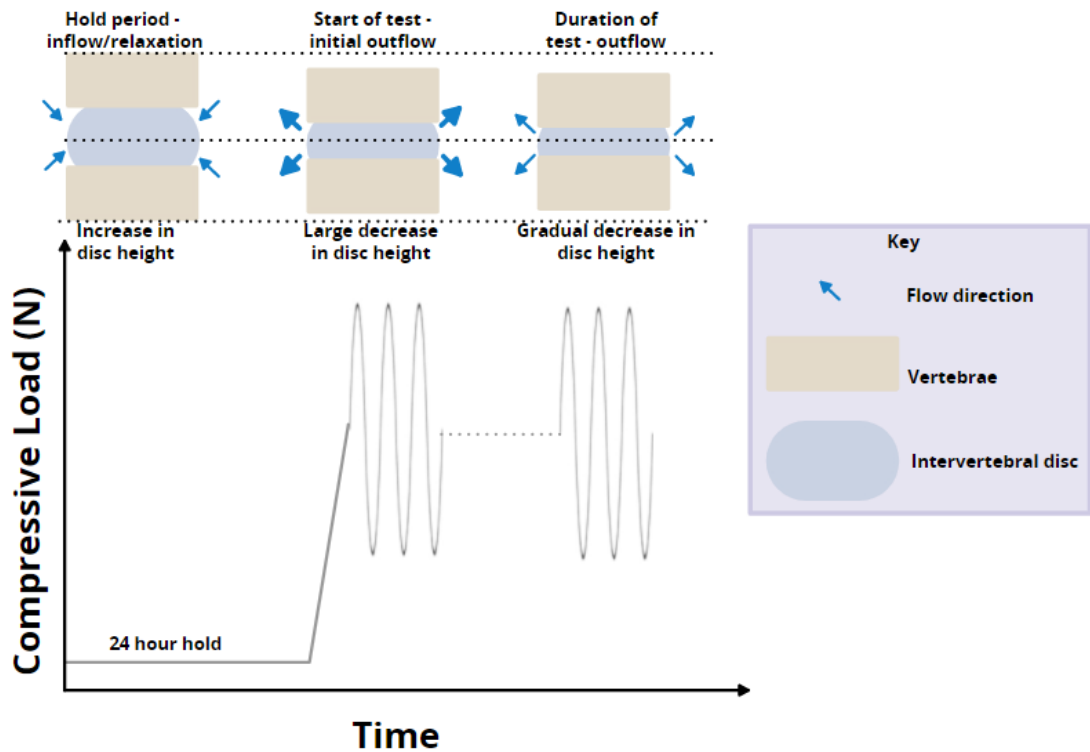


Figure 3.17 - Pictorial representation of fluid in/out flow and bone-disc-bone unit height through the duration of the test

The expelled fluid changes the disc height and was responsible for the observed change in the mechanical behaviour of the disc, an increase in stiffness. Specifically, the loss of fluid in the nucleus and inner annulus would result in a reduction to the intradiscal pressure from the nucleus leading to a reduction in the tension on the annulus. As the testing was controlled by load, the change in height compensates for the change in mechanical behaviour of the disc. Overall, this causes an increase in the stiffness.

In this study no clear height or stiffness plateau was reached throughout all the data. This indicates that the bone-disc-bone units in this study are likely above their natural 'working equilibrium'. Such a result is attributed to the high nucleus pulposus pressures applied for the cyclic loading (1.1 MPa and 2.3 MPa) in combination with no recovery time during testing. It should also be noted that the test method makes no attempt to replicate the circulatory system, where blood pressure and flow could contribute to maintaining water in the disc therefore enabling the disc to reach a working equilibrium. Fluid flow was still available for discs as they were submerged in a fluid bath where fluid was able to access both the annulus and the endplates. Another contributor to the increasing stiffness is the potential of compounding microstructural damage over the length of the test. Previous work has shown that vibrations can instigate delamination and interlamellar tearing. (Wade et al., 2016).

Direct comparison to other literature regarding cyclic compressive testing of intervertebral discs is difficult due to a given study's specific choice and preparation of tissue, reported mechanical measures, and test protocol. Cyclic bovine testing mechanical properties are reported in various ways including stiffness (Beckstein et al., 2008; Chan et al., 2013; Alsup et al., 2017), percentage strain (Thorpe et al., 2016), hysteresis (Thorpe et al., 2016; Alsup et al., 2017), neutral zone changes (Alsup et al., 2017), and Young's modulus (Thorpe et al., 2016; Schmocker et al., 2016). In general, the stiffness mechanical response of the bovine specimens was found to be similar to that of previous studies (Malhotra et al., 2012; Newell et al., 2017a); however, the specifics of the test protocol such as frequency, load, and number of cycles heavily affects the mechanical behaviour (Costi et al., 2008; Derby and Akhtar, 2015). The stiffness in this study, between approximately 2.5 and 5 kN/mm, was higher than that of similar protocols which ranged from approximately 0.6 kN/mm to 2 kN/mm (Beckstein et al., 2008; Likhitpanichkul et al., 2014; Newell et al., 2017). In general, this was attributed to the lower loads and lower number of cycles used in the other studies. An important observation of this study was the disruption identified to the typical smooth change in stiffness over multiple loading cycles. The disruption broadly fit into two categories where the magnitude of the change in stiffness was the key divider between specimens. The large change in stiffness was attributed to the hydrogel integration with the nucleus, where when initially injected the hydrogel may be localised and then is distributed throughout the nucleus during the test. Once loading started the gel could be distributed through the disc, for example into the pocket in the inner annulus, resulting in a large change in the mechanical response of the disc. In the remaining five of the thirteen disrupted samples, the stiffness shift was small and occurred quickly. In three samples this shift was believed to be due to end plate contact based on review of the CT scans. The end plate contact appeared to cause a sudden change in mechanical properties. In the remaining two samples radiographic analysis showed lateral deformation in the transverse plane. The shift in stiffness for these two samples could be exclusively caused by this deformation or the lateral deformation narrowing of the disc space resulting end plate to end plate contact. These potential causes were identified after the testing and not obvious during the test. The observed behaviour did not occur in the native state group; however, the behaviour was identified across multiple groups with no identified consistency. These behaviours were most frequent in the treated groups (12 of 13, 1 of 13 observed in the degenerate state of the degenerate group). In the treated state groups, how the hydrogel integrates, distributes or breaks down readily impacts the mechanical behaviour of the disc. Due to natural tissue variation and its response to the enzymatic protocol it is possible there are unidentified complexities of the mechanics

causing the disruption to the stiffness. It is also important to note that, there was only a 30-minute hold period between treatment and cyclic testing. This was done to mimic an outpatient appointment where a patient may be able to be active shortly after treatment. Introducing a longer hold period may reduce the observed disruptions and provide more predictable behaviour.

3.4.1.1 Direct stiffness comparison (1,000 cycles) – Degenerate model

The degenerate model used in this study consistently induced a statistically significant increase in stiffness. The sham procedure group, where saline was injected in place of the enzyme, showed no statistically significant difference between native and degenerate states. The increase in stiffness was attributed to the papain, which indiscriminately breaks down the protein-based components within the extracellular matrix. The breakdown causes the GAGs to move more freely and can allow expulsion from the disc. The reduction in GAG content in turn can reduce the ability of the disc to imbibe water. As previously discussed, this effects the mechanical behaviour of the disc. Whilst there was a statistically significant difference between the native and degenerate states, some variation in the severity of degeneration was observed due to natural tissue variation. The degenerate model was used to represent early-stage degeneration level with the induced degeneration predominantly being localised to the nucleus. This may not be fully representative of degeneration where annular tears can be observed clinically (Videman and Nurminen, 2004; Sharma et al., 2009). Instead, the degenerate model was representative of degeneration with minimal annular pathology (Jin et al., 2018) which would be an ideal target degeneration level for a nucleus augmentation treatment. The described behaviour is reflected in literature where degeneration protocols have been applied. Other work has observed a change in mechanical behaviour (Vresilovic et al., 2006; Mwale et al., 2008; Chan et al., 2013; Showalter et al., 2014; Schmocker et al., 2016; Thorpe et al., 2016; Gullbrand et al., 2017) or a change in the GAG content (Mwale et al., 2008; Roberts et al., 2008; Chan et al., 2013; Thorpe et al., 2016). As previously highlighted, it is possible that some of the observed change in mechanical stiffness was caused by microstructural changes from the high mechanical loading rather than only the enzymatic behaviour. This is reflected in the sham degeneration group, where although no statistically significant difference, there was a minor difference in the mechanical stiffness of the discs.

One key benefit of the developed protocol compared to other published models is the amount of time required to complete the degeneration. The speed of an *in vitro* methodology is vital as it reduces the chance of infection and behaviour changes as a result of tissue degradation. The bulk of current literature required a minimum of five

days to create significant degeneration to the disc (Roberts et al., 2008; Chan et al., 2013; Schmocker et al., 2016; Thorpe et al., 2016), whilst the outlined protocol takes two days to demonstrate degeneration. The reduced time in the outlined protocol is attributed to the high papain concentration alongside a high temperature hold period. Studies which use bovine tails with shorter incubation periods (two to sixteen hours) used trypsin (a serine protease) and have reported deterioration inconsistent with disc degeneration (Moore, 2000; Périé et al., 2006; Mwale et al., 2008; Alsup et al., 2017). These protocols all report the mechanical properties inconsistently due to the variations in mechanical loads and number of cycles applied. An important step in the protocol used in this study is the use of an inhibitor. Whilst this does introduce an additional needle puncture it creates a control point for the end of enzymatic activity. In doing so, any degeneration or restoration is a result of the mechanical protocol or a given treatment. The degenerate model consistently induces degeneration, therefore, to demonstrate the success of a treatment the bulk mechanical properties should show a difference between the degenerate and treated states (where the properties are altered towards the native), and no difference between the native and treated states.

3.4.1.2 Direct stiffness comparison (1,000 cycles) – Treated discs

Assessing the success of the treatments using actual data restricts the analysis to reviewing data at 1000 cycles. As shown in Figure 3.12 – Degenerate and treated state stiffnesses normalised to the native state stiffness for individual discs, split by group. Dashed lines are at 0, the native state and $\pm 10\%$ from the native., the 0.3 ml PEP:GAG group did not restore the stiffness from the degenerate state. This is primarily due to the low volume of hydrogel injected, indicating 0.3 ml is not enough of this hydrogel to restore the bulk disc properties for this level of degeneration. The 0.3 ml PEP:GAG group was only able to reduce the stiffness from the degenerate state on average (mean) by 3%. The 1 ml PEP:GAG group successfully restored the stiffness of the disc, by decreasing the stiffness from the degenerate by approximately 18%. The increased volume has enabled the hydrogel to influence the disc, triggered by either the peptide affecting the bulk stiffness, the increase in GAG content enabling more water to be absorbed, or both. As injecting to a set volume does not take into account anatomical differences or differing levels of degeneration from the enzymatic protocol, some variation and an outlier are present across the treated state for the group. These effects are also observed in the 1 ml SAL:GAG group, where the injection restored the stiffness of the disc from the degenerate state by approximately 15%. These similar results are thought to be a consequence to the higher volume injection, and the GAG imbibing the water as intended. A further issue that applies to the 1 ml groups discussed is that the data

compared is only at 1,000 cycles, meaning the injected material may not have fully dissipated from the tissue. By comparing the tissue at this early stage, the statistical testing may not be capturing the full effects of the injection. This is a limitation of the raw data from the study where 1,000 cycles were applied to the tissue in native and degenerate states to preserve the tissue prior to the final 20,000-cycle treated state test. Finally, the 1 ml SAL:SAL group showed differences between the native and treated states, as well as the degenerate and treated states (approximately 8% decrease in stiffness). The difference between the native and treated states is expected and was a result of the saline being expelled throughout the test. This also implies that for the first 1,000 cycles, the GAG and its ability to imbibe the water is the main contributor for the restorative effects.

3.4.2 Extrapolation modelling to 20,000 cycles

A further aim of this study was to assess whether the long-term behaviour of the disc can be predicted with short term test data. Two techniques were used, the first was linear regression which compared low cycle stiffness to the stiffness at 20,000 cycles, and the second was fitting mathematical functions to reduced data. As would be expected, for both techniques, as more data was used the prediction became better which is reflected by the reduction in the root mean squared error.

As shown in Table 3-8, the linear regression model using all the data found a root mean squared error below 15% at 100 cycles (0.5% of available data) which reduced to 10% at 2500 cycles (12.5% of available data). The error was attributed to natural tissue variation and the previously highlighted different specimen states. Given the potential natural variation, the errors observed are thought to be relatively low (Nerurkar et al., 2010). When looking at separate control groups, the root mean squared error was lower in all groups other than the 0.3 ml PEP:GAG group. The increased error was only present when using 100 cycles for the predictive analysis and was associated with gel-nucleus integration as the group demonstrated large changes in stiffness at low cycles. This early-stage variation in treatment groups is further reflected by the R-squared values (see Table 3-7). The control groups without a treatment (native, degenerate, and sham degenerate) all showed a strong relationship ($R\text{-squared} > 0.8$) within 1,000 cycles, whereas all the treated groups required more cycles to reach this point. One treated group, the 1 ml SAL:GAG group, demonstrated a similarly strong relationship as the non-treated groups, potentially implying that the GAG component enabled faster integration into the nucleus. A key drawback to using linear regression to predict the high cycle behaviour is that the groups have to complete the full cyclic testing (20,000 cycles).

All three mathematical models required more cycles compared to the linear regression model to achieve a root mean squared error of 10% or below. The fitted mathematical functions required at least 5000 cycles (25% of available data) to achieve a root mean squared error of 10%. The errors across all models were similar and the best overall for predicting the high cycle behaviour of the discs was the natural log function. The selected models may be too simple and a more developed model which breaks down the stiffness plots into separate sections could be more suitable. Although the method generates greater errors than the linear regression, it can be used to predict stiffness without needing either a large dataset,

Throughout the literature, other cyclic compression studies using bovine tissue apply a wide range of cycle counts, from fewer than 15 cycles (Périé et al., 2006; Alsup et al., 2017) to above 10,000 cycles (Mwale et al., 2008; Showalter et al., 2015). These studies generally assess mechanical properties based on the last set of cycles applied. Consequently, the outputs vary greatly from study to study. When using the loading protocol outlined in this study, an optimal window of test length exists where the bulk mechanical properties of the disc can be outlined with good accuracy. Although this study does not establish an upper limit on cycle number, based on the current dataset and aiming to reduce test time a suggested lower boundary of 1,000 cycles is recommended.

3.4.3 Application of extrapolation models

The linear regression predictive model was used to predict the 20,000-cycle data for the treated specimens based on the recorded 1,000 cycle data (stages 2 and 4 in Figure 3.1). This enabled comparison across states for the treated control groups at 20,000 cycles (predicted native and degenerate states, actual treated state) and the restorative effects of a treatment from the full accelerated protocol could be ascertained. In the 0.3 mL PEP:GAG and 1 mL SAL:SAL control groups, a wide range of statuses were observed with the only status not identified being over restored. These two control groups were not able to fully restore the mechanical properties of discs, which was attributed to the previously highlighted natural tissue variation, low volume injection, and expulsion of saline. The 1 mL PEP:GAG group presented restoration, over restoration, or damage which implies the treatment is having a clear restorative effect on the disc. The discs presenting over restoration or damage are thought to be a consequence of overfilling the disc. This highlights the importance of analysing the volume injected and for treatments that mimic the mechanical properties of the disc, finding an optimum individual to each disc. The 1 ml SAL:GAG control group predictive analysis yielded different results to the previous statistical analysis which showed no difference between the treated and native states at 1,000 cycles. The predictive analysis showed the discs were either not restored

or damaged. This implies that over the full length of the test discs in the group are damaged as the treatment is distributed or expelled from the disc. Although the results provide some indication of the behaviour of the treatments, there is still a wide spread in the outcome data within the groups as shown in Table 3-13. It may be possible to better distinguish between the groups by including adjusting the testing protocol. For example, by including a recovery period it may be possible to see greater differences between the GAG component treatments and the treatments that do not include GAGs. During the recovery period the treatments containing GAG components should imbibe more water back into the disc, recover more disc height, and show a reduced mechanical stiffness. A recovery period could be included into the test protocol without extending the length of by reducing the total number cycles applied to the disc. Overall, the high cycle predictive analysis reiterates the importance of investigating the high cycle behaviour and the injection volume.

3.5 Conclusions

This study has explored a sequential state methodology to evaluate injectable treatments for intervertebral discs. A rapid degenerate model has been successfully demonstrated against a sham procedure, and the degenerate model was used to analyse treatments. This degeneration method was found to be a repeatable technique which provides statistically significant differences from the native state over a short period of time enabling analysis of treatment and controls. By loading the treated specimens in a high cycle regime, this work has identified additional concerns with regards to treatment integration. Moreover, the analysis highlights the importance of injection volume and its relationship to restoration. Two mathematical prediction methods were applied to the data, and linear regression was identified as the best model to enable high cycle predictions and comparisons. Whilst some error is present, the high cycle comparisons revealed different outcomes to the 1,000 cycle data statistical analysis. These models enable comparison of mechanical behaviour at high cycles when using reduced datasets from shorter tests.

4 Injection parameter assessment in bovine tail intervertebral discs

4.1 Introduction

In previous studies, the amount of biomaterial injected for the nucleus augmentation procedure has been either to a fixed volume or based on the haptic judgement of the researcher (Schmitz et al., 2020). There has been little investigation to date on the effects of clinical variables such as the volume of injected material or the force required to deliver it. In a clinical setting, if the volume of biomaterial injected into the nucleus were too low, then there would be less restoration of disc height or biomechanical function, while too great a volume could potentially increase the risk of herniation, end-plate infraction, or over-pressurisation of the adjacent discs (Hebelka et al., 2014). The optimum volume to inject would likely be governed by the size, extracellular constituents, and degenerative state of the disc. An alternative may be to measure the mechanical resistance of the disc to filling, by monitoring the force required to deliver the biomaterial. Not only will the injection force be dependent on the state of the disc but also the fluid viscosity, the syringe, and the needle gauge and length. Whilst a force limit has not been directly investigated for injections into discs, other work identified a natural limit for manual injections at 64 N (Robinson et al., 2020).

This chapter contributes towards Objective 2 of the overall project and aims to investigate the relationship between clinically quantifiable measures of biomaterial delivery in nucleus augmentation, and the resulting mechanical performance of the augmented intervertebral disc.

4.2 Methods

4.2.1 Overview

This section builds upon methods described in Chapters 2 and 3 providing additional details where required. A total of 36 bone-disc-bone units were prepared in accordance with the methods outlined in Section 2.2.3. The discs were subjected to the previously described testing regime, where they were mechanically tested first in the native state, then following artificial degeneration, and finally following nucleus augmentation treatment. The artificial degeneration and general methods for the cyclic mechanical loading were carried out in accordance with the methods described in Sections 2.2.4 and 2.2.5. For all the tests reported in this Chapter, the cyclic loading was applied to specimens to 1,000 cycles for all disc states.

4.2.2 Treatment

The peptide and GAG components were prepared as per Section 2.2.1 and injected separately via two 25G needles into the centre of the nucleus pulposus, such that mixing and gelation occurred *in situ*. The injection was performed using a custom rig that connected two syringes in parallel to a syringe driver such that the syringes delivered both components at a constant rate. A transducer (B201-M, Flexiforce Sensor, TekScan, USA) was used to measure the force applied to the syringes ('injection force'). A 40 N axial compressive load was applied to the bone-disc-bone unit during injection, as shown in Figure 4.1.

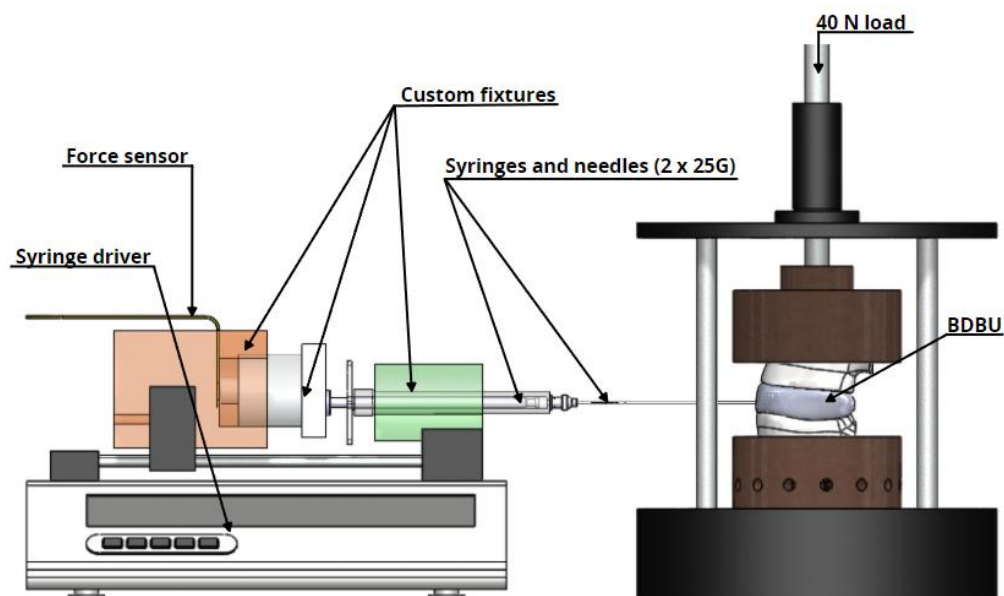


Figure 4.1 – Treatment injection fixture set up (not to scale), BDBU stands for bone-disc-bone unit

Injections were stopped when a predetermined load was reached or the syringes were empty. Three parameters relating to the injection were measured during testing: the pre and post injection bone-disc-bone unit height with a pair of Vernier callipers, the maximum injection force using the force sensor, and the volume injected using standard syringe markings. A preliminary study demonstrated that air microbubbles could be created post-injection, and tended to coalesce, as identified on radiographic analysis. To reduce the likelihood of microbubble formation, an additional step was added before treatment injection where the peptide and GAG components were sonicated using benchtop sonicator in the syringe for up to one minute.

4.2.3 Data Analysis

Specimens were excluded from the analysis if any of the following occurred: presented little or no mechanical response to the degeneration procedure, injections were not into the nucleus, or observable air microbubbles that coalesced post injection were identified on follow up radiographic analysis. As in the analysis in Chapter 3, the stiffness of each individual loading cycle was extracted and the specimen stiffness in each state was, defined as the mean stiffness from cycles 990 to 1,000, was extracted for comparison.

Statistical analysis was performed in accordance with Section 2.2.6.

To evaluate the effects of the volume of biomaterial injected, and the force of injection, the specimens were subdivided into groups. The specimens were first divided into three groups according to the total volume of biomaterial injected (low < 0.85 mL, 0.85 mL < medium < 1.25 mL, high > 1.25 mL). Paired comparison of the native and treated states was then performed on the individual groups. The specimens were then divided according to the injection force (low < 30 N, 30 N < medium < 40 N, high > 40 N) and the statistical analysis repeated.

The transverse plane cross sectional area of each disc was estimated using the CT radiographs. Estimates for the transverse plane cross sectional area were made by manual finding the best fit using the oval or polygon selections tool in ImageJ. The mechanical restoration was evaluated against the six parameters that were measurable or could be calculable in clinic using linear regressions: volume injected, volume injected/disc cross-sectional area, injection force, injection force/disc cross-sectional area, work done (integral of injection force-time plot), and change in bone-disc-bone unit height following injection (post injection height minus pre injection height).

4.3 Results

A total of 22 from the 36 specimens were successfully tested and met all criteria for analysis. A breakdown of the failed criteria for the 14 excluded specimens is shown in Table 4-1 and example images for minimal mechanical response to the degenerate procedure, injection going into the annulus, and coalesced microbubbles are shown in Figure 4.2 A, B, and C respectively.

Table 4-1 – Criteria and number of eliminated specimens.

Failure criteria	Number of specimens
Experimental error	4
Minimal response to degenerate procedure	2
Injection into annulus	1
Coalesced microbubbles	7

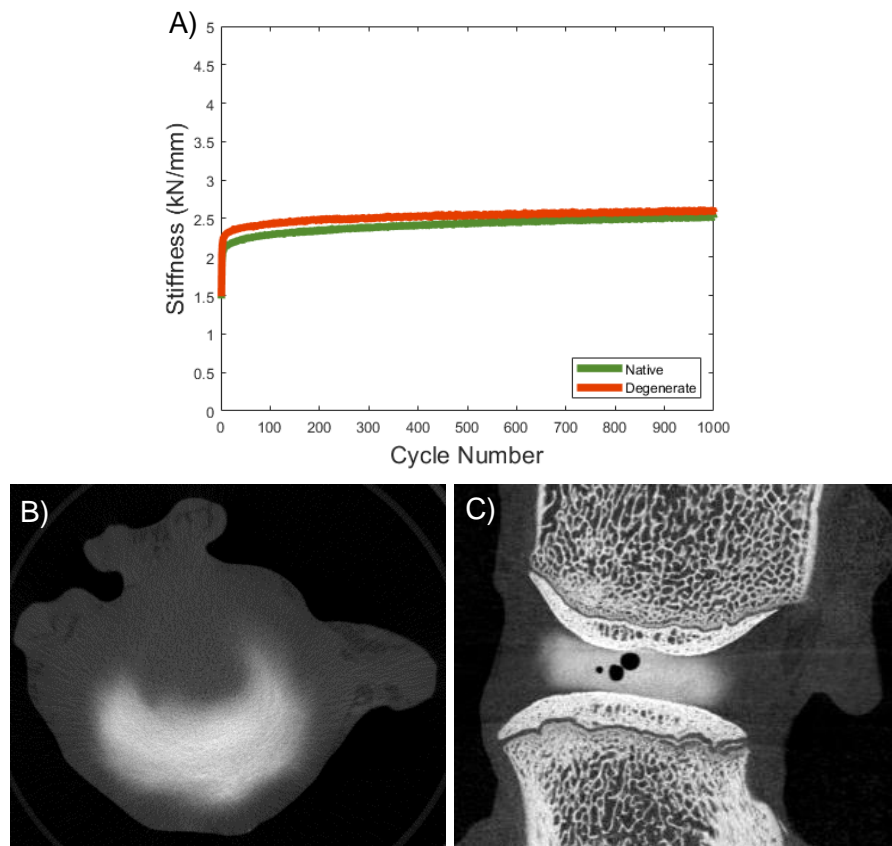


Figure 4.2 – Example images from eliminated specimens A) No response to degeneration procedure native and degenerate stiffness profiles, B) Transverse profile of disc where injection was into the annulus CT image, C) Lateral profile of disc where coalesced microbubbles were identified

During the nucleus augmentation procedure, there was an initial ramp in the injection force, followed by a period where force remained relatively steady before it rose more steeply. An example showing these three phases is shown in Figure 4.3.

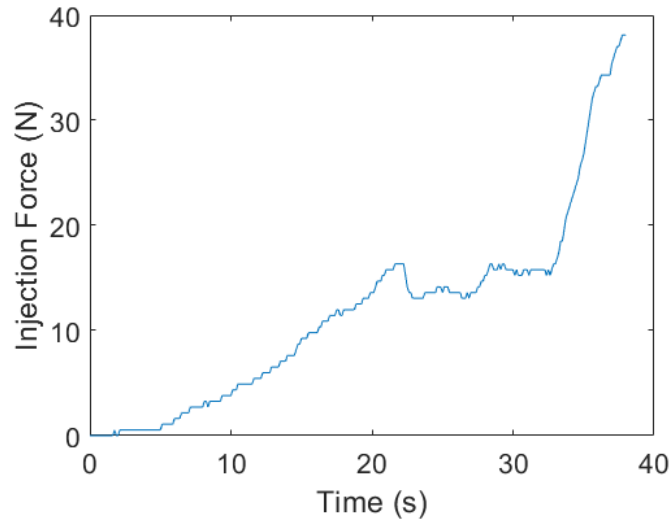


Figure 4.3 – Example typical injection force plot

The mechanical behaviour was similar to that observed in the previous chapter. The stiffness increased throughout the duration of the cyclic loading and the stiffness in the degenerated state was higher than in the native state for each specimen. No disruptions to the smooth stiffness-cycle profiles were identified in any specimen across the 1,000 cycles for each test. Typical profiles for the stiffness of a specimen across the three states are shown in Figure 4.4; the stiffness for all specimens in each state is shown in Figure 4.5.

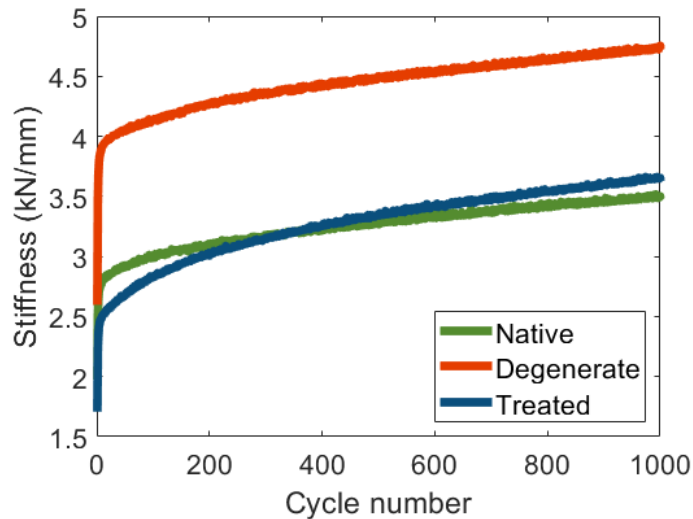


Figure 4.4 - Typical stiffness plot for different states

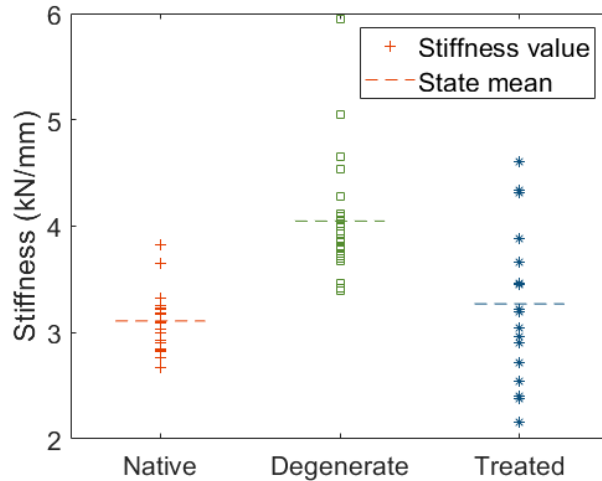


Figure 4.5 - Comparison of stiffness in different states for all specimen

The mean decrease in stiffness from the degenerate state to the native state was 28% for all the data. The mean decrease in stiffness in the low, medium, and high volume groups were 2%, 26% and 28% respectively. The mean decrease in stiffness in the low, medium, and high force groups were 17%, 16% and 24% respectively.

Shapiro-Wilk tests followed up by either repeated measures ANOVA with paired t tests or Friedmann tests with Wilcoxon sign rank tests were applied to the data. A summary of the normality tests and the selected follow up tests is shown in Table 4-2.

Table 4-2 - Shapiro-Wilk normality test p values and selected test for statistical comparison. All statistically significant results are highlighted in blue.

Shapiro-wilk test p values				
Group	Native state	Degenerate state	Treated state	Test used for comparison
All data	0.17	0.00	0.05	Friedman with Wilcoxon sign rank test
Low force	0.87	0.01	0.84	Friedman with Wilcoxon sign rank test
Medium force	0.44	0.01	0.36	Friedman with Wilcoxon sign rank test
High force	0.09	0.25	0.96	Repeated measure ANOVA with paired t-test
Low volume	0.11	0.09	0.41	Repeated measure ANOVA with paired t-test
Medium volume	0.03	0.00	0.67	Friedman with Wilcoxon sign rank test
High volume	0.02	0.26	0.87	Friedman with Wilcoxon sign rank test

The results of the statistical comparison for the different treatment groups is shown in Table 4-3

Table 4-3 — p values for the repeated measures ANOVA and follow up paired t-tests with Bonferroni correction for the different treatment groups. All statistically significant results are highlighted in blue.

Group	Friedmann or repeated measures ANOVA	Native to Treated - Wilcoxon sign rank or paired t test	Degenerate to Treated - Wilcoxon sign rank or paired t test
All data	<1E-05	0.78	6.68E-04
Low force	0.1	0.48	0.64
Medium force	0.04	0.74	0.126
High force	1.40E	0.06	1.51E-04
Low volume	2.80E-04	0.3	0.7353
Medium volume	4.00E-03	0.09	0.02
High volume	1.60E-03	0.07	3.86E-04

The stiffness ratio for the degenerate and treated states with respect to the native state is shown in Figure 4.6A. Mechanical restoration, the ratio of the native state stiffness to the treated state stiffness, was compared against parameters of interest, an example is shown in Figure 4.6B. The R-squared and p values for linear regressions for all parameters are shown in Table 4-4.

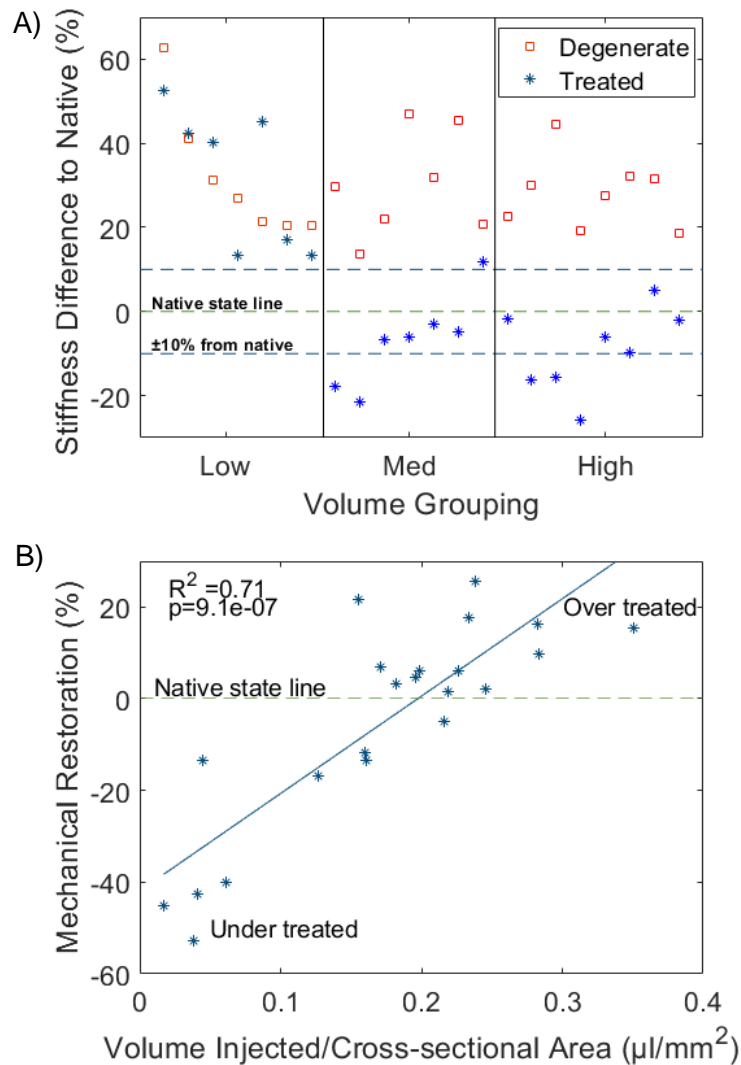


Figure 4.6 - A) Summary of stiffness differences compared to native state for low, medium, and high-volume specimens, B) Linear regression relationship between mechanical restoration, the ratio between the native state stiffness and the treated state stiffness, and volume injected/cross sectional area

Table 4-4 – Relationship (linear regression) between parameters and treatment stiffness mechanical restoration

Parameter	R-squared	P value
Volume injected (ml)	0.63	1.20E-05
Volume injected/Cross sectional area (µl/mm ²)	0.71	9.10E-07
Max Injection force (N)	0.23	0.02
Max Injection force/cross sectional area (N/mm ²)	0.28	0.01
Work done (J)	0.31	0.01
Change in height (pre injection – post injection) (mm)	0.79	3.60E-08

Although there was a weak relationship between the force related parameters and stiffness restoration, a cut-off point was identified where the disc was over treated. The cut off points were 55 N, 0.1 N/mm², and 3500 j injection force, normalised injection force and work done respectively. The linear regression for the injection force with a proposed cut off region is shown in Figure 4.7.

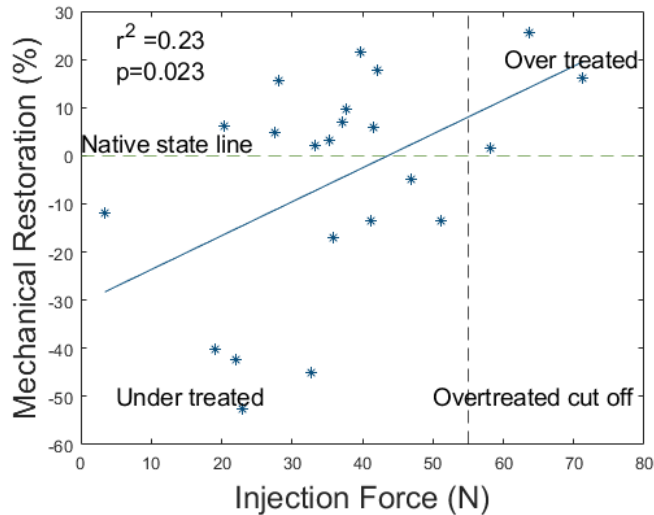


Figure 4.7 – Linear regression relationship between mechanical restoration, the ratio between the native state stiffness and the treated state stiffness, and injection force with a proposed cut off region.

4.4 Discussion

The objective of this work was to assess the use of clinically relevant quantitative measures for injection of restorative intervertebral disc injectable treatments. Three key variables were measured: the volume injected, the injection force, and the change in disc height from injection. The results of this study showed that the treatment could restore biomechanics, with no statistically significant difference across all the data between the native and treated states.

Unlike in the mechanical testing in Chapter 3, no disruptions to the smooth stiffness vs. cycle number profiles were identified in any state. In Chapter 3, the large disruptions seen in the treated state profiles were associated with hydrogel disruption during testing. It was thought that because the injection was performed under load, some of the hydrogel distribution occurred during injection rather than during testing. The small disruptions reported in Chapter 3 were associated with joint space narrowing causing bone on bone contact or lateral deformation. This was not observed during the testing because of the reduced number of cycles used (1,000 cycles instead of 20,000 cycles).

When divided into the subsets based on the volume injected or the applied force, a minimum volume was required to achieve mechanical restoration (Figure 4.6A). The amount of restoration observed in the medium and high volume groups (~25%) was higher than that observed in other similar studies where an increase of ~12% was found (Malhotra et al., 2012; Varma et al., 2018). The differences in the amount of stiffness increase was attributed to different injection volumes where one study injected up to 0.35 mL into ovine discs (Malhotra et al., 2012), and the other up to 0.75 mL into bovine discs (Varma et al., 2018). The statistical testing showed differences between

degenerate state and treated state in the low and high-volume groups. This highlights that volume injected is likely an important variable when assessing mechanical restoration. On top of this, it was found that the volume of biomaterial injected, the volume normalised by disc cross-sectional area, and change in disc height from injection, provided good indicators of the level of mechanical restoration of disc biomechanical properties. The strongest relationship identified was with the change in disc height pre and post injection, which is unsurprising given the relationship between height and stiffness. Overall, the relationship between these direct measurements and the level of stiffness restoration was much better than for the measurements derived from the applied injection force.

Clinically, these measurements may be readily implemented. Volume can be monitored on syringes and change in disc height may be approximated with fluoroscopy during surgery. The volume of injected biomaterial normalised by the disc cross-sectional area was better correlated to the mechanical restoration than the volume alone. The curved nature of the endplates meant the consistent measures of disc height were more difficult to derive from the CT data, so only the disc cross-sectional area rather than the disc volume was used to normalise the injection volume. Clinically, there would be potential to better estimate all of the disc dimensions from additional magnetic resonance imaging (Deneuille et al., 2021).

The injection force was monitored as a parameter to provide a quantitative measure of the haptic feedback used clinically to determine intradiscal pressure. As the hydrogel is injected into the disc, the expansion of the nucleus will be resisted by the tensioning of the annulus tissues and the intradiscal pressure will increase. The force required to inject the biomaterial was therefore expected to increase during the delivery (Panjabi et al., 1988; Cannella et al., 2014). This study found that the injection force initially increased to a steady value, which was maintained for a period before finally rising steeply. In the *in vitro* model used here, the artificial degeneration of the disc is thought to be caused by a loss of GAG and fluid content in the nucleus; there is therefore little resistance to the injection initially as the disc 'refills'. It is only once the annulus becomes tensioned that the force rises more steeply. Whilst the maximum injection force would, in theory, be a good indicator of fill, all measures associated with injection force poorly correlated with the mechanical restoration of biomechanical function. It is likely that *in vivo*, the progressive degeneration of the disc and remodelling of the surrounding tissues would provide greater resistance to injection in the initial stages, and the injection force would be more difficult to interpret. Therefore, injection force alone does not appear to provide sufficient data to be used as a clinical measurement tool during nucleus augmentation.

Nevertheless, when used in conjunction with the directly measured volume and height parameters, injection force could still provide a meaningful upper limit measurement.

In clinic, these relationships could be beneficial and may act as a guide for the operating surgeon. It may be possible to provide a surgeon with a series of recommended volumes based on the degeneration level and the size of the disc. Based on the degeneration model used in this study, a volume of approximately 1 mL provides the closest restoration to the native state. Whilst the force relationship was weaker than the volume relationship, an upper force value of between 50 and 60 N appears to be a good indicator of overfilling. The direct monitoring of intradiscal pressure could be an alternative to the injection force measured in this study. However, this would require a pressure transducer to be inserted into the disc. The hydrogels in this study were designed specifically to be delivered down fine bore needles to avoid the risk of annular damage that could further the degenerative process (Elliott et al., 2008; Wang et al., 2021). The inclusion of a pressure transducer would require either an additional needle or a wider diameter needle to accommodate the sensor, and so was not considered in this study.

In this study, the biomaterial used for the nucleus augmentation was a previously developed peptide-GAG hybrid hydrogel (Miles et al., 2016; Warren et al., 2021). The hydrogel used in this project is able to mimic the healthy nucleus tissue's ability to imbibe water (Miles et al., 2016; Warren et al., 2021). By having a similar GAG composition to the native nucleus, and a hydrogel with a high water content, the aim was that the natural balance between the load and osmotic pressure would reduce risks associated with overfilling. It should, therefore, be noted that while the results of this study are applicable to other nucleus augmentation materials, the ranges of the measured injection parameters likely depend on the biomaterial used and its properties. It is likely that materials with different osmotic potential, gelation mechanisms or mechanical properties could result in different biomechanical outcomes for a given injected volume. The needle gauge and length used for injection will also affect the applied forces. Although the relationships between injection parameters and resultant biomechanical performance may be unique to a given material, the parameters and techniques developed in this work could readily be applied to other biomaterials.

4.5 Conclusion

This research clearly demonstrates that mechanical restorative outcomes for nucleus augmentation vary with injection parameters. Specifically, the maximum force required to inject the hydrogel has a weak relationship with mechanical restoration but could

provide upper and lower limits for injection. Whereas the volume injected and change in height from injection have strong relationships with mechanical restoration and could be used to predict outcomes.

5 Application and adaptation of methods for human spinal tissue

5.1 Introduction

In this chapter, an initial study is described where the methods in Chapters 4 and 5 are adapted for human tissue testing. As discussed in Section 1.5.4, bovine intervertebral discs can be a good model for human discs, but human discs are different in morphology and have naturally occurring degeneration. This chapter addresses Objective 3, which was to adapt the developed animal tissue testing for use with human tissue. The work presented in this chapter begins with preliminary testing which evaluated how effectively the bovine methodology could be directly applied to human discs. The chapter then presents an altered test method based on the outcomes of the preliminary testing.

5.2 General Methods

The two sets of testing reported in this chapter, preliminary testing and the main study, share methods. The general methods section outlines the shared techniques used.

5.2.1 Donor spine selection

After ethical approval (Yorkshire & The Humber - Sheffield Research Ethics Committee, REC reference: 15/YH/0096, IRAS ID: 170894) a list of available donor spines from Leeds GIFT 2 Research Project through St James's University Hospital, Leeds, were assessed based on donor medical history. Three spine segments were available for use in this study, the details of the specimens is shown in Table 5-1.

Table 5-1 -Donor details and segment lengths of selected segments for the study

Spine number	Donor age	Segment details
1	97	T6 to T12
2	81	T11 to S1
3	47	T11 to S1

The lumbar region of Spine 1 had been used in a previous study (Norbertczak, 2019) and had undergone four freeze-thaw cycles. This spine segment was known to have spinal pathology in the form of advanced diffused idiopathic skeletal hyperostosis. Diffused idiopathic skeletal hyperostosis is an arthritic condition where the tendons and ligaments of the spine become calcified. To maximise the use of this previously used tissue, Spine 1 was used to for initial test method transfer and preliminary testing.

5.2.2 Human tissue handling

All human tissue used in this project was handled with care and respect and in accordance with the Human Tissue Act 2004. Samples were tracked using unique codes in an electronic tracking system (Achiever, Interactive Software, UK). The tracking system recorded history of storage locations and transfers for tissue.

5.2.3 Imaging of spines

All spines were scanned using MRI by Dr. Nagitha Wijayathunga. Prior to the day of the MRI scan, spines were taken out of the storage freezer and defrosted overnight at 4°C. Imaging was performed using a Siemens Magnetom Verio 3T scanner (Siemens Healthineers, USA). Three high quality sequences were used (spin echo, 3D-SPACE and T1-VIBE) that had been optimised previously for the analysis of cadaveric spinal tissue (Wijayathunga et al., 2019).

From the images, any observed spinal pathology was identified and individual discs were graded in accordance with the Pfirrmann classification (Pfirrmann et al., 2001) by

Dr. Nagitha Wijayathunga. The Pfirrmann score of the scanned discs is shown in Table 5-2.

Table 5-2 - Specimens used in testing and degeneration levels.

Spine	Unit	Pfirrmann score
Spine 1	T6-T7	IV
	T7-T8	IV
	T9-T10	IV
	T10-T11	IV
	T11-T12	IV
Spine 2	T11-T12	III
	T12-L1	III
	L2-L3	III
	L3-L4	III
	L4-L5	III
Spine 3	T11-T12	IV
	T12-L1	III
	L1-L2	III
	L2-L3	III
	L3-L4	IV
	L4-L5	III

5.2.4 Bone-disc-bone unit preparation

On the day of the MRI scan, spinal segments were dissected to bone-disc-bone units in a similar manner to the method outlined in Chapter 2. First, surrounding soft tissue and fat were carefully removed from the spine segment. Posterior processes were removed by cutting through the pedicles with an oscillating saw. After the dissection, transverse cuts were made through the centre of the vertebrae with an oscillating saw, using the MRI imaging data for reference. This resulted in bone-disc-bone units as shown Figure 5.1.

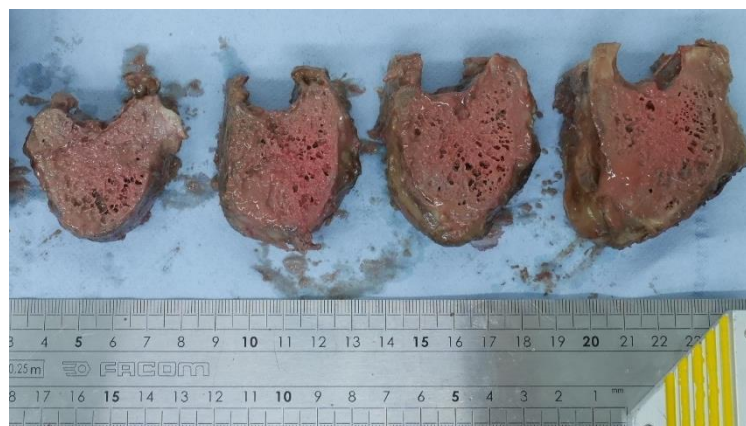


Figure 5.1 - Prepared bone-disc-bone units prior to the being cleaned with the water pik.

Once the bone-disc-bone units were separated, the bone was cleaned using a surgical Water Pik (Pulsavac Plus Wound Debridement System, Zimmer Biomet, USA). Once cleaned, the discs were soaked in sodium citrate for 24 hours in sealed polymer bags at 4°C. After the soak period was completed, the specimens were drained, rinsed with PBS, sealed in plastic bags once again and frozen in a -20°C freezer until the day of testing.

5.3 Method Development

5.3.1 Introduction

This section describes how the developed methodology for bovine specimens reported in Chapters 3 and 4 was initially to human tissue to develop the human tissue testing method.

5.3.2 Methods

Four bone-disc-bone units were used for the method development, three bone-disc-bone units from Spine 1 (T9-T10, T10-T11, and T11-T12) which were Pfirrmann grade IV with skeletal hyperostosis, and one specimen from Spine 2 (L1-L2) Pfirrmann grade III. The methods were iterated from one specimen to the next based on the outcomes of the testing.

5.3.2.1 Hold period in testing machine - Spine 1 T10-T11, Spine 1 T11-T12

The first two specimens, Spine 1 T10-T11 and Spine 1 T11-T12 were tested in the material testing machine for a 24-hour hold period at 0.1 MPa (77 to 85 N) followed by 20,000 cycles of compressive loading at 1.1 MPa (851 to 933 N) to 2.4 MPa (1779 to 1950 N) intradiscal pressure. Intradiscal pressure was calculated as for the bovine loads, by multiplying cross section area with the target intradiscal pressure and a correction factor. For the bovine tissue load calculation, a mean cross sectional area was used for all specimens, whereas for the human tissue a cross sectional area was calculated for each specimen and used to calculate the loads. After cyclic loading the specimens were CT scanned using the same protocol as the bovine specimens and placed in a -20°C freezer.

5.3.2.2 Hold period in PBS bath – Spine 1 T9-T10, Spine 2 L1-L2

For the remaining two specimens, the 24-hour hold period for Spine 1 T9-T10 and Spine 2 L1-L2 was completed outside the materials testing machine in a fluid bath under an 80 N load (~0.1 MPa intradiscal pressure). In these cases, as in the bovine tissue testing, the cyclic loading was prefaced with a 30-minute hold period in the materials testing machine. All mechanical testing was carried out in treated PBS held at 37°C. After

mechanical testing in the native state, specimens were CT scanned using the previously outlined protocol (See Section 2.2.3).

5.3.3 Results

5.3.3.1 Hold period in testing machine - Spine 1 T10-T11, Spine 1 T11-T12

The 24-hour hold period in the material test machine showed a reduction in specimen height for the duration of the test. The change in height over a one hour period was reduced to below 0.1 mm for both specimens after approximately 4 hours. During 24-hour hold period for Spine 1 T11-12, a data logger error occurred at approximately 10 hours into the test. The loading was not removed but the data capture was stopped for this time. When the error was found the test was resumed so the cyclic loading portion of the test could be completed. The change in disc height for the two specimens is shown in Figure 5.2.

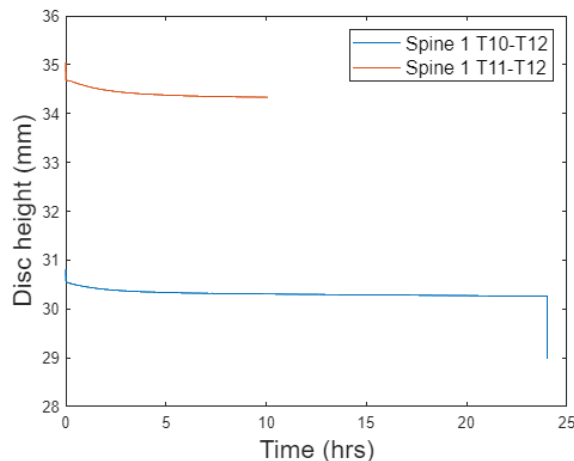


Figure 5.2 - Change in disc height during the 24-hour hold period for the first two specimens

The cyclic loading for the first bone-disc-bone unit (Spine 1 T10-T11), the incorrect cyclic loading was applied. Instead of the corrected load for the human tissue, the bovine loads were applied to the disc. This was a machine set up error where only the cyclic amplitude was changed but not the control loop target loads. The machine applies the cyclic amplitude with the aim of reaching the target loads. It then uses a control loop to reduce the amplitude based on the stiffness of the specimen to ensure the target loads are attained. For this specimen, the cyclic testing continued to 20,000 cycles at the bovine loads. The stiffness for these cycles was calculated and is shown in Figure 5.3.

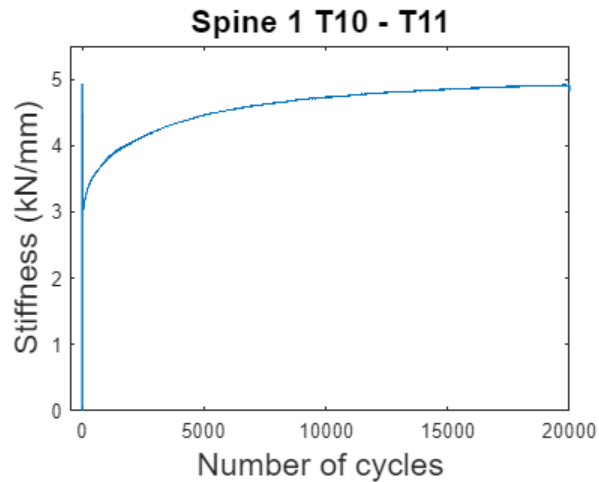


Figure 5.3 - The stiffness for Spine 1 T10-T11 throughout the duration of the test. The incorrect load control loop targets was applied to the specimen. The initial overshoot from the targets from the increase amplitude can be seen at the start of the test.

For the second specimen, Spine 1 T11-T12, the testing was resumed after the datalogger failure, the cyclic loading was commenced. However, due to one of the control loop target loads being in tension rather than compression, the cyclic testing failed and the testing was stopped. As the error was not immediately clear on the day of test, the testing was stopped for this specimen.

5.3.3.2 Hold period in PBS bath – Spine 1 T9-T10, Spine 2 L1-L2

The testing was corrected for the remaining two bone-disc-bone units which completed the 24-hour hold period in a separate PBS bath. Spine 1 T9-T10 completed the 20,000-cycle test. During testing of Spine 2 L1-L2, the test stopped at 1,911 cycles due to the metal fixtures making contact. Stiffness was evaluated for the two specimens that completed cyclic testing at the correct loading, Figure 5.4 shows the stiffness for these specimens.

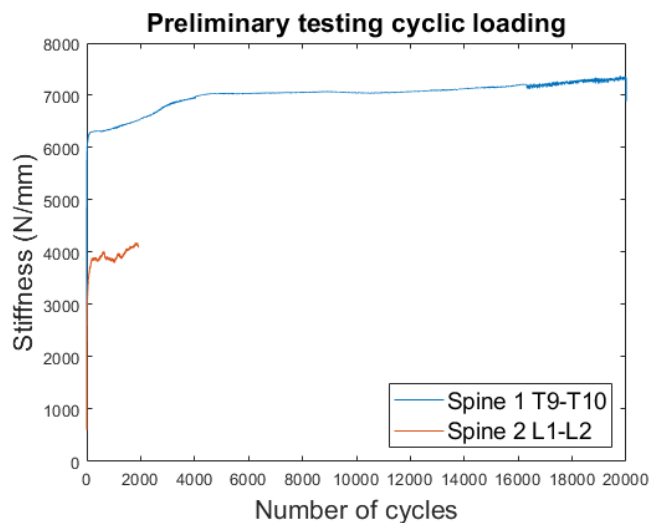


Figure 5.4 – Stiffness profiles for two bone-disc-bone units that completed correct loading

The bridging bone, from the advanced diffused idiopathic skeletal hyperostosis, in the Spine 1 specimen cracked over the duration of the test. An end plate fissure, where the soft tissue had ruptured through the end plate, was identified for the disc from Spine 2. Pre and post test coronal μ CT slices from both discs are shown in Figure 5.5.

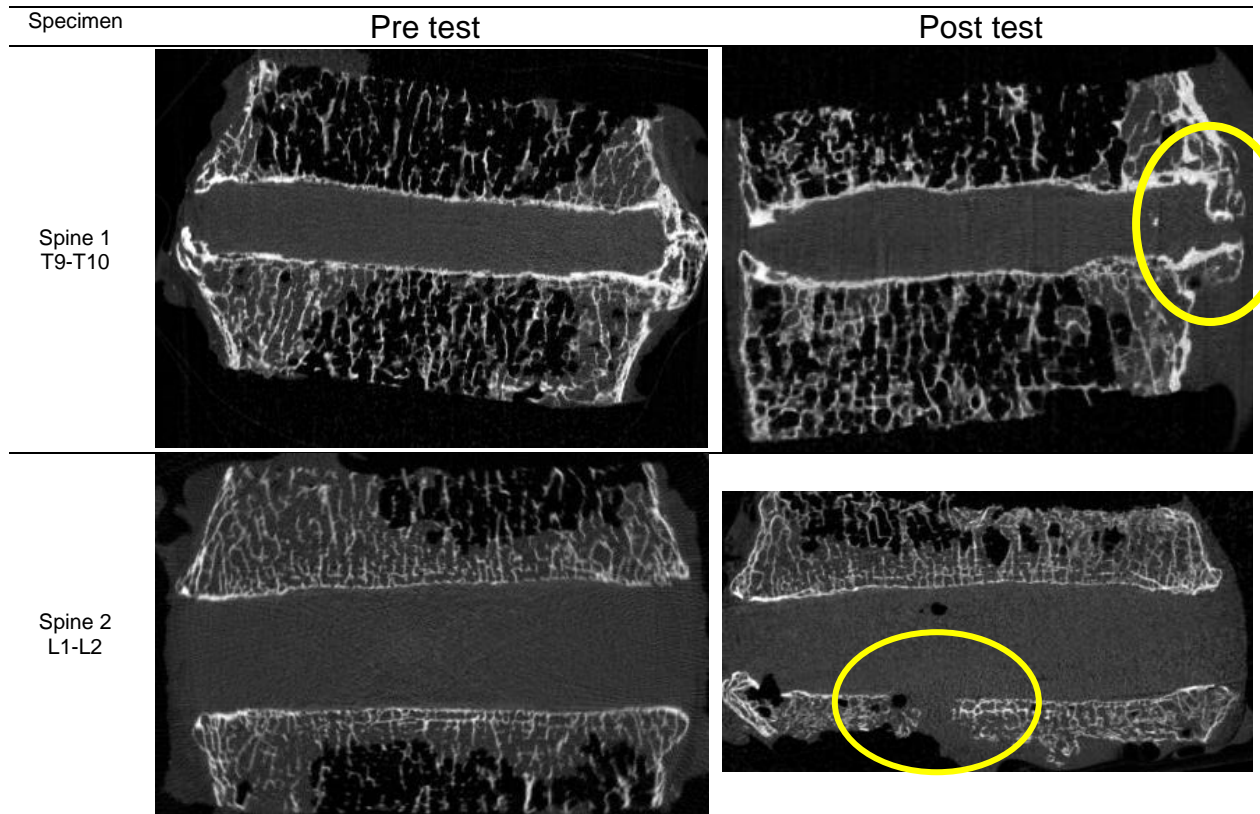


Figure 5.5 – CT scan pre and post test screenshots with bone damage circled

5.3.3.3 Summary

A summary of the test outcomes identified in the preliminary testing is shown in Table 5-3.

Table 5-3 - Summary of preliminary testing hold location and test notes

Spine	Unit	Test notes
Spine 1	T9-T10	Damage to bone from cyclic testing
	T10-T11	Incorrect loading profiles – bovine loading applied
	T11-T12	Data logger failure during 24-hour hold Cyclic loading fail as attempted to apply tension load
Spine 2	L1-L2	Damage to bone from cyclic testing

5.3.4 Method development conclusion and recommendations

An important result from the two specimens tested in the mechanical testing machine, was that the change in disc height during the hold reduced to below 0.1 mm for both

specimens after approximately 4 hours. The 24-hour hold identified in the bovine testing appears to be suitable for the human tissue testing as well and will account for variation across specimens.

The two specimens which were tested at the correct cyclic loading resulted in damage to the vertebral bone. This was thought to have two main contributing factors: the magnitude of the load was too high, and the bone density was too low. When comparing the two discs, it is likely that the calcified soft tissues were able to better support the disc from Spine 1, enabling it to complete the full test.

Overall, the test development identified it is not possible to apply the high loading used in the bovine testing. Future testing will need to reduce the magnitude of the loading and provide some reinforcement to the bone to prevent endplate collapse.

5.4 Methods

5.4.1 Overview

Based on the method development a test method was developed to evaluate the discs in the native state, treat the discs, and evaluate them in the treated state. The methodology is summarised in Figure 5.6 and is expanded upon in this section. No artificial degeneration was used in this human tissue testing as the tissue presented natural degeneration. A total of 11 bone-disc-bone units from Spines 2 and 3 were prepared for testing between T11 to L5 (most cranial unit: T11-T12, most caudal unit: L4-L5). The Pfirrmann scores for all discs can be found in Table 5-2.

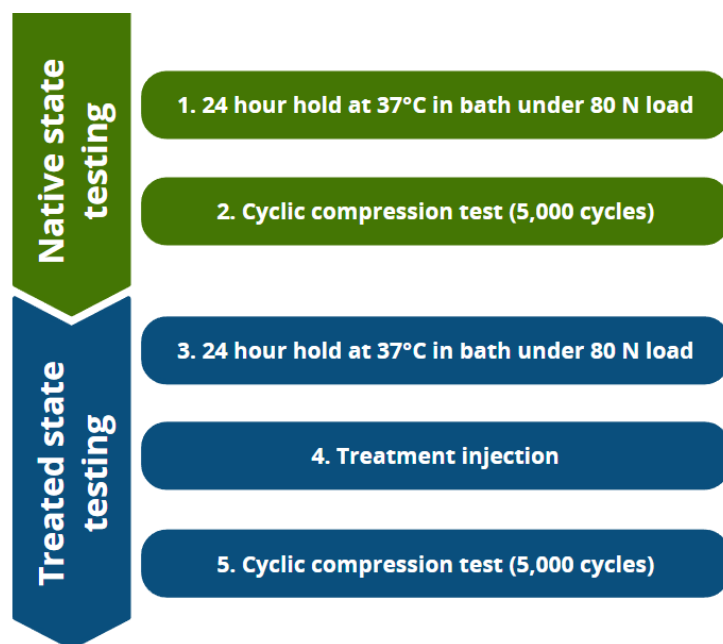


Figure 5.6 - Flow chart with details of testing completed

5.4.2 Additional bone-disc-bone unit preparation

Specimens used in this study were first prepared in accordance with the method described in Section 2.2.3. Once prepared and prior to starting the 24-hour hold period, specimens were pressed approximately 5 mm into a 10mm thick mantle of PMMA cement on both the cranial and caudal side. This was done to reinforce the bone because in the development testing the bone was found to fracture when loaded against the platens. Adding cement mantles to either side of the bone-disc-bone unit will affect the mechanics of the disc as it can limit the fluid flow through the bone and end plates. This was seen as a necessary compromise to ensure the mechanical behaviour observed during testing was from the disc and not a result of bone deformation.

5.4.3 Step 1, 2, 3, & 5: Biomechanical testing

The biomechanical testing steps were based on the bovine testing and the preliminary testing. Testing began with a 24-hour hold period under an 80 N compressive load in a treated PBS bath (steps 1 and 3, see Figure 5.6). This load was selected because it was close to the ideal 0.1 MPa intradiscal pressure (between 76 N and 139 N) and was the maximum capacity of the rig. The applied 80 N load was below the 0.1 MPa intradiscal pressure for some specimens

At the start of the mechanical loading (steps 2 and 5, see Figure 5.6), the specimens underwent a 30-minute hold period at the calculated force for 0.1 MPa intradiscal pressure. As with other testing carried out in this project, this was done to compensate for any fluid loss during transfer to the testing machine. After the hold period, compressive sinusoidal cycles were applied to the sample between 0.5 and 1.1 MPa intradiscal pressure at 1 Hz for 5,000 cycles. The loads were lowered from the preliminary testing based to reflect different physiological activities. Loads were calculated from the cross-sectional area measurement of each disc and the range of loads and representative activities are shown in Table 5-4. The frequency of loading remained the same, at 1 Hz. The number of cycles was selected based on analysis in Chapters 3 and 4, where stiffness disruptions were mainly observed before 5,000 cycles.

Table 5-4 - Summary of loads applied during testing with the intradiscal pressure/activities the load represents based on (Nachemson, 1981; Wilke et al., 1999; Dreischarf et al., 2015)

Protocol stage	Representative Activity	Intradiscal pressure (MPa)	Load range (N)
Hold period	lying in supine position	0.1	76 - 139
Upper limit	unsupported sitting, standing flexing forwards, holding a 20 kg weight close to the body	1.1	1016 - 1532
Lower limit	Relaxed standing, walking barefoot (lower load), climbing stairs (lower load)	0.5	462 - 696

5.4.4 Step 4: Treatment

The treatment (step 4, see Figure 5.6) was carried out in the same manner as Chapter 4 where discs were injected using a syringe driver under a load whilst injection force was monitored. The general set up can be seen in Figure 4.1, Section 4.2.2. Injection was stopped based on one of three criteria: the end of the syringe was reached (1.6 ml), a force based stop criteria was reached, or a leak was observed on the disc. The force based stop criteria were either that the injection force exceeded 65 N (based limit of manual injection proposed by Robinson et al., 2020) or multiple consecutive slips occurred on the syringe driver. Bone-disc-bone unit height was measured pre and post injection using a pair of vernier callipers. The T11-T12 bone-disc-bone unit for each spine was used as a control specimen and was not treated. The control specimens were therefore, cyclically tested twice without treatment.

5.4.5 Data analysis

Change in specimen height, hysteresis and mechanical stiffness were defined and examined using the same methods as described in Chapter 3. The injection parameters (maximum force, volume injected, and change in disc height from injection) were recorded and assessed with respect to the stiffness values.

5.5 Results

For all specimens the bone-disc-bone unit height decreased throughout the duration of the test. An example plot of the decrease in height is shown in Figure 5.7.

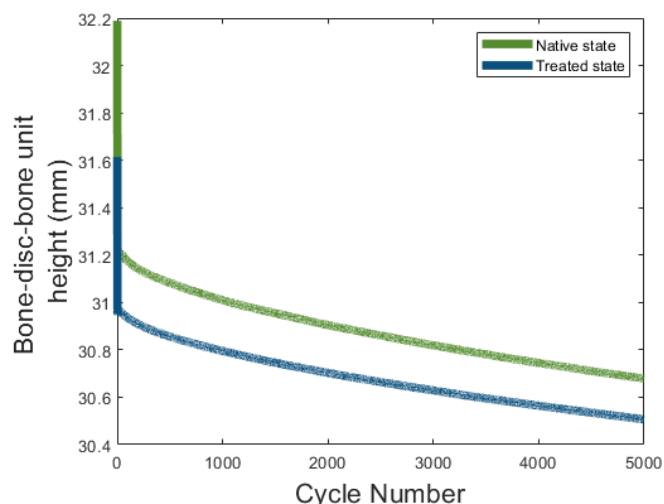


Figure 5.7 - Example of decreasing specimen height throughout duration of test, data taken from specimen Spine 2 T11-T12

The change in height over the duration of the test was dependent on the state. A summary of the change in height for each specimen is shown in Figure 5.8. The greatest change in bone-disc-bone unit height from the start to the end of the test was in the treated state specimens at 4 mm. The smallest change was in the native state, with 1.1 mm. Statistical analysis was applied to the change in height and no statistically significant difference was found between the two groups ($p=0.31$).

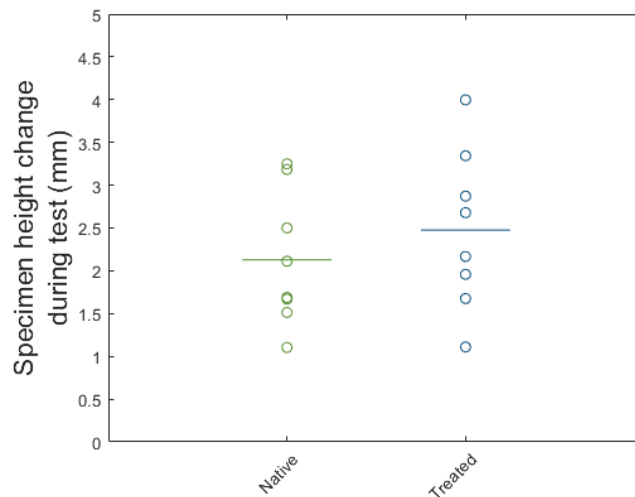


Figure 5.8 - Summary of the change in height for specimens in the native and treated states

Hysteresis was calculated for each cycle and was found to decrease rapidly at the beginning of the test then remain low for the rest of the test. An example plot of the hysteresis behaviour is shown in Figure 5.9. The change in hysteresis between cycles was found to change by less than 0.5% in all specimens for both native and treated states after 32 cycles.

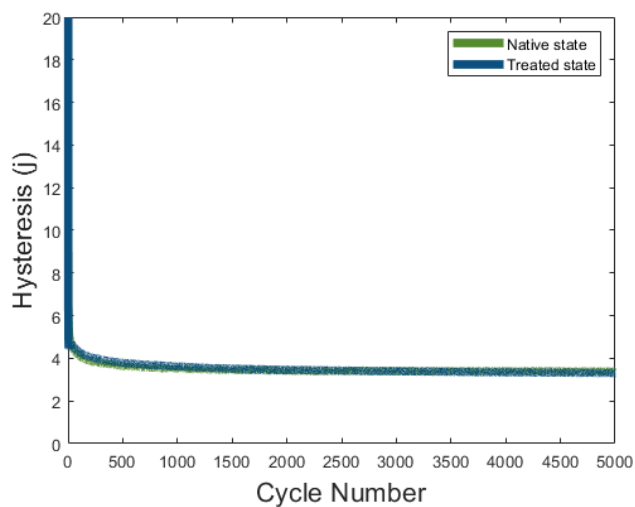


Figure 5.9 - Example of a typical change in hysteresis across the duration of the test, data taken from specimen spine 2 T11-T12

The general mechanical behaviour observed was similar to that observed in bovine tissue, where the stiffness of the disc increased over the duration of the test. A typical example stiffness change over the duration of the test is shown in Figure 5.10.

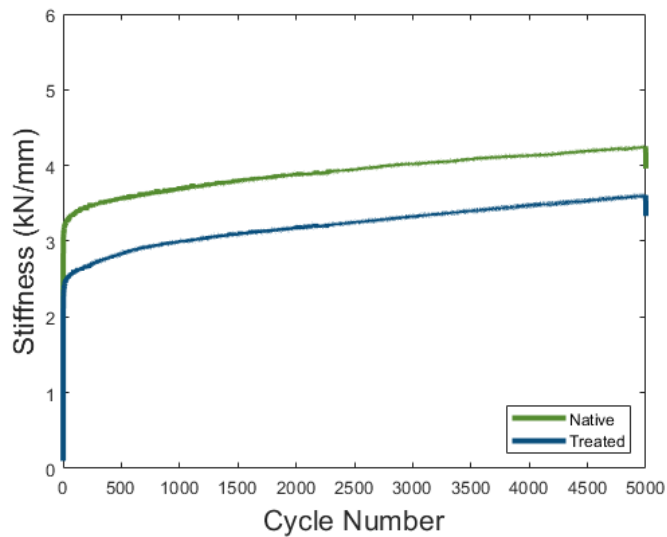


Figure 5.10 – Example typical change in stiffness over length of test from Spine 3 T12 to L1

All but two tests followed the smooth typical profile shown in the figure. The treated state test for Spine 2 T12-L1 showed a drop in stiffness that gradually recovered over approximately 500 cycles as shown in Figure 5.11A. The cause of this was a manual error where the disc was not placed flush in the fixture with the cement mantle at an angle. This caused a sudden drop in height as the cement flattened against the fixture mid test. The other specimen was Spine 2 L4-L5 which had a sudden drop at cycle 3,531 as shown in Figure 5.11B. This was due to having to pause the test because of a leak from an o-ring break. Loading was not removed whilst the test was paused. Neither of these specimens were removed from the overall analysis and comparison to other discs.

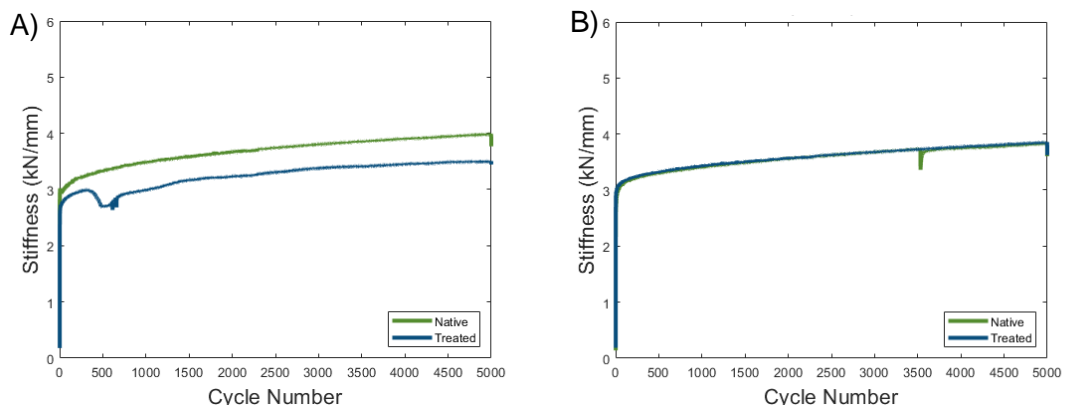


Figure 5.11 – Stiffness change in specimens where drops were observed, A) Spine 2 T12-L1, B) Spine 2 L4-L5

During testing, three specimens showed signs of infection in the hold period PBS bath. For two of these discs, Spine 3 T11-T12 and Spine 3 L3-L4, testing was stopped after

the native cyclic testing. For the remaining disc, Spine 3 L1-L2, the PBS was refreshed and the testing was completed. After these infections, the sodium azide PBS bath (see Chapter 2) was used for all future testing. As it was not possible to know what effect the infection could have on the mechanics of the disc, these specimens were not taken forward for analysis. Seven bone-disc-bone units were taken to completed of the testing, along with one control unit which did not receive treatment. A summary of the testing and where specimen deviated from the standard methods is shown in Table 5-5.

Table 5-5 – Summary of testing, specimens highlighted in light red were not used for further analysis.

Spine	Unit	Native state testing	Treated state testing
Spine 2	T11-T12	-	Control specimen
	T12-L1	-	Non-flush placement of bone-disc-bone unit
	L2-L3	-	-
	L3-L4	-	-
	L4-L5	O-ring break	-
Spine 3	T11-T12	-	Infection, not tested
	T12-L1	-	-
	L1-L2	Infection, bath refreshed, testing continued	-
	L2-L3	Sodium azide bath	-
	L3-L4	-	Infection, not tested
	L4-L5	Sodium azide bath	-

The stiffness values for these seven specimens alongside the control specimen, and the reason to finish injection are shown in Figure 5.12.

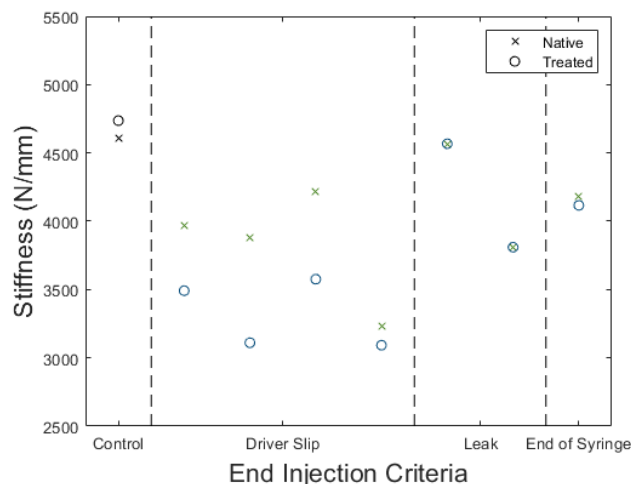


Figure 5.12- Native and treated state stiffness for specimens alongside injection end criteria and control specimen (for which the cross is the first test and circle the second test).

Driver slip was the most common reason to end injection (four of seven discs) and a typical injection force profile for driver slip plot is shown in Figure 5.13A. The injection into the remaining discs was stopped either due to identification of a leak (two of three discs) or due to reaching the end of the syringe (one of three discs), typical injection force

profiles for a leak and reaching the end of the syringe are shown in Figure 5.13B and C respectively.

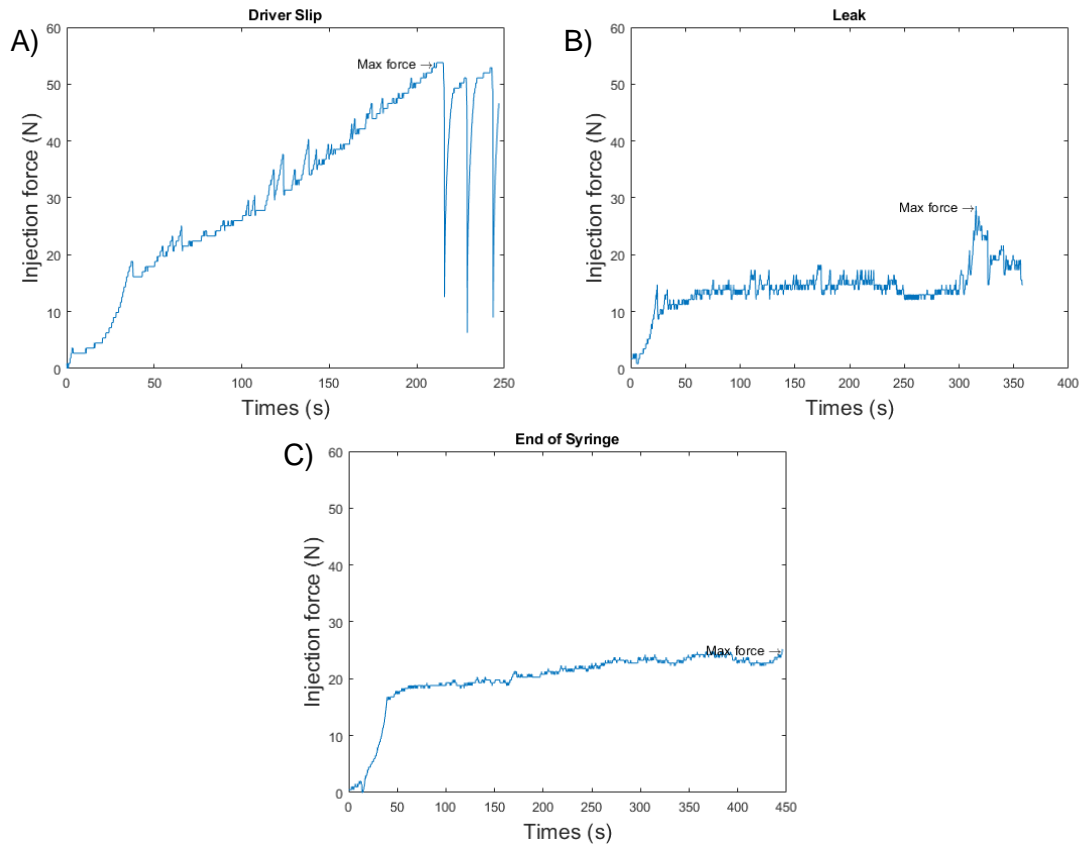


Figure 5.13 - Injection force plots for different end criteria: A) typical driver slip, B) Typical leak, C) End of syringe

Change in stiffness at the end of the test (mean of the last ten cycles), between native state and treated state was assessed. The largest difference in stiffness was in Spine 3 T12-L1 at 0.77 N/mm, and the smallest in the control specimen -0.13 N/mm. The treatment reduced disc stiffness in all but one disc, Spine 2 L4-L5, which leaked and reduced in height during injection. No trends were identified between the change in stiffness and the injection parameters (volume injected, maximum injection force, and change in height). A summary table showing the change in stiffness, volume injected, maximum injection force, change in height pre and post injection, and reason that the injection was stopped reason is shown in Table 5-6.

Table 5-6 – Summary of human tissue testing showing stiffness difference, volume injected, maximum injection force, change in height from injection, and the end injection criteria for the given disc with location of leaks where appropriate.

Family	Disc	Stiffness Difference, Native to Treated (%)	Volume injected (ml)	Max injection force (N)	Height change (mm)	End injection criteria
	T11 T12	2.72	Control Specimen – no injection			
Spine 2	T12 L1	-11.9	0.8	46.9	0.1	Driver slip
	L2 L3	-2.6	1	35.6	0.5	Leak (Anterior)
	L3 L4	-1.6	1.6	32.7	0.8	End of Syringe
	L4 L5	1	1.3	28.6	-0.5	Leak (Lateral)
Spine 3	T12 L1	-19.8	0.6	53.8	1.1	Driver slip
	L2 L3	-15.2	1.1	49.4	1.2	Driver slip
	L4 L5	-4.4	1	47.2	1.4	Driver slip

5.6 Discussion

Following the protocol adjustments identified in the preliminary testing of this chapter, the bovine tissue methodology was adapted for human tissue. The methodology enabled assessment of the mechanical behaviour of the disc across multiple states following injection of a hydrogel.

5.6.1 Developed methodology

The general mechanical behaviour of the discs was similar to previous work, where a gradual increase in stiffness throughout the duration of the test can be seen. As outlined in Chapter 3, the changes in mechanical properties over the duration of the test were likely a consequence of changes to the fluid distribution or fluid outflow (Showalter et al., 2014). Two key changes to the methodology from the bovine testing were made: the addition of a cement mantle and the reduced magnitude of loading. The additional cement mantle may have reduced fluid outflow from the disc by preventing fluid flow through the vertebral bone. Overall, the cement mantle appeared to have minimal effect on mechanical behaviour where the stiffness increased during the testing in a similar manner to previous Chapters. In the bovine specimens the stiffness ranged from approximately 2.5 kN/mm to 5 kN/mm, similarly in this human tissue study the stiffness ranged from approximately 3.2 kN/mm up to 4.7 kN/mm. Based on the data gathered, it is unclear whether there would have been a greater change in stiffness without the presence of the cement. Although only a single specimen, the specimen in the preliminary testing which completed 20,000 cycles at the bovine loads showed a stiffness of 4.5 kN/mm. This could indicate that the cement mantle is not having a large effect on the mechanical behaviour of the disc. The reduction of loading was done to ensure testing could be completed across varying bone densities. The loading was reduced within physiological ranges (0.5 MPa to 1.1 MPa intradiscal pressure) and was similar to other protocols applying cyclic loading to human tissue (Arthur et al., 2010; Smith et al., 2014; Showalter et al., 2015). The original goal of the higher loading used in the bovine tissue was to accelerate potential physiological extremes over a low number of cycles (Dixon et al., 2021). Although no disruptions to the smooth stiffness profile were identified in this testing, the lower loading behaves as a reasonable compromise between accelerating potential issues and successfully running the test.

5.6.2 General mechanical behaviour

Mechanical behaviour of human discs is known to vary greatly and is dependent on degeneration level, age, gender, spinal level, and test methodology (Wilson et al., 2013; Alkalay et al., 2015; Newell et al., 2017; Newell et al., 2020). Like with animal tissue

testing, different mechanical measures are used to report disc biomechanics performance, for example modulus (Showalter et al., 2015; Li et al., 2020), change in disc height (Brinckmann and Grootenboer, 1991; Arthur et al., 2010), or range of motion (Spenciner et al., 2006; Cannella et al., 2014; Pelletier et al., 2016; Dupré et al., 2016). Although this makes it difficult to make direct comparisons to other studies, comparable studies which load the disc up to 800 N show disc axial stiffnesses between 2-3 kN/mm (Arthur et al., 2010; Cannella et al., 2014). These values are similar but slightly lower than the values in the conducted study which were between 2.3-4.2 kN/mm. The slightly higher stiffness observed in the conducted study was thought to be due to the larger loading applied which causes an increase in the intradiscal pressure and a shift in the mechanical behaviour of the disc. A higher stiffness where larger loads were applied to the disc has been observed in similar studies where stiffness was calculated across increasing loads (Arthur et al., 2010; Cannella et al., 2014; Vergroesen et al., 2014).

5.6.3 Effect of treatment

Given the transfer of the method, it was possible to assess the effect of the hydrogel injection on the disc. Several specimens showed expected behaviour where the stiffness was reduced in the treated state. In general, the treatment decreased the stiffness of the disc. The control specimen showed an increase in stiffness of approximately 3% which gives an indication of the possible natural tissue degradation range from this testing. Three out of four specimens which had a percentage change in stiffness above the control, had a change above 10%. The specimen which did not show a large change was at L4-L5. The small stiffness change in the L4-L5 disc may be a result of the disc being larger (and the treatment not filling the disc as well). Reviewing the summary data in Table 5-6, the relationship between the change in disc height from injection and stiffness difference, three of four discs had a height increase above 1 mm from the injection. One of the T12-L1 discs showed a height increase of 0.1 mm. One consistency in the four specimens with a stiffness difference greater than the control was the maximum force of approximately 50 N was reached. In the specimens with a stiffness change less than the control, the force was approximately 35 N. The end values of injection force are likely a result of the test method (the end injection criteria), however, indicate it could be a useful measure for future studies. Looking across all the data, there was little consistency in the magnitude of stiffness difference between the native and treated states throughout this study as visualised in Figure 5.12. The inconsistency in the data is highlighted when reviewing the relationship between injection variables shown in Table 5-6.

It is difficult to define an ideal amount of stiffness reduction to restore to a healthy state (Pfirrmann grades I to II) as the disc mechanical properties are dependent on degeneration and level (Zirbel et al., 2013; Muriuki et al., 2016). These studies applied different range of motion loads and found grade V degenerative discs can show a rotational stiffness up to 1.5 times greater than grades II and III (Muriuki et al., 2016). Between grades II and III the difference was smaller and was approximately 15%. In this performed study, in the tissue where the treatment was believed to be successful there was a decrease in stiffness of approximately 10%. Therefore, it is believed the treatment was able to generate a meaningful amount of restoration.

In general, no clear relationship was identified between the inputs, volume injected and injection force, to the outputs, change in disc height and stiffness. This is likely due to a combination of natural tissue variation, unique specimen degeneration pathology, and the small sample size used for this methodology development.

5.6.4 Injection end criteria

Two possible force related reasons to stop injection were proposed, a force above 65 N was reached (Robinson et al., 2020) or the syringe driver repeatedly slipped. The maximum injection force criteria was not reached instead slipping of the syringe driver was the only force related criteria that results in stopped injection. In four of the seven treated specimens, injection was stopped due to driver slips and all but one specimen showed a decrease in stiffness greater than 10%. All the driver slips started at approximately 50 N which implies that the pressure in the disc, needle and syringe system is greater than the injection force applied by the syringe driver, causing the syringe driver to slip. This is lower than the expected maximum of 65 N which was selected based on the limit of manual injection in literature (Robinson et al., 2020). The 50 N force value is not as high as the injection force observed during injection of some bovine specimens observed in Chapter 4. The difference between studies was thought to be due to minor wear to the thread or motor in the syringe driver from use in this and other studies. In the remaining three discs, injection was stopped due to identification of a leak or due to reaching the end of the syringe. These three discs were from neighbouring discs in spine 2 (L2-L3, L3-L4, and L4-L5) and all demonstrated a change similar in magnitude to that of the control. For two of these specimens this was attributed to the leak identified on the specimen. The third disc reached the end of the syringe. It was thought there was an unidentified leak on this specimen because the disc was anatomically located between the two that leaked during injection, the minimal mechanical response to the hydrogel, and the similar injection force profile to the leaked specimens. This highlights a limitation to the method as leaks were identified visually by

checking for the carboxyfluorescence dye through a narrow field of view in the fixturing. Leaks are likely a result of fissures extending through the annulus to the outside of the disc. The native mechanical testing may have exacerbated minor annular fissures present in the tissue (Wade et al., 2022). Disc height and stiffness were reviewed as possible indicators for potential leaks, however, possibly due to high interspecimen variability, no clear indication was identified. The three discs which had leaks were all Pfirrmann Grade III indicating a distinction between annulus and nucleus and no collapse of the disc space (Pfirrmann et al., 2001). This does not directly address potential fissures in the annulus and more detailed image review may be required specifically assessing annular integrity. This is a limitation of the grading scale and fissures may need to be considered in the future for nucleus augmentation treatments. During follow-up image assessment, fissures were identified in both Spine 2 and Spine 3 with slightly more fissures identified in Spine 2. Although fissures were identified in the discs which leaked, none of the fissures clearly lead to the edge of the disc. As a leak may not be readily identifiable, it may be useful to use imaging contrast agents alongside intra-operative imaging may be necessary for nucleus augmentation surgeries. Sample MRI slices for spines 2 and 3 in the coronal, sagittal, and transverse planes have been collated and can be found in Appendix 2.

Alternatively, the leaks may be a limitation to *in vitro* testing where the surrounding soft tissue such as ligaments or muscles were removed. These soft tissues may help prevent leaking. Importantly, these leaks may indicate injection of a hydrogel is not suitable for degenerate discs with severe annular fissures.

The different responses to the hydrogel across the tissues is likely due to natural morphological variations, such as size and degeneration. This is highlighted in the specimens where a leak was identified during injection, as the leak was not at the needle insertion site. The study currently conducted visual analysis and grading of the tissue. Further image analysis reviewing the annular structure in detail may be able to identify specimens which will be unresponsive to a hydrogel injection due to annular defects.

5.7 Conclusion

Overall, a method has been transferred from animal tissue to human tissue for evaluation of mechanical properties of intervertebral discs that have undergone nucleus augmentation. Alterations to the animal tissue methodology were made due to low bone densities in the human tissue, specifically, the loading was lowered, and a cement mantle was added. A preliminary dataset using this new method was completed which indicated nucleus augmentation can reduce the stiffness of the disc. There was little consistency

across the data due to morphological changes, specifically leaking of the hydrogel during injection was observed. This was not capture pre-treatment with only Pfirrmann grading and were not identified in follow-up image review. This highlights the need for further test method development. Overall, a method to assess the effects of nucleus augmentation on human tissue has been developed. The method was applied and an initial set of outcomes have been reviewed.

6 Delivery device design and evaluation

6.1 Introduction

The work completed in this chapter addresses Objective 4 which entails the development and evaluation of a prototype medical device for injection of the University of Leeds self-assembling peptide:GAG hydrogel. This chapter presents the design requirements for the delivery system, the design development, and the final used design. A series of evaluation studies are then presented including *ex-vivo* surgical assessment, needle puncture evaluation against standard hypodermic needles, and a rheological evaluation.

The device was designed to demonstrate the proof of technical concept that the gels could be delivered into a degenerate disc. Specifically, the design was informed by the requirements of a parallel *in vivo* study, where the nucleus augmentation procedure would be performed on aging sheep. The *in vivo* study involved a collaboration with veterinary and orthopaedic groups at the Universities of Cambridge and Nottingham.

6.2 Device design development

6.2.1 Nucleus augmentation general surgical workflow

As discussed in Chapter 1, the goal of a nucleus augmentation surgery is to deliver a biomaterial to the nucleus pulposus of the disc. The proposed surgical approach starts by navigating a large bore 'introducing' needle to the outside of the annulus. It is anticipated that fluoroscopy imaging would be used to check the positioning of the introducing needle. Once the introducing needle is in place, a small bore 'delivery' needle is inserted down the introducing needle. As with the introducing needle, the location of the delivery needle would be assessed using fluoroscopy. Next, the biomaterial would be injected into the degenerated nucleus and finally the needles would be removed, completing the surgery.

6.2.2 Design requirements

A set of initial user needs and intended uses alongside corresponding design inputs for the proposed delivery device for the *in vivo* study were generated and are shown in Table 6-1. The design requirements were refined throughout the design development. These requirements were assessed and developed in consultation with the veterinary team at the University of Cambridge and the multidisciplinary team at the University of Leeds.

Table 6-1 - Initial overview of user needs and intended uses with corresponding design inputs

User Needs or Intended use	Design input
1 Device must be sterile when used	The device should be able to withstand normal clinical cleaning and sterilisation methods for example autoclaves (up to ~134°C for 10 minutes)
2 Deliver the two solutions to the centre of the nucleus pulposus	Two lumens required for delivery The device must be able to penetrate from outer annulus fibrosus to centre of nucleus pulposus
3 Ensure equal ratio of each solution injection	Syringe interface design must ensure equal ratios of each solution are injected simultaneously
4 Must allow spontaneous gelation of a self-supporting hydrogel	Needle orientation and design must allow spontaneous gelation at the delivery site. This requirement is discussed further in Section 6.2.3.2
5 Minimise damage to annulus fibrosus during delivery	Device should minimize bore diameter of AF penetration as far as possible. This requirement is discussed further in Section 6.2.3.1 Orientation of needles should minimise damage to AF as far as possible. This requirement is discussed further in Section 6.2.3.2
6 Delivery to be accomplished by surgeon	Injection to be completed by surgeon without the need for specialist assistance Device should be easy to manipulate and hold in the correct orientation
7 Prepare solutions in sterile field	Simple back table assembly of device
8 Identifiable in the body	All parts of device that enter the body to be fluoro-opaque
9 Intraoperative injection measurement	Device enables assessment of injection parameters volume injected and injection force intraoperatively

6.2.3 Additional design details

6.2.3.1 Needle diameter

Design Requirement 5 shown in Table 6-1 reflects the clinical concern regarding damage to the disc caused by the needle penetration. It is currently unclear what constitutes recoverable damage to the annulus fibrosus. As highlighted in Chapter 1, previous studies have identified that needle puncture *in vivo* can cause a degenerate cascade and even small gauge needles can have a microstructural effect on the annulus (Michalek et al., 2010). The bulk mechanics, however, do not reflect this where a needle diameter to disc height ratio below 40% shows no significant differences in various mechanical properties (Elliott et al., 2008).

One advantage of the University of Leeds peptide:GAG hydrogel used in this study is that the two solutions can be delivered through fine bore needles. Previous work in the laboratory has shown delivery down short needles of 30G was possible. However, during testing with clinical members of the proof-of-concept project, the more viscous GAG

solution was found to be difficult to inject down 30G needles of the required length for this application. Preliminary tests were undertaken by the veterinarian completing the surgery using a range of needle diameters (25G to 30G). As stated in Requirement 3, an equal ratio of each solution must be injected, therefore different diameter needles would not be possible. The best compromise between usability and needle gauge size was identified as the 29G needle. Therefore, 29G needles for the both of the solutions were used for design development.

Disc height to needle diameter ratio for ovine, bovine, and human tissue for a range of different needle gauges and is presented in Table 6-2. It shows the University of Leeds product delivery sits between a 22G needle and 23G needle and would be sufficiently small to limit the risk of annular damage across different species.

Table 6-2 - Nominal needle outer diameter to mean disc height ratio for ovine, bovine and human tissue (disc heights taken from Monaco et al., 2016)

Needle Gauge	Nominal needle outer diameter (mm)	Nominal Needle outer diameter to disc height ratio		
		Ovine (lumbar)	Bovine (tail)	Human (lumbar)
18	1.27	26%	10%	12%
22	0.7176	15%	6%	7%
2 x 29 G needles	0.6732	14%	5%	6%
23	0.6414	13%	5%	6%
29	0.3366	7%	3%	3%

6.2.3.2 Needle orientation

Another feature relating to design requirements in Figure 6.1 that needs consideration is the orientation of the needles. Needle orientation and design will affect two key parameters: the damage to the AF (Requirement 5), and the mixing and therefore gelation of the peptide:GAG hydrogel (Requirement 4). Thus far, testing had been completed using bevel tipped needles. This type of needle has three needle tip orientations: M-shaped, in parallel, and back-to-back as shown in Figure 6.1.

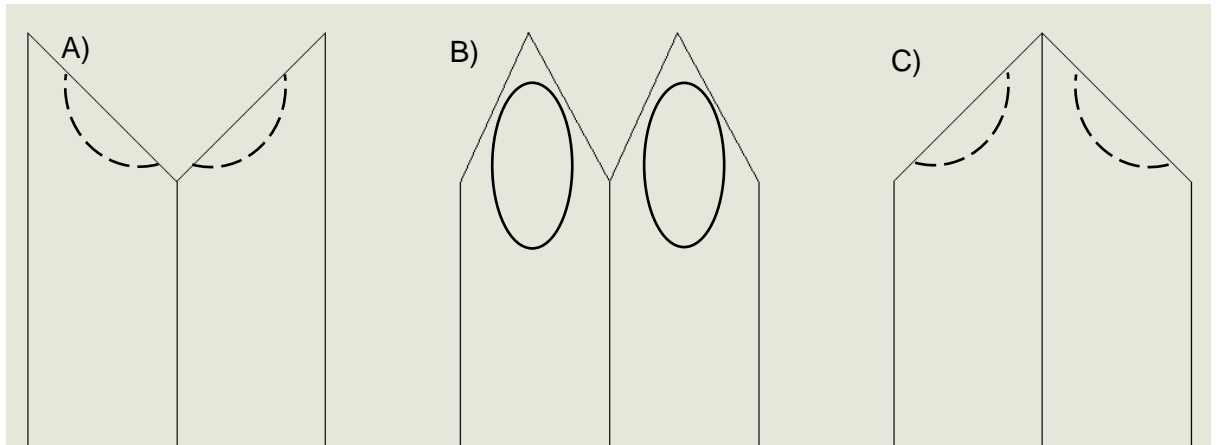


Figure 6.1 - Bevel needle orientations with representative inside diameters. A) M-shape orientation, B) parallel orientation, C) back-to-back orientation.

It was thought that reducing the distance between the needle tips will aid in reducing AF damage. Therefore, the back-to-back orientation was proposed to cause the least damage, while the M-shaped orientation would cause the most damage. Preliminary studies were conducted in-house by Dr James Warren (unpublished data shared via private communication) and it was found that only the M-shaped and parallel orientations permitted sufficient mixing to allow gelation to occur. Since the parallel orientation was thought to reduce potential damage, it was adopted for this study. Given the uncertainty around the needle diameter damage and the tip damage, a separate study was undertaken to examine these factors and is presented in Section 6.4.

6.3 Design development

The design development was broadly split into three phases: initial development, manufacturing development, and finalising the prototype device for use in the *in vivo* study. A summary of these phases is shown in Figure 6.2 A, B, and C.

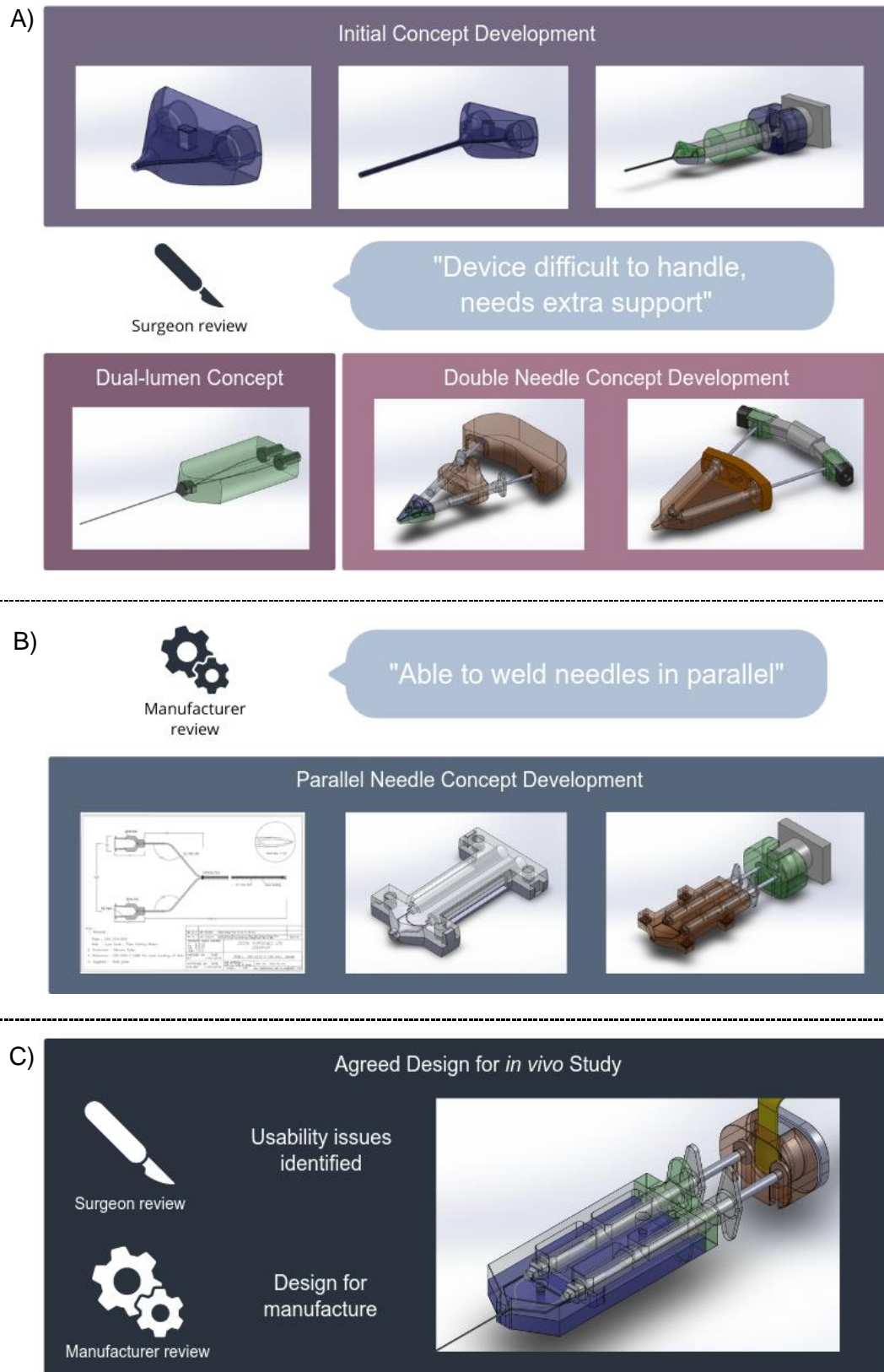


Figure 6.2 - Design development timeline, A) Phase 1: Development of initial concepts with clinical team feedback followed up a second wave of design concepts, B) Phase 2: Manufacturer development where it was possible to silver braise and bend small diameter needles, C) Phase 3: The agreed design for the *in vivo* study

In the initial development, a set of concepts were developed based on the lab testing set up and shared with clinical stakeholders (Figure 6.2A). These concepts used channels to guide two needles together alongside a rear syringe mounting plate to enable even injection (Requirement 3).

During the design review, a concern was raised around the handling of the device intraoperatively (Requirement 6). Based on this, a large body encompassing the syringes was added to the design. Once the handling of the device was addressed, several concepts were developed to ensure successful delivery of the two components of the peptide hydrogel (Requirements 2 and 3).

Two broad concepts were developed: a dual-lumen concept, and a double needle concept, (Figure 6.2A). The dual-lumen concept was two lumens held together over the length of the needle. Whereas the double needle concept was two separate needles that were either pressed together or held in place with small locking rings. Specifically, the double needle concept was intended to use long readily manufacturable needles that have been used in previous studies of this project (Chapters 3 and 4).

During the next phase, the concepts were taken to expert manufacturers to assess the potential for manufacture (Figure 6.2B). The double needle concept was eliminated as a possibility due to basic experiments using 3D printed prototype. In initial discussions with manufacturers, Barber Medical (UK), confirmed they were able to add silver braising to the length of needles joining them to create the dual-lumen concept.

Next, several design iterations for the dual-lumen concept were developed altering the needle length and needle angles. Needle length was a compromise between manufacturability, with longer needles being more difficult to apply the silver braising to, and ensuring enough length to reach the centre of the nucleus. The needle angles were a compromise between length and not blocking flow from kinking the needles. Alongside the specialist dual-lumen needle development, the handling device was refined for by reducing material on the device and adding syringe wings onto the body of the device to aid injection. Additionally, two syringe mounting devices were developed, one standard device and one with two parts which enabled force sensor integration.

Finally in phase 3, a design was agreed after several design iterations and feedback from both the clinical team and manufacturing teams (Figure 6.2C). A CAD render of the final agreed design disassembled and assembled are shown in Figure 6.3. A summary table outlining the material and manufacturing details for each component is shown in Table 6-3.

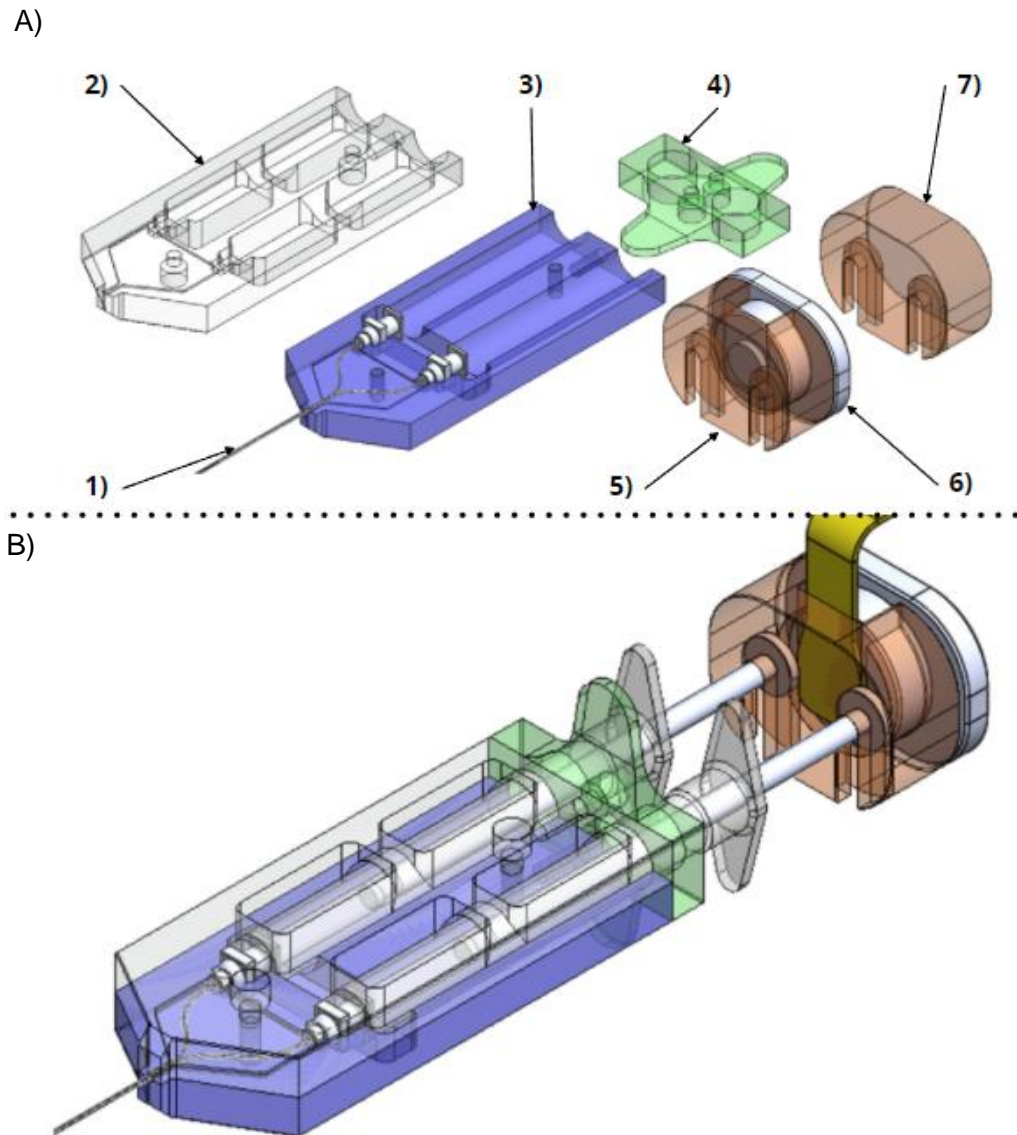


Figure 6.3 - Solidworks renders of agreed design for in vivo study A) Disassembled and B) Assembled

Table 6-3 - Agreed design for in vivo study part manufacture details

Part number	Part Name	Material	Manufacturer	Manufacture method
1	Specialist needles	Stainless steel	Barber Medical	Position and apply silver braising along needle length
2	Device top	Acetal (Delrin)	Barkston Plastics	CNC machined
3	Device bottom	Acetal (Delrin)	Barkston Plastics	CNC machined
4	Rear plate	Acetal (Delrin)	Barkston Plastics	CNC machined
5	Syringe attachment	Acetal (Delrin)	Barkston Plastics	CNC machined
6	TekScan press	Acetal (Delrin)	Barkston Plastics	CNC machined
7	Blanked Syringe Attachment	Acetal (Delrin)	Barkston Plastics	CNC machined
8	TekScan Sensor	Polyester	TekScan	N/A (off the shelf component)

There are two parts to the main body of the device, a top and bottom, which bolt together into helicoils. The top component has a set of windows to enable manufacture and to see the volume in the syringes intraoperatively. The windows are not present on the bottom part of the device, instead a channel has been added to the needle hub area for manufacturing purposes. These two parts hold the specialist needle hubs in place prevent them from moving. Next there is a rear plate part which bolts into the back of the top and bottom components. Four M5 bolts are required to fully assemble the handling device. The rear plate was designed to enable ease of handling by providing larger syringe wings for injection. Finally, two syringe presses were designed which ensured even injection. The syringe attachments have two guides that sit over the rounded plunger on the syringe. The first syringe attachment has a blank on the other end. The second syringe attachment is designed to accommodate the TekScan sensor used in Chapters 4 and 5. The syringe attachment consists of two parts, a section that attaches to the syringes, and a press section. A full set of technical drawings of the final needle and device components can be found in Appendix 3.

6.4 *In vitro* needle puncture evaluation

The aim of the study in this section was to evaluate mechanical differences in from needle punctures through to the nucleus from different needles. Specifically, the goal was to compare the specialist designed needle against convention straight needles of varying diameters.

6.4.1 Methods

A total of 32 bovine bone disc bone units were prepared in accordance with the methodology outlined in Chapter 2. Once prepared, the units were mechanically tested in the native state, punctured with a needle, and mechanically tested again in the puncture state. The mechanical test followed by needle puncture was repeated up to three needle punctures. A summary of the methodology is shown in Figure 6.4.

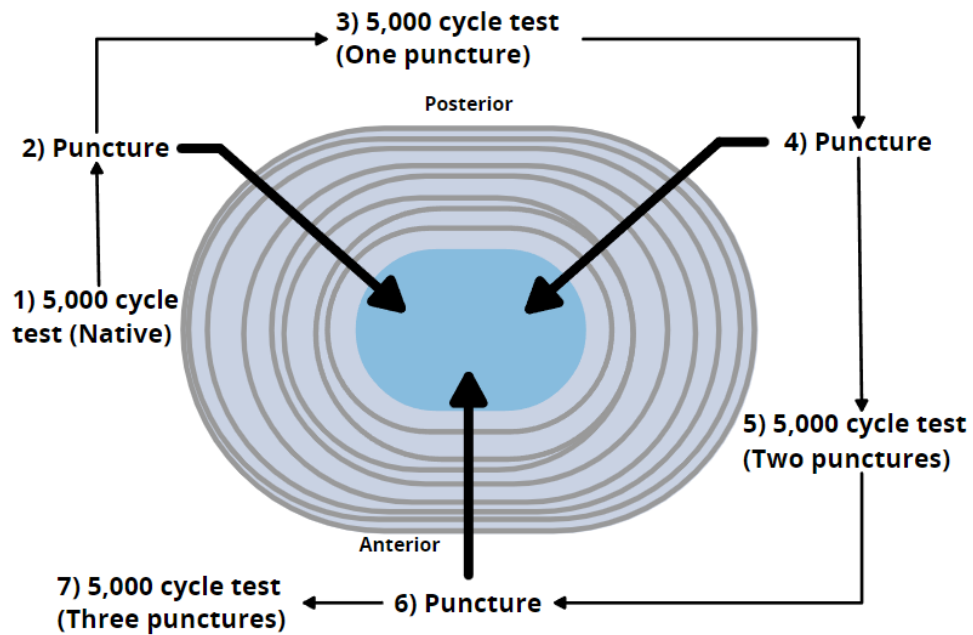


Figure 6.4 - Methodology for the needle puncture evaluation, showing the order of the testing and the position of each needle puncture, starting posterior lateral and at approximately 120° for the two set of punctures.

The mechanical testing load and frequency were performance as described in Section 1.2.3, with a 24-hour hold period followed by cyclic loading for 5,000 cycles (steps 1, 3, 5, and 7). The number of cycles was selected based on Chapters 3 and 4 as a compromise between test length, specimen throughput, and capturing a meaningful level of data. As with other testing in this project, a CT scan was completed after the cyclic loading. Needle punctures were completed immediately after the post cyclic loading CT scan. The specimens then started the mechanical testing cycle again by completing a 24-hour hold period in its new punctured state. Three punctures were completed in total, the first two punctures were completed posterior laterally on opposite sides and the third puncture was anterior, each puncture was approximately 120° apart. The needle punctures were spaced out in this manner to maximise damage throughout the entire disc, increasing likelihood of observing mechanical differences in the specimens.

The 32 specimens were split into four groups, a no puncture group (n=8), a 12G puncture group (n=6), a 21G puncture group (n=6), and a specialised needle puncture group (n=6). The specialised needle group used the developed needle described in Section 6.3 where two 29G needles were soldered together. The no puncture and 12G puncture groups were used as negative and positive controls. The 21G group was used as it is a commercially available hypodermic needle and has the outer diameter (0.81mm) similar to the specialist needle (0.67mm).

The stiffness of the specimens were assessed as described in previous chapters, applying a linear fit to the load portion of each load-displacement cycle. The stiffness for a given testing stage was defined as the mean of the last 10 loading cycles. For each group, comparisons were made between the native state (Step 1, Figure 6.4) and the one, two, and three puncture states (steps 3, 5, and 7, Figure 6.4). Statistical testing was performed to the different groups as described in Section 2.2.6.

6.4.2 Results

The mechanical behaviour of individual discs throughout the testing was similar to that of the previous testing, where the stiffness increased throughout the length of the test. In general, stiffness increased as states progressed, where the native state had the lowest stiffness and the 3 x puncture state had the highest. Although this was the general trend, the magnitude of the stiffness difference between states varied across groups. When comparing the magnitude of differences between the puncture states and the native, the 12G group showed the largest differences and the 21G group showed the smallest difference for all three punctures states. A comparison of the stiffness is shown in Figure 6.5, where the stiffness of each specimen in the different states is displayed.

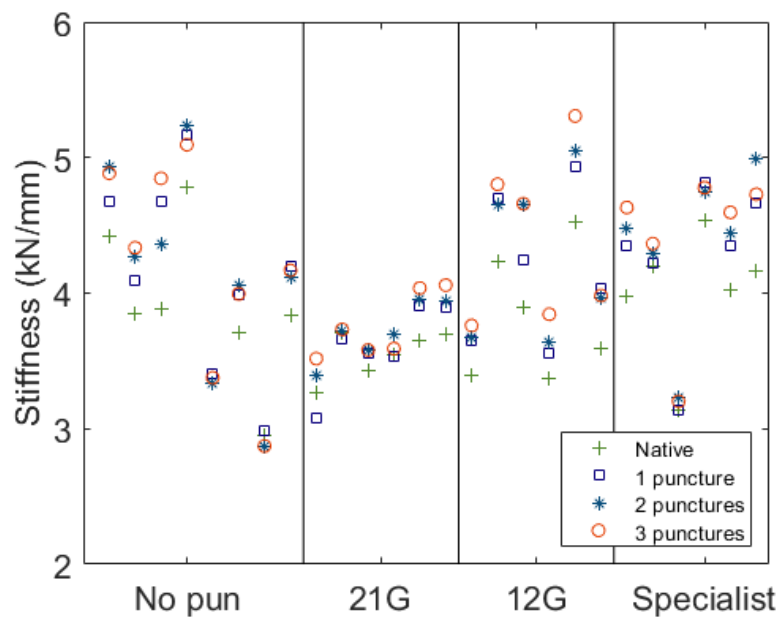


Figure 6.5– Stiffness in the native, 1 x puncture, 2 x puncture, and 3 x puncture states for all specimens

The magnitude of the stiffness difference between the native and punctured states in the no puncture group was small (below 0.3 kN/mm >10%) from state to state and was similar in the no puncture group and the 21G and specialist needle groups. The 12G group showed larger stiffness differences (above 0.4 kN/mm, <12%) than the no puncture controls across all three punctures.

When applying the Shapiro-Wilk test to assess for normality, one dataset was identified as not having a normal distribution. However, as this dataset had an specimen size of 6 the repeated measures ANOVA with post hoc paired t-tests was used for comparisons. The p value results of the Shapiro-Wilk normality test and the selected test for comparison for the different treatment groups is shown in Table 6-4

Table 6-4 - Shapiro-Wilk normality test p values and selected test for statistical comparison. All statistically significant results are highlighted in blue.

Group	Shapiro-Wilk test p values			
	Native state	1 x puncture	2 x puncture	3 x puncture
12G punctures	0.51	0.77	0.33	0.44
21G punctures	0.40	0.39	0.75	0.13
Specialist needle punctures	0.21	0.12	0.22	0.01
No puncture	0.90	0.96	0.89	0.64

The repeated measures ANOVA was applied within each specimen group and showed statistically significant differences across states. Post hoc paired t-tests comparing the needle puncture states to the native showed statistically significant differences in all cases other than the 1 x 21G puncture. A table showing the p values from the repeated measures ANOVA and the paired t-test with Bonferroni correction is shown in Table 6-5.

Table 6-5 - Statistical testing for needle puncture groups, tests where the p value is below 0.05 are highlighted in blue

Group	Repeated measures ANOVA	Paired T-tests		
		Native to 1 x puncture	Native to 2 x puncture	Native to 3 x puncture
12G	>0.01	1.80E-05	0.01	0.00
21G	0.01	1.00	0.03	0.07
Specialist	>0.01	0.08	0.08	0.04
No Pun	>0.01	0.02	0.02	0.05

6.4.3 Discussion and conclusions

It was observed that the test protocol alone generated a change in the stiffness of the disc, where the no puncture group each test resulted in an increase in stiffness. This was attributed to tissue degradation. Tissue degradation was thought to be a large factor in the change in stiffness as differences were identified in the no puncture group. Tissue degradation was expected as part of the testing process which applies large loads to the disc and does not attempt to preserve natural biological behaviours.

The statistical testing shows there was no significant difference between the native and the 1 x puncture groups for the 21G and specialist needles. However, statistically significant differences were identified between the native state and after one puncture in the 12G group and the no puncture group. The significant difference between the native

and one puncture in the no puncture control group is surprising and highlights the spread of the data. Although some degeneration is expected from the testing process, the difference between the no puncture, specialist, and 21G groups is likely a limitation stemming from the low specimen numbers used in this testing. This limitation highlights the importance of looking at the stiffness values for individual specimens to understand whether the specialist needle was having a large effect on the disc.

Although no statistically significant difference was found, a possible cause for a difference between the 21G group and the specialist needle is the parallel needle orientation. The specialist design has more cutting edge and once inserted would create an elliptical gap rather than circular gap.

As shown in Figure 6.5, the change in mechanical stiffness was similar in the control, specialist needle, and 21G groups and larger in the 12G group. Therefore, needle puncture from the 12G was thought to also affect the mechanical behaviour of the disc.

Given the similar change in stiffness observed between the no puncture group, specialist needle group, and the 21G group, it was thought that the different design of needle did not affect the mechanical behaviour of the disc.

6.5 Rheological evaluation

This section compares the viscoelastic properties of the hydrogel when using the specialist designed needle and conventional straight needles of varying lengths. All testing and the basis of the analysis completed for this rheological evaluation was completed by Mr Matthew Culbert as part of his PhD project. The data has been included in the chapter as it is an important aspect towards the evaluation of the developed medical device.

Individual peptide:GAG hydrogels solutions were prepared in the same manner outlined in Section 2.2.1. Rheological measurements were performed on a Kinexus Pro rheometer (Malvern, USA) with a cone-plate geometry (cone angle: 1°, diameter: 50 mm, gap: 0.03 mm). To allow comparison of the specialist needle, rheological evaluation was completed on four needle configurations: the specialist needle (29G x ~150mm with bends see Figure 6.3), straight 29G needles, and no needle. The straight needles were at three different lengths (100mm, 150mm, and 200mm). Two amplitude sweeps were carried out for each sample (1 Hz and 20 Hz). A full description of the rheological test developed has been previously published (Miles et al., 2016; Warren et al., 2021). The amplitude sweeps informed the linear viscoelastic region and measurements were carried out with a frequency sweep. All measurements were repeated on fresh samples

three times. The mean of viscoelastic properties from the three samples for each step in the frequency sweep was calculated and used for comparison. Comparison of data was made at 1 Hz and student t-tests were performed between needle configurations to a significance level of 0.05.

The mean of the three repeat specimens for each needle configuration at 1, 5, and 20 Hz for the complex modulus is shown in Figure 6.6.

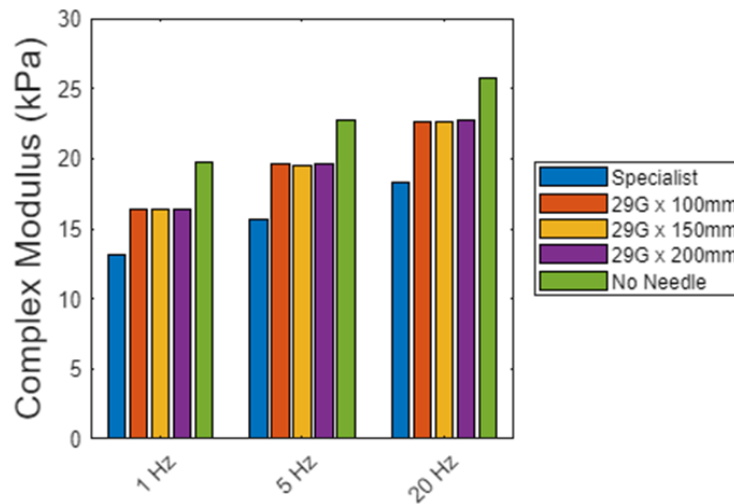


Figure 6.6 - Mean complex moduli for different needle configurations

The t-tests comparing between the different groups at a frequency of 1 Hz are shown in Table 6-6.

Table 6-6 – Statistical testing of various needle configurations, ANOVA with Bonferroni correction was used to compare all groups and student t-tests were used for the intergroup comparisons, statistically significant results are highlighted in blue ($p < 0.05$).

Groups	Complex modulus	Elastic modulus	Viscous modulus
Specialist and 29G x 150mm	0.03	0.03	0.03
Specialist and no needle	0.02	0.02	0.01
29G x 150mm and no needle	0.14	0.14	0.10

The rheological evaluation aimed to assess whether using the specialist needle design influenced the mechanical properties of the hydrogel. Some variation in the hydrogel mechanical properties were observed when the hydrogel was prepared down different needle configurations. When comparing across groups, injecting down a set of needles resulted in a reduction of the mechanical properties. This is thought to be due to the additional shear forces on the injection components when injected down a needle. These shear forces are thought to align the long chondroitin sulphate molecules altering the gelation behaviour of the gel. Statistically significant differences were identified when comparing different needle configurations to the specialist needle. Although there was a statistically significant difference, the material properties were still within the anticipated

clinical range for the nucleus pulposus (6 to 22 kPa) (Iatridis et al., 1997; Bron et al., 2009; Kuo and Wang, 2010). Given the advantages of single injection and reduction in annular damage from the specialist needle, the slight reduction in gel mechanical properties were considered acceptable. A limitation to this study no natural tissue assessment was completed. Applying the same rheological test to natural tissue would confirm the hydrogel mechanical properties are within natural tissue ranges. Further rheological assessment with natural tissue which has been injected with the hydrogel would provide understanding of mixing behaviours and the impact of the hydrogel on the tissue. Another option for future investigation is the tunability of the hydrogel, it may be possible to account for the differences from various needle injection by tuning the gel, adjusting the mechanical properties of the disc (Warren et al., 2021). Overall, the specialist needle appears to consistently produce a hydrogel with mechanical properties similar to the native nucleus pulposus.

6.6 *Ex vivo* surgical assessment

An evaluation of the developed design was completed during a preliminary study at the Royal Veterinary College. In this study, a recently sacrificed sheep from a separate project was acquired and used to evaluate the surgical process. The goal of the study was to identify and practise a surgical approach for the *in vivo* study and assess the proposed devices and solution preparation methods throughout the workflow. The surgical process was performed to mimic the real operating procedure on the full sheep cadaver by Dr Jane McLarenn (University of Nottingham) and Dr Graham Hagger (Royal Veterinary College). An intraoperative X-ray imaging device was used to visualise the position of the needles during injection.

Injections were performed on a total of three lumbar discs. In the first two discs, the injection process was unsuccessful and the needles were not located in the centre of the nucleus. These tests were used to identify markers for the correct positioning of the devices. The third disc was successfully injected with the hydrogel.

In general, the device was successful and was enabled the surgery to be performed. However, the surgical use of the device did highlight some limitations. It was found that it was difficult to manually press the syringes, even using the 29G needles. First, two people were needed to complete injection to prevent the device and needle sliding deeper into the outer introducing needle and therefore, the disc. It was proposed a small piece of medical tubing cut on the during surgery could be used to manage this issue. Second, it was difficult to deliver a set volume of hydrogel, instead syringes were depressed until empty. During the study, it was noted that the injected solutions were

able to move up the introducing needle. This indicates that there is an upper limit on the amount that could be injected. It was also identified that using the current force sensor device would not be possible in clinic. For future developments, the force sensor could be wireless and integrated into a single part. Overall, this *ex vivo* study has demonstrated the use of the developed device. It has highlighted several important learning points for the future of the device.

6.7 Discussion and Conclusions

A prototype medical device for the University of Leeds two-part hydrogel that is ready for use in an *in vivo* study has been design and evaluated. A set of user needs and intended uses alongside design requirements have been developed for the device. As the device continues to progress towards commercialisation, these requirements can be refined, and formal verification and validation activities can be generated. On top of this for commercialisation, design history file documentation will need to be generated including design input/outputs, design and process failure modes and effects analysis, plans for design transfer, and completed validation/verification activities.

The developed specialist needle provided the advantages of minimising damage to the annulus fibrosus and enabling simultaneous delivery of the two components. Future review of the specialist needle and its handling device should assess the design and manufacturing techniques. Several potential other design options are available which may improve the usability of the device including addition of a driver to the handling system, use of dual lumen medical tubing rather than the specialist needle, and integration of a wireless force sensor into the syringe press. Further investigation into the manufacturers and manufacturing techniques may be of benefit to reduce prices and improve the manufacturing scalability of the device.

A set of initial evaluations have been completed for the prototype device. The specialist needle was evaluated against standard hypodermic needles using *in vitro* bovine mechanical testing and rheological testing. The *in vitro* testing assessed the mechanical effects of puncturing discs with the specialist needle. Puncturing the disc with the specialist needle had no greater bulk mechanical effect than similar sized standard hypodermics or the no puncture control group. Future testing which investigates annular fibre damage may provide more meaningful insight into the effects of the specialist needle. The rheological evaluation found that the specialist needle altered the mechanical properties of the gel, however, the properties were still within the required range for natural tissue. A nucleus augmentation surgery was completed using the device in an *ex-vivo* ovine study. Further use of the device and feedback will come with

the *in vivo* study to enable meaningful future design developments. The surgery was successful and important feedback for using the device was identified Overall, a novel prototype medical device has been developed and through different types of evaluation has been shown to be suitable for use in an *in vivo* ovine study.

7 Discussion and Conclusions

7.1 Introduction

The aim of this project was to develop *in vitro* models for the testing of intervertebral disc nucleus augmentation injectable treatments. A further aim was to develop and evaluate a device that meets the specific requirements of the patented University of Leeds peptide hydrogel. A sequential state *in vitro* testing method was applied to bovine tail intervertebral discs using high load magnitude cyclic loading across a large number of cycles. This was done to evaluate the behaviour of the injectable hydrogel on the intervertebral disc (Chapter 3). Based on predictive modelling from the testing in Chapter 3, another set of tests were performed on discs which used significantly shorter test time and aimed to optimise clinically measurable parameters for injectable treatments (Chapter 4). The developed animal tissue *in vitro* test method was then transferred and modified for the testing of human intervertebral discs. An initial dataset was generated using human tissue (Chapter 5). A prototype medical device was developed to address the specific requirements of the University of Leeds hydrogel (Chapter 6). The device was evaluated with three different assessments, a set of *in vitro* needle puncture tests, rheological analysis, and finally, an *ex vivo* clinical evaluation.

7.2 *In vitro* testing for nucleus augmentation treatments

A novel approach for *in vitro* mechanical testing of nucleus augmentation materials in bovine tissue has been utilised. Compared to other bovine tissue testing literature (Milani et al., 2012; Schmocker et al., 2016; Peroglio et al., 2017; Varma et al., 2018), the method applies large loads to exacerbate the tissue aiming to accelerate potential issues, such as herniation, from the nucleus augmentation treatment. As discussed in Chapter 1, it is not possible to perform the ten million cycles expected for medical device testing when using tissue (ISO, 2011). Therefore, exacerbating potential negative outcomes, such as herniation or subsidence, is vital for *in vitro* testing.

There were consistent changes in the mechanical behaviour of the disc during the cyclic mechanical loading. Throughout the duration of all tests the disc height decreased, and the mechanical stiffness increased smoothly. In the testing the hysteresis was found to decrease sharply at the beginning of the test and remain low. The shift in mechanical behaviour during testing was expected and matches that seen in similar testing in the literature (Beckstein et al., 2008; Malhotra et al., 2012; Alsup et al., 2017; Newell et al., 2017). Stiffness was selected as the mechanical property for comparisons as the viscoelastic properties (the hysteresis) reduced sharply within the first 50 cycles. Whilst stiffness was able to identify bulk changes to the mechanical behaviour of the disc, it may not be sensitive enough to detect all minor mechanical changes in the disc, such as small needle punctures. In some treated state tests, large disruptions were identified during the first 1,000 cycles of the typically smoothly increasing stiffness profiles (change in stiffness of over 2 kN/mm). These disruptions were associated with hydrogel migration or distribution within the disc and were observed in testing which did not apply a load during treatment injection. Applying a load during injection is more physiologically relevant and likely a better representation of the clinical environment. As no disruptions were observed in the testing which were loaded during injection, having the loading on the disc during injection appears to alter the manner in which the hydrogel is distributed in the disc. Although the project was unable to confirm this behaviour, it was thought that it is important to use the most clinically relevant test set up. A limitation to this work is that specimens were imaged only after testing, therefore it was not possible to confirm whether it was hydrogel distribution causing the changes in stiffness.

The testing performed in this project did not apply any form of range of motion (flexion/extension, lateral bending, or axial rotation). In doing so, the complexity of the test set up was reduced. This limitation meant there may be additional mechanical effects of the nucleus augmentation procedure that were not identified. Additionally, the high

loading used in this project was not representative of daily living physiological loading and consequently the observations represent an extreme loading case. Specifically, the disruptions identified in the work may be removed by applying an extended low load period, representing lying down several hours post operation. Alternatively, as the gel is instantaneously formed, a short low hold period may not be a driving factor for the gel integration.

The cyclic bovine testing was performed to either 1,000, 5,000, or 20,000 cycles. The upper value of 20,000 cycles, when combined with the high load, was thought to be an extreme loading case. The load profile does not represent average daily living, as it would simulate moving a weight around the body in different ways for six hours. Instead, the loading profile intended and succeeded in exacerbating issues within the disc where end plate contact or transverse plane motion were identified.

It was found that the mechanical properties of the disc in the native and degenerate state at the end of the 20,000-cycle test could be predicted by using a reduced number of cycles. To increase specimen throughput, other studies in this project applied 1,000 or 5,000 cycles. Although no specific ideal number of cycles was identified, it is likely a suitable compromise between specimen throughput and capturing sufficient mechanical data sits between 1,000 and 10,000 cycles.

As previously discussed, having a suitable artificial degenerate method for animal tissue is necessary to evaluate the effectiveness of a nucleus augmentation procedure. Throughout the project, an enzymatic degeneration method was used, which was able to instigate statistically significant differences between the native and degenerate states. A sham procedure was performed and did not show statistically significant differences between the native and sham degenerate states. This indicates that the enzyme was responsible for the change in mechanical behaviour.

The main benefit of the performed enzymatic degeneration method used was how quickly the method was able to instigate degeneration. The degeneration procedure occurred over two days whereas other methods using similar enzymes take six to ten days (Chan et al., 2013; Malonzo et al., 2015; Schmocker et al., 2016). However, these longer timeframe degeneration methods are usually performed in a bioreactor and aim to preserve the cellular behaviour of the disc.

By reducing the time taken, specimen throughput can be improved which enables assessment of different variables relating to the nucleus augmentation procedure. A unique feature of the degeneration method was the use of an inhibitor. Other methods do not use an inhibitor, instead relying upon natural enzyme degradation over time (half-

life of approximately 7 days for chondroitinase ABC (Hettiaratchi et al., 2020)) to control the severity of the degeneration. Other studies use a long degeneration time where the disc will be in an equilibrium state at the end of the degeneration period. By using a shortened time, whilst better for the preservation of the tissue, there is need to ensure the equilibrium of the disc is reached in its degenerate state. Therefore, an additional 24 hour hold period after the injection of the inhibitor was required. As other studies used longer periods of time no inhibitor was used. Use of an inhibitor could also improve the consistency in the level of degeneration, ensuring an early stage of degeneration was reached for each disc. This method may create a basis for future comparison of the mechanical effects of different hydrogels. The degeneration was associated with the activity of the papain; however, the mechanical testing, needle puncture, and higher temperature hold period may have further contributed to the degeneration. Testing in this project where the enzyme was not applied, the 'sham' procedure group from Chapter 4, showed minimal or non-detectable effects from these other variables. This was possibly due to only assessing the disc through bulk mechanical means, and further testing, such as a GAG assay, may show specific differences between disc states.

It is not possible, however, to attribute the entire degeneration to the enzymatic behaviour, as it has previously been discussed the mechanical loading and needle punctures can also instigate degeneration. This change is shown in the needle puncture evaluation, where a statistically significant difference was observed in the no puncture control native state and the 1 x no puncture state.

The main difference across the two studies (the 'sham' group in Chapter 4 and the no puncture group in Chapter 6) was a different number of cycles applied during testing. The 'sham' group applied 1,000 cycles to the disc in the native state whereas the no needle puncture group applied 5,000 cycles to the disc in the native state. It may be that the increased number of cycles instigated additional degeneration.

A limitation of this *in vitro* testing method was that it did not take into consideration the cellular behaviour of the disc. This was done due to the natural low cell density of the disc and to focus solely on the mechanical behaviour of the disc. Whilst this is suitable for the University of Leeds hydrogel, which is acellular, the method may not be appropriate for cellular hydrogels (Wan et al., 2016; Schmocker et al., 2016; Thorpe et al., 2017). For cellular hydrogels, the outlined method is meaningful, as it will provide an understanding of the mechanical behaviour from injection which may be indicative of any mechanotransduction effects occurring (Fearing et al., 2018). Additional testing investigating the cellular behaviour will be required for such cellular treatments.

The *in vitro* bovine tissue model developed in this project can instigate consistent degeneration rapidly. The method can enable comparison of different hydrogels to a standard model, assessment, and optimisation of clinical variables, and can be an accessible method to eliminate mechanically unsuitable, injectable hydrogel candidates.

The use of animal tissue models is a necessity in the development of *in vitro* methods due to accessibility and ethics. As it is readily available from the food chain, animal tissue is valuable as a precursor to *in vitro* testing with human tissue. Whilst similar, there are no food chain animal intervertebral discs with comparable dimensions to the human intervertebral disc (O'Connell et al., 2007; Beckstein et al., 2008; Monaco et al., 2016). In human tissue studies, the loading for can be calculated by scaling up the intradiscal pressure based on the larger cross-sectional areas. The direct transfer of the method was unsuccessful and resulted in damage to the vertebrae of the prepared bone-disc-bone units. Two changes were made to the testing based on literature: the loads were lowered (Arthur et al., 2010; Dupré et al., 2016; Costi et al., 2021), and a cement mantle was added to either side of the bone-disc-bone unit (Cannella et al., 2014; Marini et al., 2015; Amin et al., 2016; Costi et al., 2021). By taking these two steps *in vitro* testing of human tissue was successfully performed. Although the effect of each individual change was not assessed, a method has been outlined for the transfer of animal tissue test methods to human tissue.

The mechanical behaviour of the human tissue discs was similar to that observed in the bovine tissue, where the stiffness increased throughout the duration of the test. In general, the observed mechanical restoration of the disc was lower than that observed in the bovine tissue. This result was not surprising given the volume injected was approximately the same and the human discs were larger than the bovine disc. This highlights the need for *in vitro* human tissue testing in the development of injectable nucleus augmentation treatments.

7.3 Treatment delivery and clinical implications

An important question addressed in this project was what quantity of a material should be injected into the disc for a nucleus augmentation procedure. This was primarily evaluated in Chapter 4, where clinically measurable injection parameters were compared against mechanical restoration. The overarching goal of assessing these variables was to provide meaningful advice to clinicians to ensure the best possible treatment outcomes. Overall, this project identified direct measurements of the disc as the best indication of restoration, where volume injected and change in height showed a strong relationship with mechanical restoration. Similar assessment has been

demonstrated in literature comparing disc mechanical restoration to disc height (Cannella et al., 2014). Although fewer parameters were assessed in the literature, a positive relationship with disc height and mechanical properties was identified. As discussed in Chapter 3, injection parameters appeared to be dependent on the treatment injected, degeneration level, size, and shape of the disc.

It was possible to use the identified bovine relationships to assess the volume or force that should be used for the human tissue testing. However, it was found that to gain a similar level of restoration as observed in the bovine tissue, over 2 mL would need to be injected. This volume was not injected as 2 mL is significantly larger than any other studies, both in literature and in this project (Dixon et al., 2021). It also may not be physically possible to inject such a large quantity without specialist equipment.

The mean percentage stiffness decrease from the degenerate state to the treated state in the bovine tissue studies with a 1 mL injection was ~17% (Chapter 3) and ~25% (Chapter 4). This decrease in stiffness is slightly larger than observed in another study where a mean increase of 12% was found (Malhotra et al., 2012; Varma et al., 2018). In the human tissue study conducted, the mean decrease in stiffness was approximately 10%. The lower percentage is unsurprising as a similar volume was injected into the human tissue as the bovine tissue and the human tissue was generally larger than the bovine. It is difficult to define a healthy state for the human tissue as generally tissue used for *in vitro* testing is typically already in a degenerate state. As discussed in Chapter 5, the compressive stiffness can change by approximately 15% between pfirrmann grades I and III (Muriuki et al., 2016). Although the decrease in stiffness observed in the conducted human tissue study is lower than 15%, the treatment is able to change the overall mechanics of the disc towards a lower degeneration grade.

Unlike in the bovine testing, no strong relationship was found between the injection parameters and the mechanical restoration in the human tissue samples. This lack of relationship in the human tissue was thought to be a result of the low sample numbers in the human tissue study, and the consistent degeneration in the bovine study. The artificially instigated degeneration in the bovine tissue specimens was excellent for assessing the impact of different variables, however; the degeneration level did not fully represent the range of degeneration present in the human tissue. The enzyme likely created localised degeneration in the nucleus, which would represent early-stage degeneration. As a result, it cannot represent other degenerative features such as annular fissures. For example, it is unlikely that the enzymatic degeneration would cause the severe fissures observed in the human tissue in this project. It may be possible to further adjust the mechanical aspect of the degenerate model to include loading

specifically intended to cause annular fissures. For example, disruptions to the microstructure of the disc can be instigated with high frequency loading (frequencies greater than 5 Hz) (Wade et al., 2016). A recent review suggested the use of a combination degeneration model which utilises enzymatic degeneration alongside mechanical loading to have a model that better reflects *in vivo* situations (Rivera Tapia et al., 2022). Although not confirmed, with a larger sample size of successful tests it was thought a relationship between injection parameters, degeneration level, and mechanical restoration could be identified for human tissue.

The work has shown that the mechanical outcomes of a nucleus augmentation procedure could potentially be predicted based on injection parameters and dimensions of the disc. The project has shown the degree of degeneration in the disc affects the mechanical outcomes, where discs with severe annular fissures may not respond to the treatment. The testing implies that the nucleus augmentation procedure could be optimised based on clinically measurable factors for clinical use. The final objective in this project was to develop and analyse a medical device that meets the unique requirements of the University of Leeds hydrogel. A specialist needle was developed which minimises annulus damage by enabling gelation to occur at the end of the needles. A handling device was designed which enabled easy use of the specialist needle.

When transferring the usage of the hydrogel from benchtop testing to a clinical application, additional testing needs to be considered. Three areas were identified that may affect the use and performance of the hydrogel: needle puncture, gel rheological behaviour, and clinical usage. This project applied the developed *in vitro* bovine sequential state mechanical testing to discs to assess the impact of the specialised developed needle. There was no significant difference between the native and one puncture state for the specialist needle or a similar sized hypodermic needle. However, there was a significant difference in the control groups (no puncture and 12G punctures). Although the raw stiffness values were statistically different, the change in stiffness between the native state and the single puncture state was similar for the native, specialist needle, and 21G groups. Further investigation into the effects of the needle puncture would be of benefit to the development of the device. Rheological assessment was able to evaluate changes to the hydrogel mechanical behaviour with the specialist needle. The rheological analysis identified changes to the hydrogel properties based on needle bore size, needle length, and needle design. The clinical usage primarily focuses on usability and accessibility of the surgery. An *ex vivo* assessment was performed and identified a series of important changes to the design for future development of the overall medical device. A common clinical concern with injectable treatments was

damaging the annulus by needle puncture (Culbert et al., 2022). This highlights the need to assess a potential treatment through using the anticipated delivery system rather than preparing the material in an ideal state on a benchtop.

The different evaluation methods used in this project were able to assess some of the anticipated challenges when transferring from benchtop to application. The testing performed has highlighted the need to expand testing focus to the delivery of the hydrogel as well as the gel itself. Moreover, the project has provided an initial guideline that can be built upon for future testing and assessment of injectable nucleus augmentation treatments.

The testing and analysis performed in this project could contribute to the regulatory pathway for cellular (advanced therapeutics) and acellular (medical device) nucleus augmentation materials. Specifically, the test methods developed could contribute to the verification and validation of a material. With further testing and development, it may be possible to inform a standard or become part of a wider suite of testing standards. The analysis has highlighted important considerations for the design input phase of the regulatory pathway.

An important consideration for injectable nucleus augmentation treatment is what time of the day should the injection be conducted. As discussed in Chapter 1, the disc undergoes a natural cycle, where water is slowly expelled during the day and the water is recovered during the night. Based on this, it may be possible to inject more at the end of the day. The testing in this project simulated a 24-hour supine position prior to treatment. The intention of this was to reach an osmotic equilibrium and prevent over injection, which has the potential to cause a severe adverse event (herniation). A 24-hour rest period could be accomplished clinically, however, may not be practical. Overall, it is currently unclear when to perform an injection in clinic and whether it has a meaningful impact on the treatment.

7.4 Future work and limitations

Future work for the development of nucleus augmentation treatments needs to address the perceived challenges from clinical staff and regulatory bodies. Other testing, outside of the project scope, is important for the future of nucleus augmentation treatments and has been discussed in depth in recent review studies (Schmitz et al., 2020; Dixon et al., 2021; Culbert et al., 2022). This section will discuss future work that builds upon the work in this project.

7.4.1 *In vitro* testing for nucleus augmentation treatments

The focus of this project was developing a set of *in vitro* mechanical testing methods and techniques that enabled evaluation of injectable nucleus augmentation treatments. An observation from the *in vitro* testing was the large, treated state disruptions to the smooth stiffness profile. The shift in the mechanical behaviour was thought to be a result of the gel redistributing itself within the disc. A limitation of this work was that the radio-opaque agent has the ability to migrate away from the formed hydrogel. This made detecting the behaviour of the gel less reliable. An area of interest for further research is how the gel integrates into the nucleus. There are several experimental methods which could begin to investigate these effects. Firstly, including more imaging throughout testing may be beneficial. For example, using fluoroscopy during injection or an additional CT scan prior to loading, could provide an initial starting point for gel migration comparisons. Another experimental option would be to transversely dissect discs at different timepoints after injection, such as immediately after injection, after the hold period, or part way through cyclic loading. Alternatively, further analysis on the specimens tested in this project is possible by dissecting and sampling parts of tissue. Rheological or histological analysis of the tissue from different states may provide insight as to how the hydrogel has integrated into the nucleus. More in-depth image analysis on the current data set is another option to better understand the distribution behaviour of the gel. Use of formal image analysis with thresholding may provide new insight in the comparison of the disrupted treated state discs with the standard smooth profile discs.

7.4.2 Treatment delivery and clinical implications

In general, existing literature focuses on whether mechanical restoration is possible with a given biomaterial. A limitation to the studies completed in this project is that mechanical restoration can vary greatly depending on injection parameters. Given this variation, even when the parameters are kept constant, future investigations into injectable treatments should include details of the injection parameters. A further recommendation to address this limitation is to load the disc during injection. Not only does this better

mimic the anticipated surgical situation better, but also appears to affect the immediate distribution of the injected material within the disc. These two recommendations for future testing should enable better consistency in mechanical evaluation of injectable treatments. Finally, more detailed analysis of the CT data from the produced dataset may enable more meaningful evaluation of the injection parameters with relation to the mechanical restoration. Automating the analysis and applying machine learning may identify features that will cause a treatment to fail for a given disc. This is beneficial for testing, where failed discs could be identified earlier and may have clinical benefit in identifying unsuitable discs for injectable treatments.

A parameter of interest for injectable nucleus augmentation treatments, which was not investigated in this project, was disc recovery. This was not investigated as the goal of this work was to generate a method to evaluate the mechanical effect of injecting a hydrogel. Nonetheless, given the natural day and night, loading and recovery the disc undergoes, assessing the recovery behaviour of a treated state disc would be of interest. Assessment of this behaviour can be readily achieved by adding a hold period in the mechanical testing after the cyclic loading or adding a height measurement, such as linear variable differential transformers, to the hold rig.

7.4.3 Delivery device

This project developed an initial prototype of a medical device for use in an *in vivo* ovine trial, however, further design work is required for clinical use. There are several design developments discussed in Chapter 6. A series of relevant evaluations were performed to assess the suitability of the product. The studies highlighted the need to develop a delivery device alongside development of the treatment. The assessments were performed for the designed device and specific hydrogel. Any treatments that require additional steps or products that are not currently in clinical use will also require similar considerations and testing. Although the mechanical testing (rheology and *in vitro* needle puncture) provided useful insight, clinical feedback and review is particularly important for such treatments as this enables actual use in clinic.

7.5 Conclusions

The overall goal of this project was to develop a set of *in vitro* tests to evaluate injectable nucleus augmentation treatments. A sequential state testing method was used to compare the native, degenerate, and treated states for intervertebral discs. A high magnitude cyclic load was used up to a large number of cycles to comprehensively evaluate the mechanical behaviour of the discs in the different states. The test method was able to show restorative effects and identified exacerbated mechanical issues from treatment integration. Predictive models showed that it was possible to accurately assess the high cycle mechanical properties using a reduced dataset. Different outcomes were identified for the treated state discs for the low cycle statistical testing and the high cycle predictive modelling. Based on the predictive modelling, a rapid *in vitro* testing method was developed that was able to evaluate different parameters relating to the nucleus augmentation surgery. Volume injected and change in disc height from injection showed a strong relationship with mechanical restoration. The method was transferred to human tissue and an initial dataset was assessed. A design that met the unique requirements of a patented hydrogel was developed. A series of studies showed the success of the device and highlighted important testing requirements for development of other devices. This project has developed a suite of mechanical testing that can be used to assess the mechanics of injectable nucleus augmentation treatments. The testing can enable optimisation of the treatment injection, ideally, reducing the potential risk of adverse clinical events. A series of recommendations for future mechanical testing were made to aid the translation of these treatments into clinic.

References

- Cannella, M., Isaacs, J.L., Allen, S., Orana, A., Vresilovic, E. and Marcolongo, M. 2014. Nucleus implantation: The biomechanics of augmentation versus replacement with varying degrees of nucleotomy. *Journal of Biomechanical Engineering*. **136**(5), p.051001.
- Deneuille, J.P., Yushchenko, M., Vendeuvre, T., Germaneau, A., Billot, M., Roulaud, M., Sarracanie, M., Salameh, N. and Rigoard, P. 2021. Quantitative MRI to Characterize the Nucleus Pulposus Morphological and Biomechanical Variation According to Sagittal Bending Load and Radial Fissure, an ex vivo Ovine Specimen Proof-of-Concept Study. *Frontiers in Bioengineering and Biotechnology*.
- Elliott, D.M., Yerramalli, C.S., Beckstein, J.C., Boxberger, J.I., Johannessen, W. and Vresilovic, E.J. 2008. The effect of relative needle diameter in puncture and sham injection animal models of degeneration. *Spine*. **33**(6), pp.588–596.
- Hebelka, H., Nilsson, A. and Hansson, T. 2014. Pressure increase in adjacent discs during clinical discography questions the methods validity. *Spine*.
- Malhotra, N.R., Han, W.M., Beckstein, J., Cloyd, J., Chen, W. and Elliott, D.M. 2012. An injectable nucleus pulposus implant restores compressive range of motion in the ovine disc. *Spine*. **37**(18).
- Miles, D.E., Mitchell, E.A., Kapur, N., Beales, P.A. and Wilcox, R.K. 2016. Peptide:glycosaminoglycan hybrid hydrogels as an injectable intervention for spinal disc degeneration. *Journal of Materials Chemistry B*. **4**(19), pp.3225–3231.
- Muriuki, M.G., Havey, R.M., Voronov, L.I., Carandang, G., Zindrick, M.R., Lorenz, M.A., Lomasney, L. and Patwardhan, A.G. 2016. Effects of motion segment level, Pfirrmann intervertebral disc degeneration grade and gender on lumbar spine kinematics. *Journal of Orthopaedic Research*. **34**(8), pp.1389–1398.
- Panjabi, M., Brown, M., Lindahl, S., Irstam, L. and Hermens, M. 1988. Intrinsic disc pressure as a measure of integrity of the lumbar spine. *Spine*. **13**(8), pp.913–917.
- Rivera Tapia, E.D., Meakin, J.R. and Holsgrove, T.P. 2022. In-vitro models of disc degeneration – A review of methods and clinical relevance. *Journal of Biomechanics*. **142**(August), p.111260.
- Robinson, T.E., Hughes, E.A.B., Bose, A., Cornish, E.A., Teo, J.Y., Eisenstein, N.M., Grover, L.M. and Cox, S.C. 2020. Filling the Gap: A Correlation between Objective and Subjective Measures of Injectability. *Advanced Healthcare Materials*.

- Schmitz, T.C., Salzer, E., Crispim, J.F., Fabra, G.T., LeVisage, C., Pandit, A., Tryfonidou, M., Maitre, C. Le and Ito, K. 2020. Characterization of biomaterials intended for use in the nucleus pulposus of degenerated intervertebral discs. *Acta Biomaterialia*. **114**, pp.1–15.
- Varma, D.M., Lin, H.A., Long, R.G., Gold, G.T., Hecht, A.C., Iatridis, J.C. and Nicoll, S.B. 2018. Thermoresponsive, redox-polymerized cellulosic hydrogels undergo in situ gelation and restore intervertebral disc biomechanics post discectomy. *European Cells and Materials*. **35**, pp.300–317.
- Wade, K.R., Schollum, M.L., Robertson, P.A., Thambyah, A. and Broom, N.D. 2016. ISSLS prize winner: Vibration really does disrupt the disc. *Spine*. **41**(15), pp.1185–1198.
- Wang, J.Y., Mansfield, J.C., Brasselet, S., Vergari, C., Meakin, J.R. and Winlove, C.P. 2021. Micro-mechanical damage of needle puncture on bovine annulus fibrosus fibrils studied using polarization-resolved Second Harmonic Generation(P-SHG) microscopy. *Journal of the Mechanical Behavior of Biomedical Materials*.
- Warren, J.P., Miles, D.E., Kapur, N., Wilcox, R.K. and Beales, P.A. 2021. Hydrodynamic Mixing Tunes the Stiffness of Proteoglycan-Mimicking Physical Hydrogels. *Advanced Healthcare Materials*.
- Zirbel, S.A., Stolworthy, D.K., Howell, L.L. and Bowden, A.E. 2013. Intervertebral disc degeneration alters lumbar spine segmental stiffness in all modes of loading under a compressive follower load. *Spine Journal*. **13**(9), pp.1134–1147.

Appendix 1 – General stock solution preparation

8 General stock solution preparation

8.1 Sodium citrate

Sodium citrate is an anticoagulant and was used in the specimen preparation. Sodium hydrogen carbonate (3.96g) (S/42000/60, Fisher Scientific, USA) and Citric Acid monohydrate (7.86g) (20276.292, VWR, USA) were added to 200 mL deionised water, then pH balanced to pH 7. The solution was then autoclaved and made up to 2 L by adding 1716 mL sterile PBS, 80 mL penicillin/streptomycin, and 4 mL aprotinin.

8.2 Phosphate buffer saline

PBS was used a hydration medium during mechanical testing. As per the manufacturer's instructions (Oxiod, UK), ten tablets of PBS were dissolved per litre of distilled water. A treated PBS bath was used in this project to maintain tissue hydration over time. The PBS prepared for the bath was dissolved the PBS as outlined and then sterilised in an autoclave (Tractol 2, Priorclave, UK). The PSB bath was then supplemented with: 1 mL/L penicillin (5000 U/mL) /streptomycin (5 mg/mL)(P4458, Sigma Aldrich, USA) , 0.5 mL/L amphotericin B (250 µg/mL))(A2942, Sigma Aldrich, USA), and 0.25mL/L aprotinin (10,000 KIU/mL))(AP-R, Nordic Pharma, UK) or prepared to be a solution of 0.3% sodium azide (40-2000-01, Severn Biotech, UK).

8.3 Papain

Papain was the selected enzyme used in this project to degenerate the disc. A digestion buffer was prepared by mixing 0.788 g L-Cysteine Hydrochloride (C1276, Sigma Aldrich, USA) and 1.8612 g disodium ethylenediaminetetraacetic acid (E/P140/65, Fisher Scientific, USA) into 1 L PBS using a magnetic stirrer. The pH was adjusted to 6.0 ± 0.1 . 40,000 KIU papain (A3824.0100, Applichem, GER) was then dissolved in 5 mL of the digestion buffer, for a concentration of 1.6 kU/mL. The papain was the frozen and stored at -20°C until day of use.

8.4 Ebselen

Ebselen was used to stop the papain enzymatic activity and create a controlled end point for the degeneration. Ebselen (25 mg) (E3520, Sigma Aldrich, USA) was dissolved in 5 mL PBS as a stock solution. This was then diluted to 42 mL with 37 mL PBS for a

concentration of 0.064 μM , then to 5 mL bijoux. The Ebselen solution was aliquoted and stored at -20°C until day of use.

8.5 Peptide hydrogel

The peptide hydrogel consisted of two functional components: an amino acid peptide variant (Ac-SSRFOWOREQQ-NH₂) (CS11082, CS Bio, USA) and chondroitin sulphate (ScanDroitin, ZPD, DEN). Both components were dissolved in the same 'working' solution. The working solution consisted of three components: saline, 5,6-carboxyfluorescein (72088-94-9, Merk, USA), and a radio-opaque agent. Sodium chloride (S/3160/63, Fisher Scientific, USA) was dissolved in distilled water to prepare a 130 mM saline solution and then the pH was adjusted to 7.4. The 5,6-carboxyfluorescein solution was dissolved in a portion of the previously made saline to a concentration of 5 mg/mL. The radio-opaque agent was one of two clinically used agents, trade names Ultravist (300, Bayer, UK) and Onmipaque (300, GE Healthcare, USA). The three components were mixed at a ratio of 2:1:1 for saline:carboxyfluorescein:radioopaque agent and then sterilised using an autoclave. The peptide and chondroitin were dissolved separately in the working solution to concentrations 24 mg/mL and 136 mg/mL respectively. The solutions were then mixed with a vortex mixer for 30 seconds.

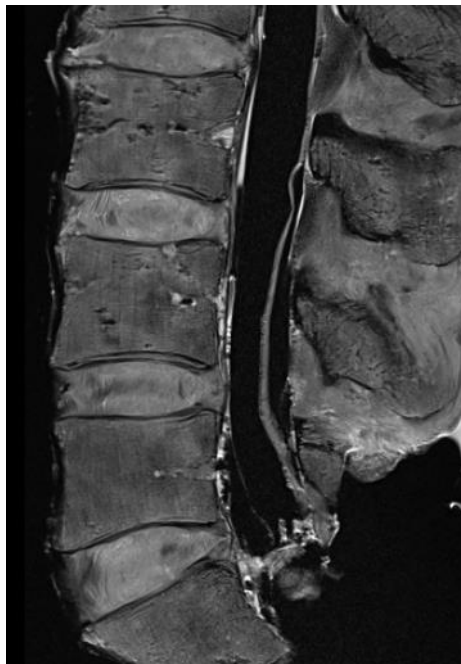
Appendix 2 – Human tissue MRI scans

9 Human tissue MRI scans

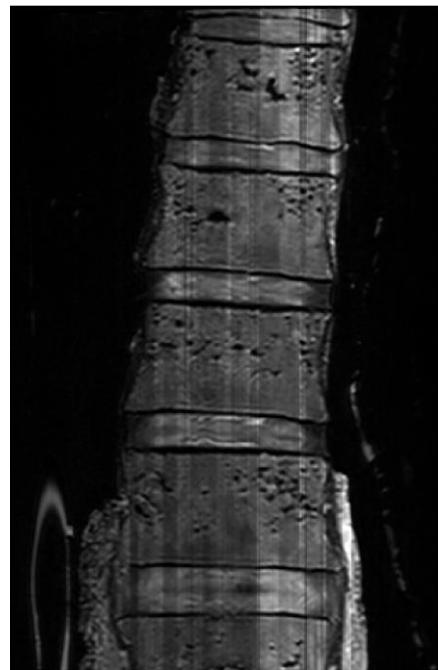
9.1 Spine 2

Scan type: T2 weighted turbo-spin-echo fat saturated imaging. Transverse plane images show cranial to caudal.

Sagittal

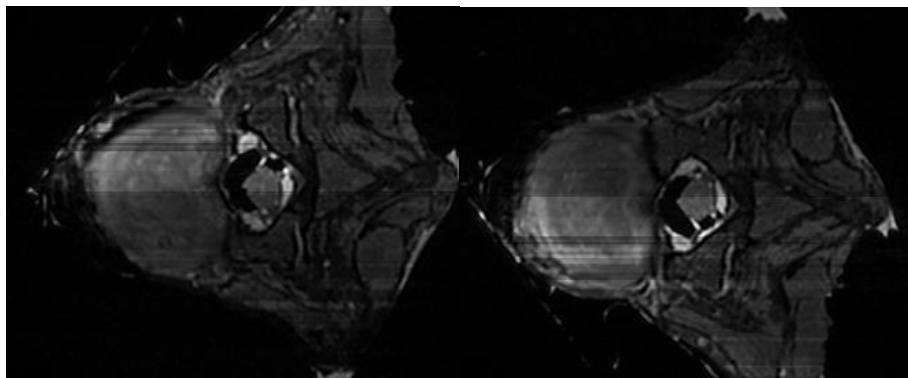


Coronal

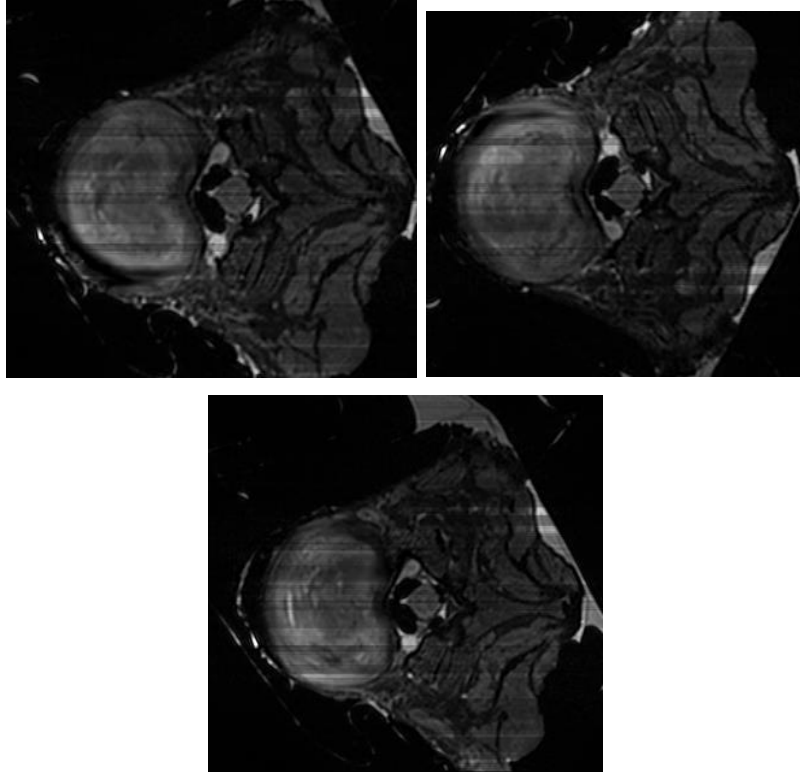


Transverse slices

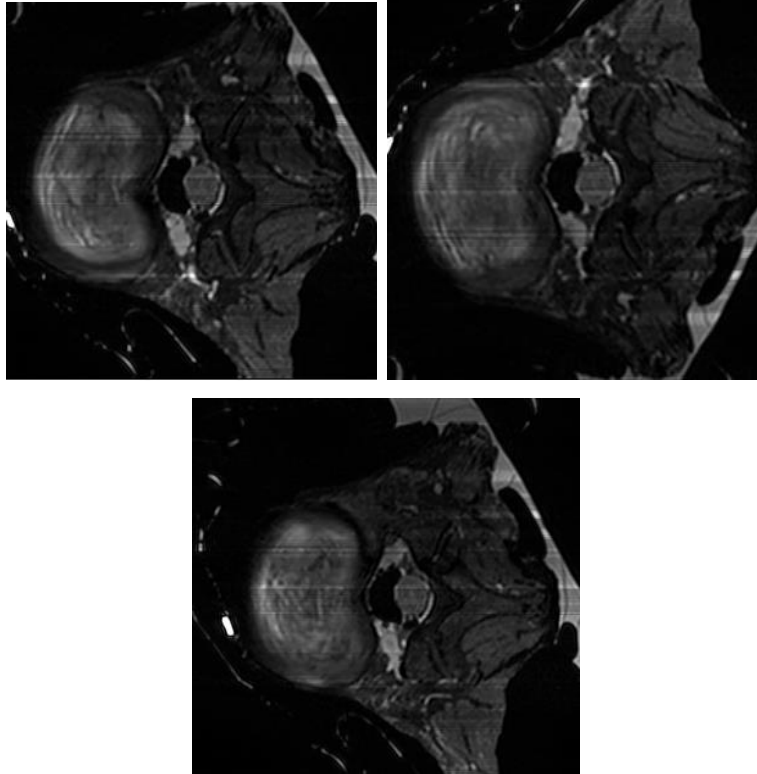
T12-L1: Pfirrmann Grade III



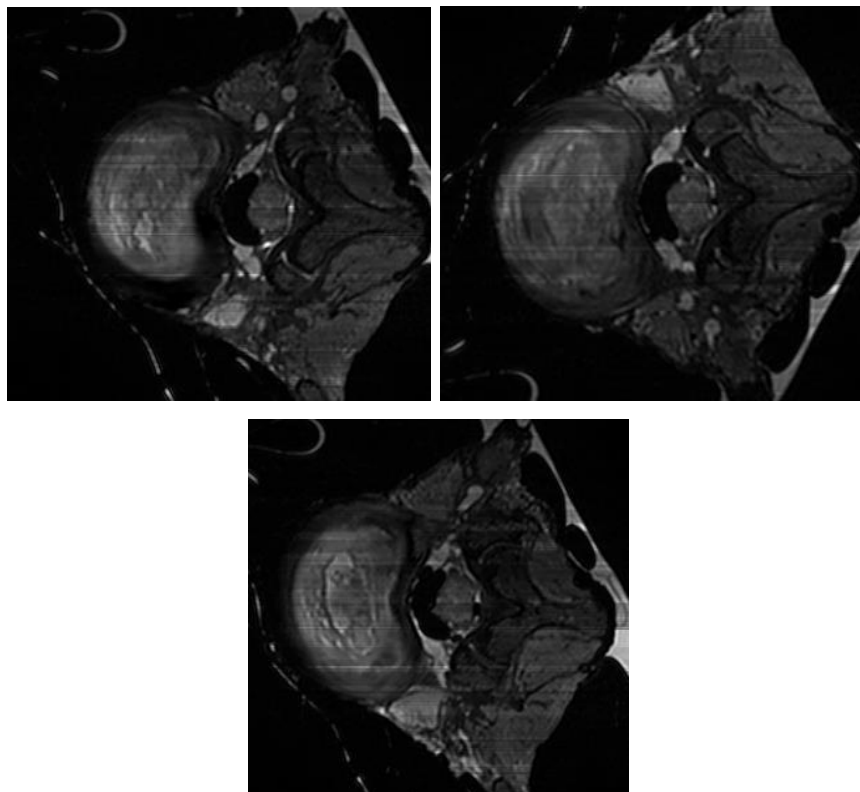
L1-L2: Pfirrmann Grade III



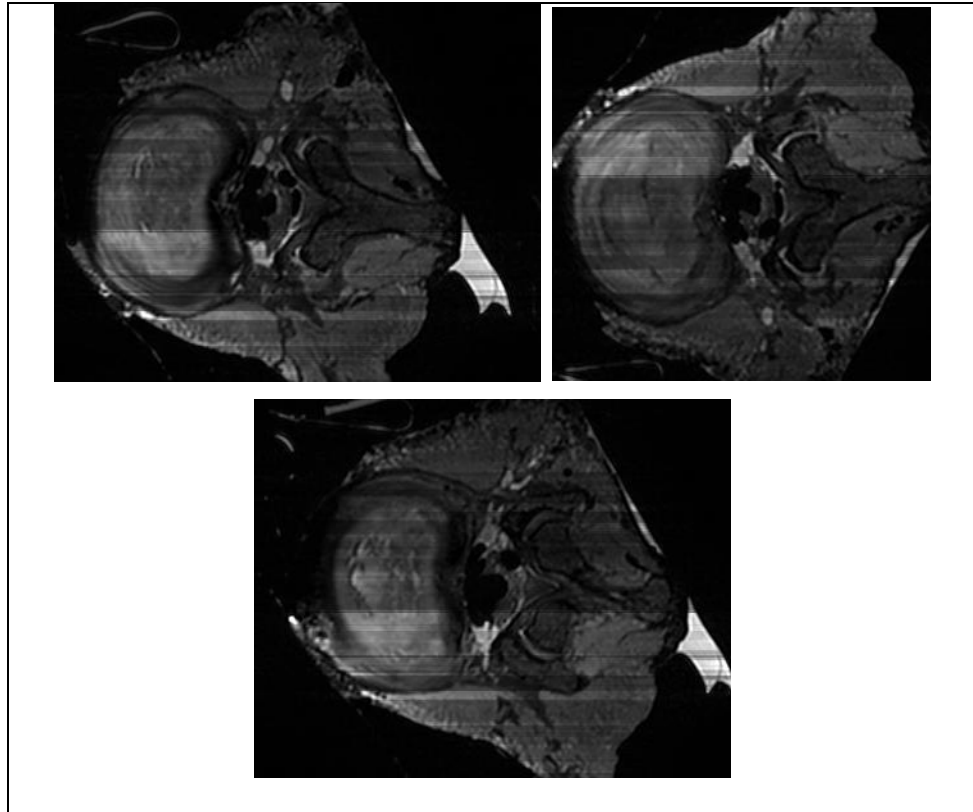
L2-L3: Pfirrmann Grade III



L3-L4: Pfirrmann Grade III



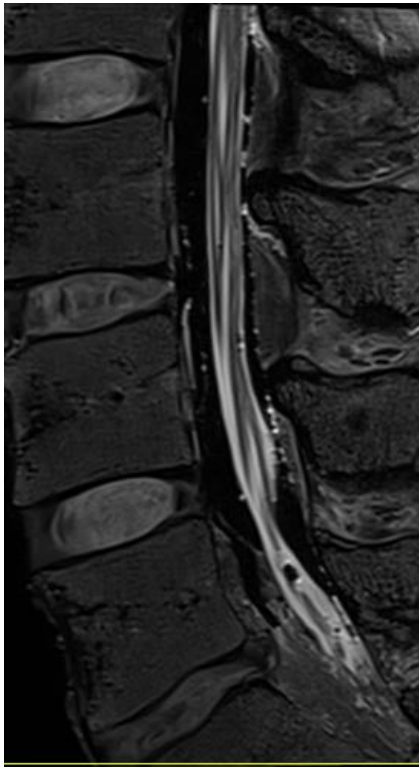
L4-L5: Pfirrmann Grade III



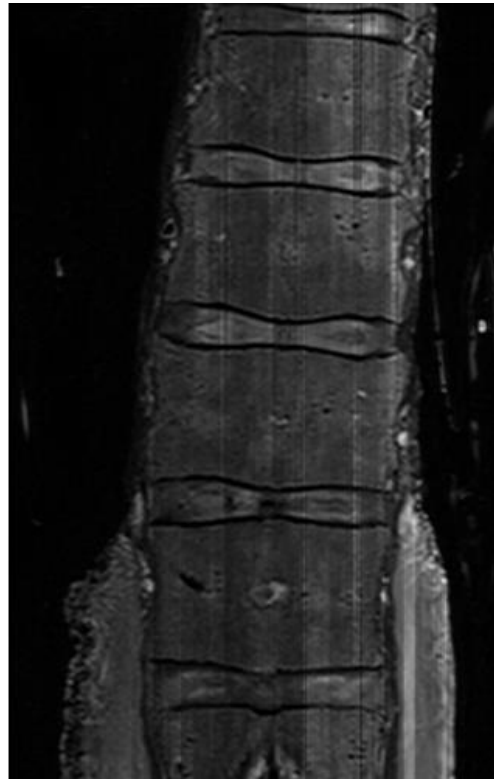
9.2 Spine 3

Scan type: T2 weighted turbo-spin-echo fat saturated imaging. Transverse plane images show cranial to caudal.

Sagittal

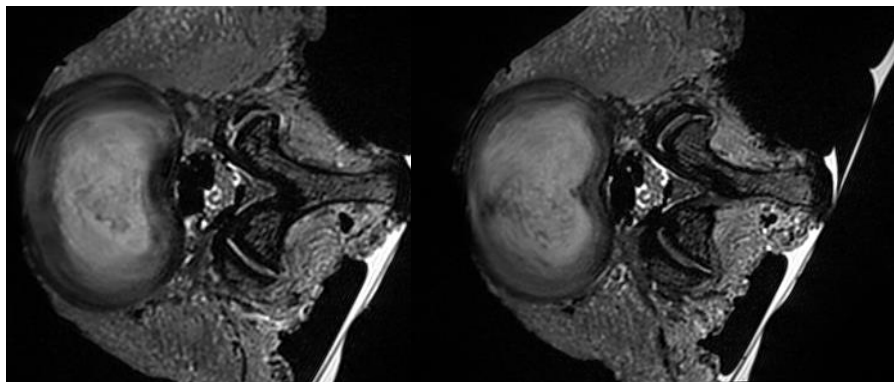


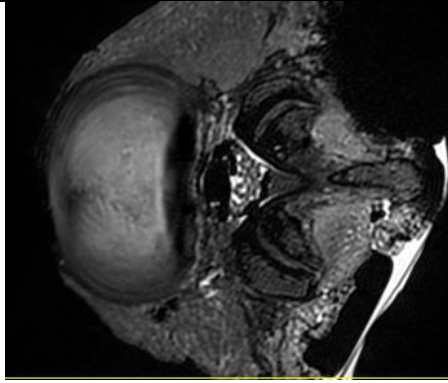
Coronal



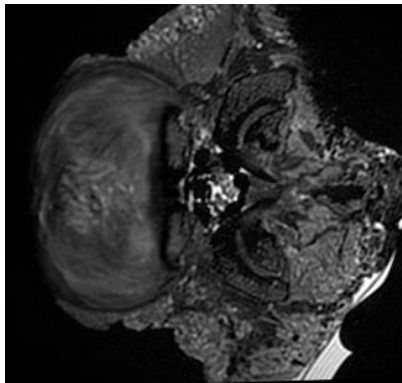
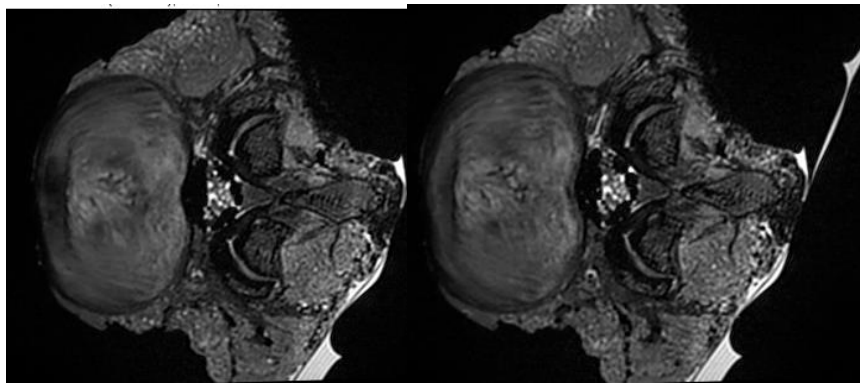
Transverse slices

L1-L2: Pfirrmann Grade III

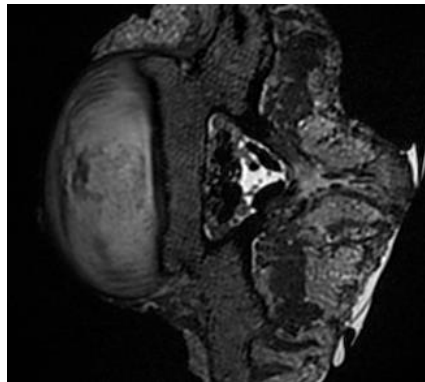
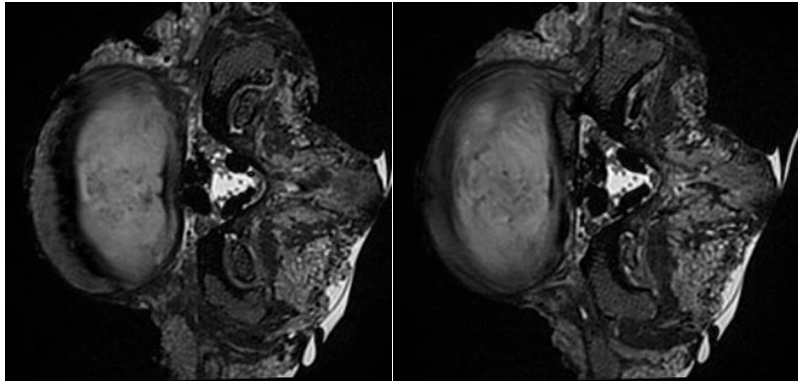




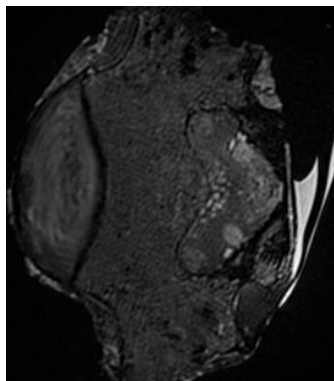
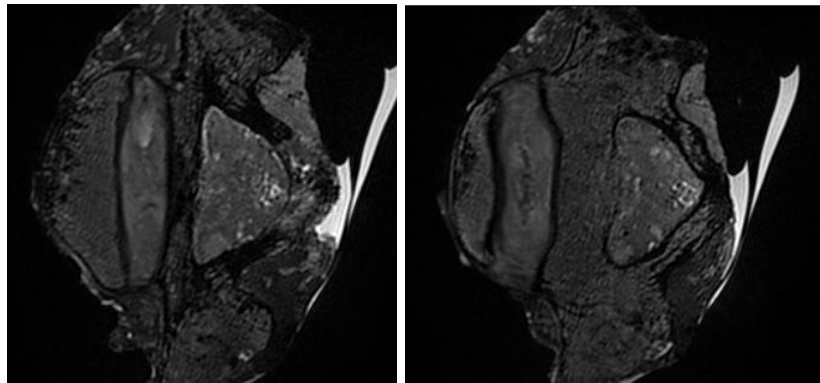
L2-L3: Pfirmann Grade III



L3-L4: Pfirrmann Grade IV

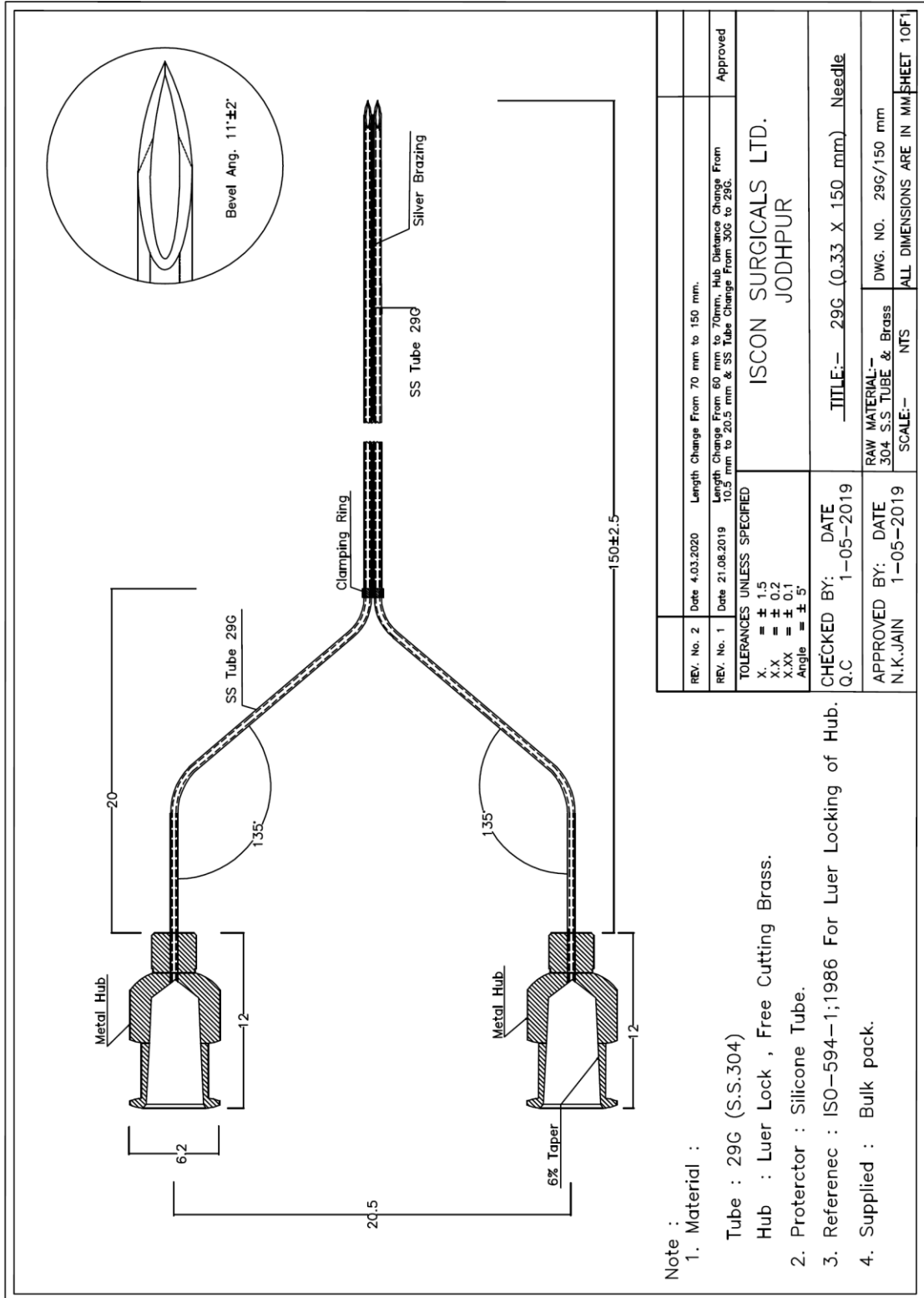


L4-L5: Pfirrmann Grade III



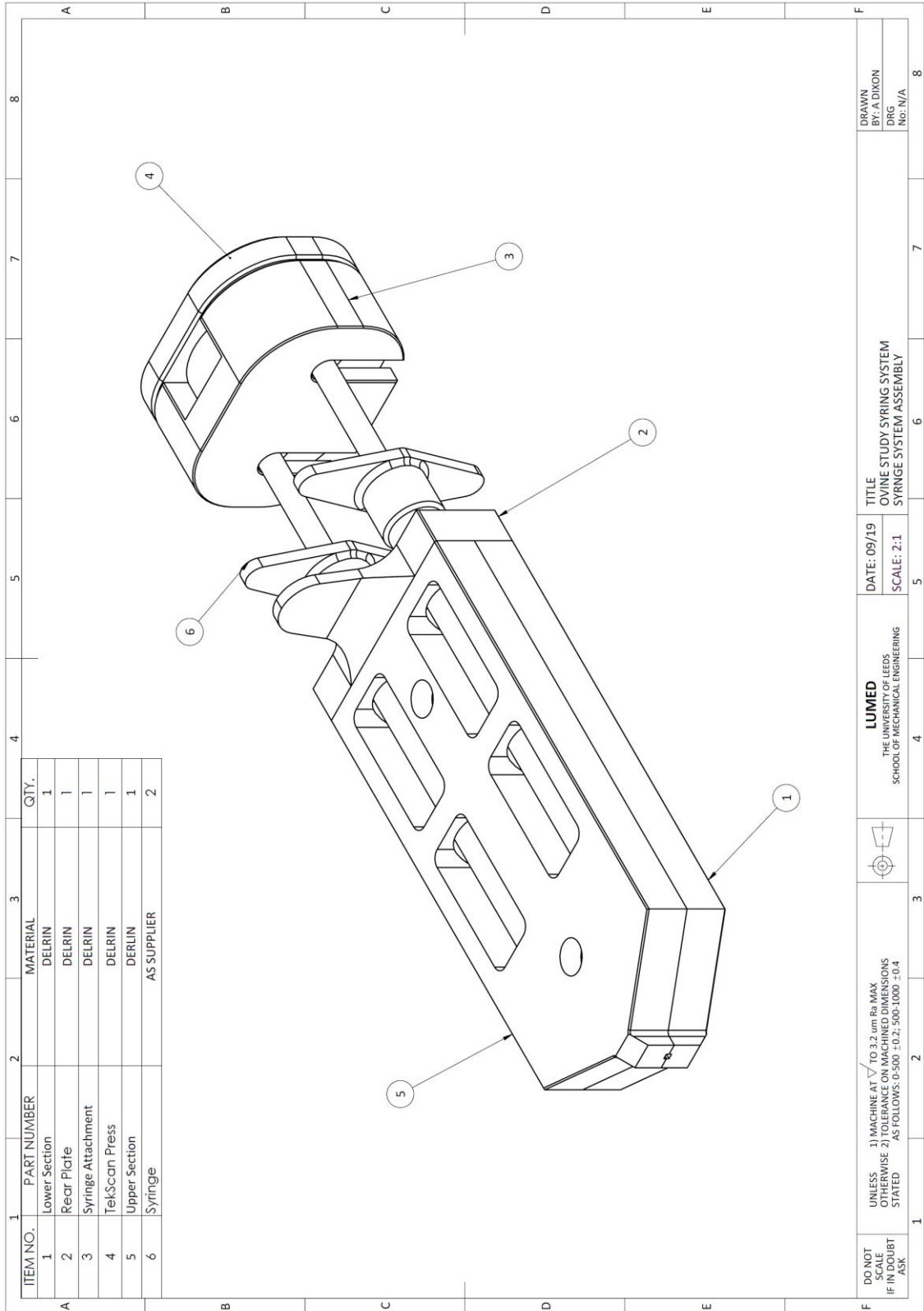
10 Appendix 3 – Technical Drawings

10.1 Specialist needle technical drawing

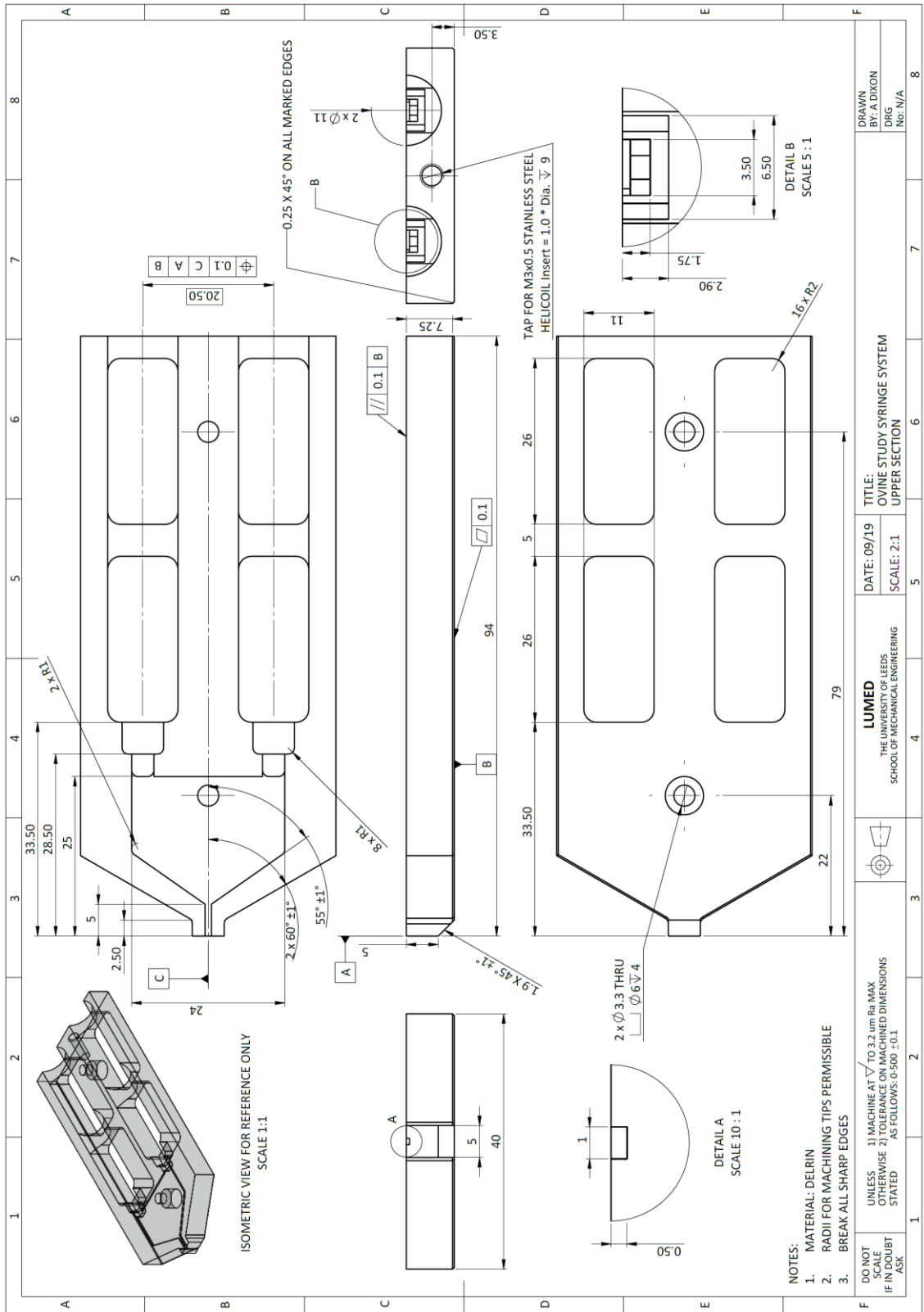


10.2 Handling device technical drawings

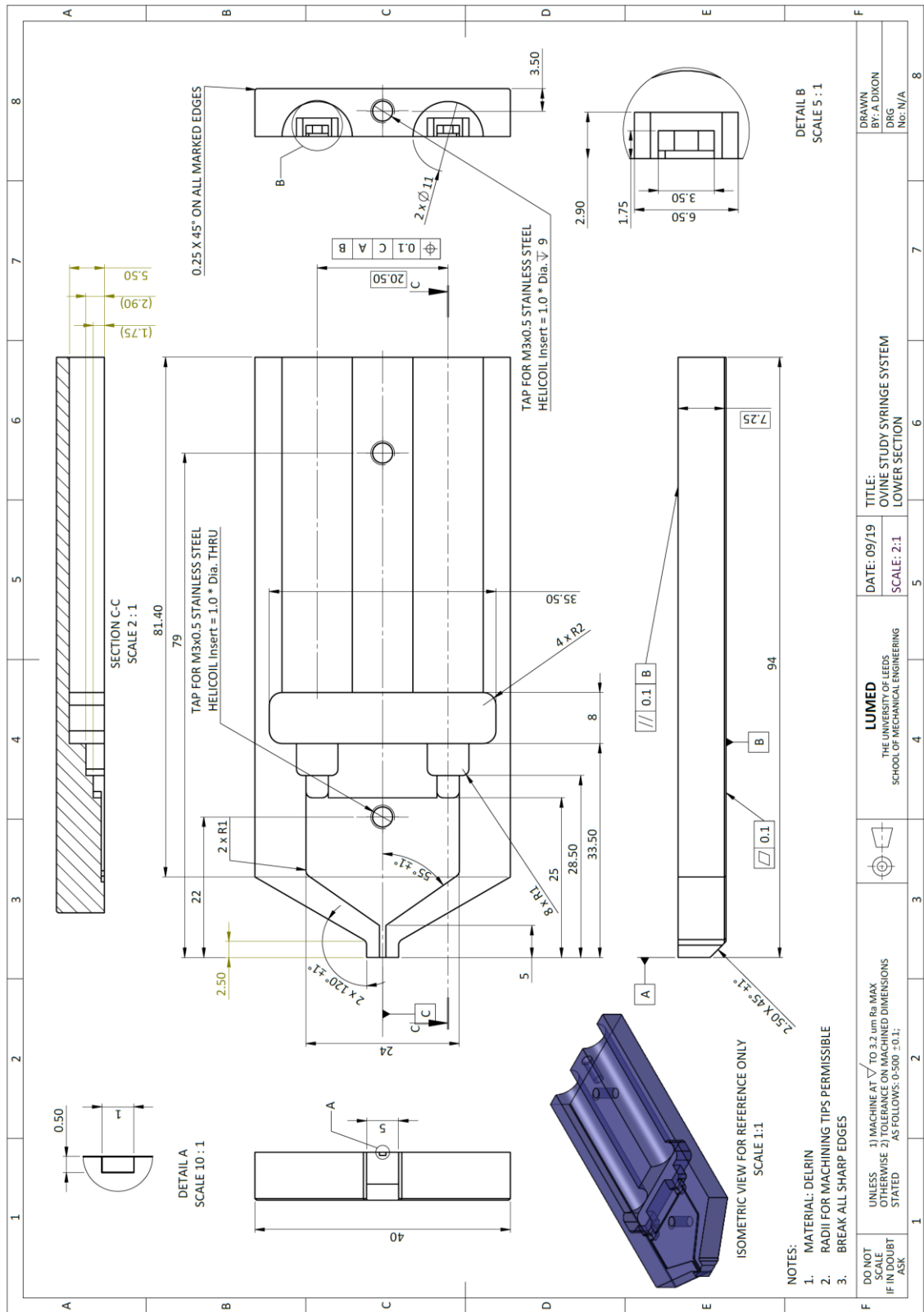
10.2.1 Assembly



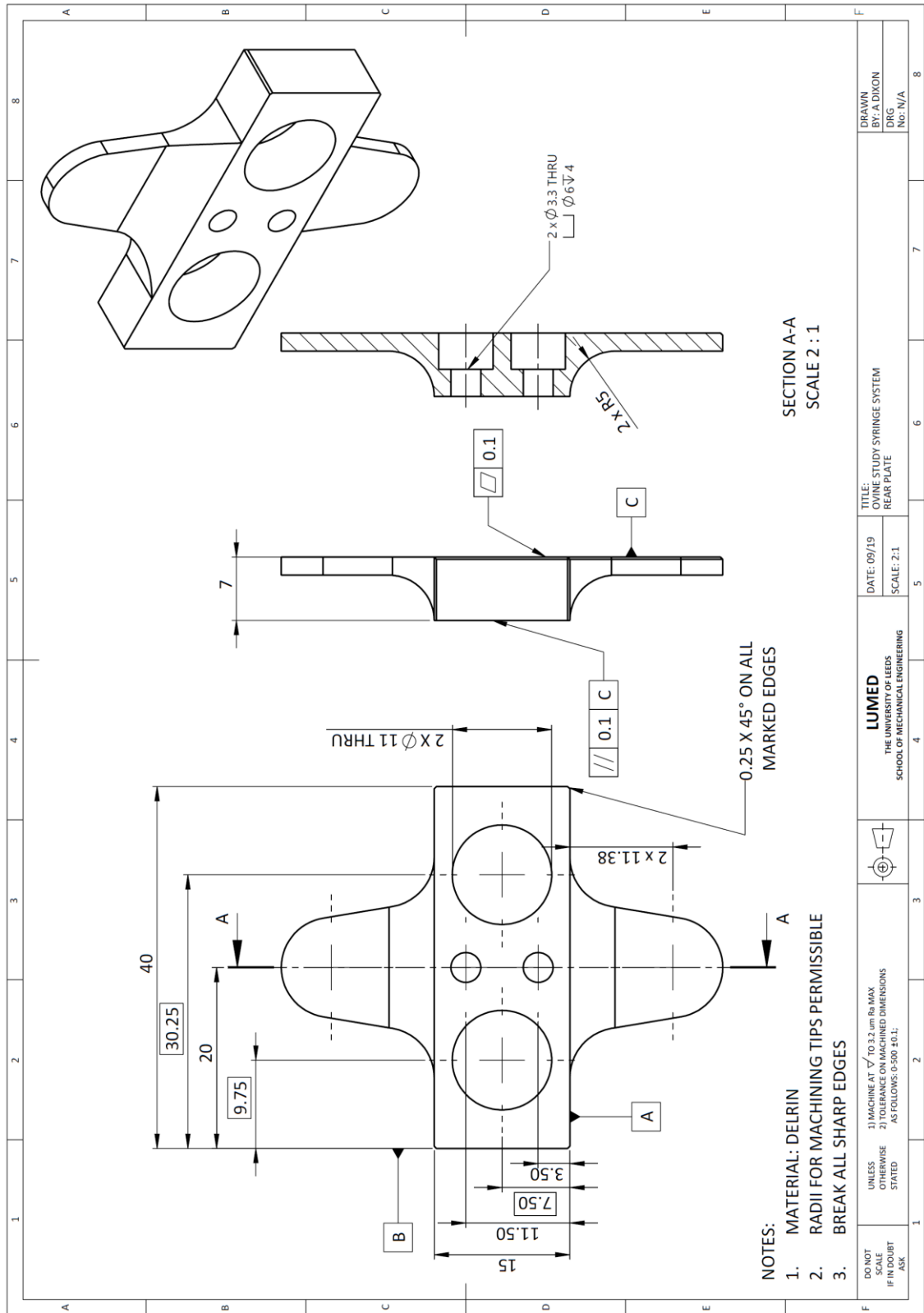
10.2.2 Device Top



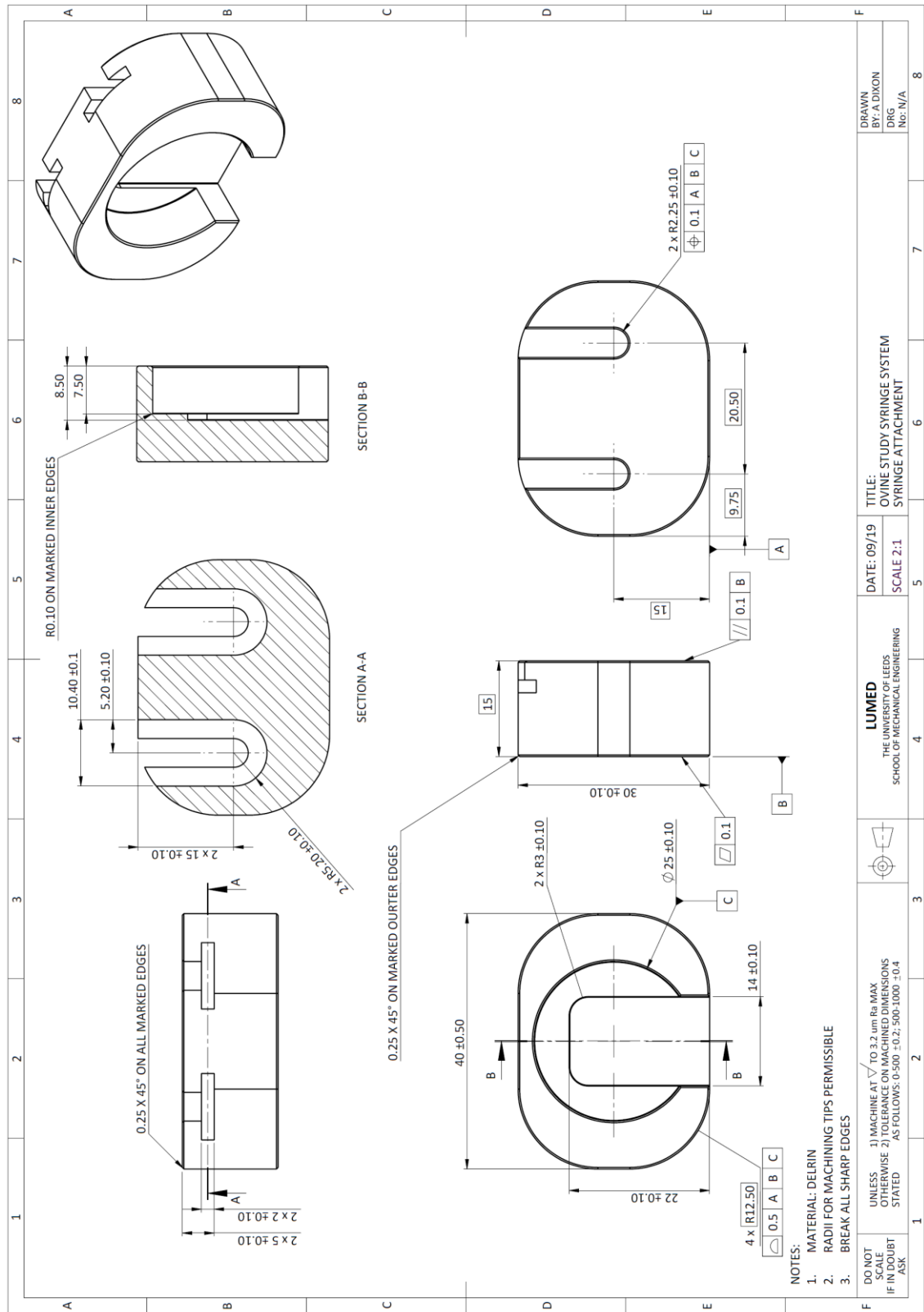
10.2.3 Device bottom



10.2.4 Rear plate



10.2.5 Syringe attachment



NOTES:
 1. MATERIAL: DELRIN
 2. RADI FOR MACHING TIPS PERMISSIBLE
 3. BREAK ALL SHARP EDGES

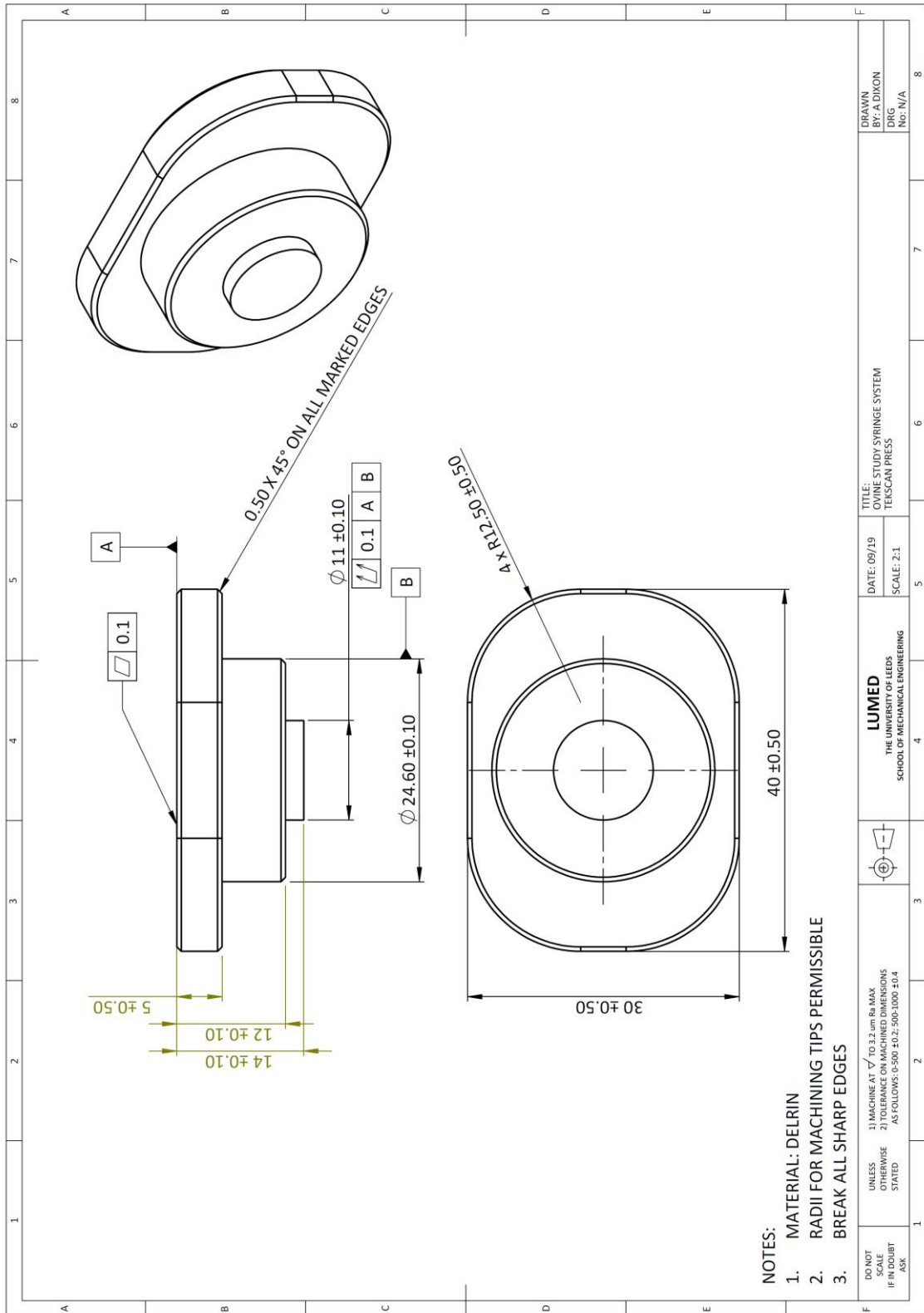
DO NOT SCALE IF IN DOUBT ASK
 UNLESS STATED OTHERWISE AS FOLLOWS:
 1) MACHINE AT $\sqrt{0.3, 0.4, 0.5, 0.6, 0.8, 1.0, 1.5, 2.0, 3.0, 4.0, 6.0, 8.0, 10.0, 15.0, 20.0, 30.0, 40.0, 60.0, 80.0, 100.0}$
 2) TOLERANCE ON MARKED DIMENSIONS AS FOLLOWS: 0-500 ± 0.2 ; 500-1000 ± 0.4

LUMED
 THE UNIVERSITY OF
 SHEFFIELD
 SCHOOL OF MECHANICAL ENGINEERING

DATE: 09/19
 SCALE 2:1
 TITLE: OVINE STUDY SYRINGE SYSTEM
 SYRINGE ATTACHMENT

DRAWN BY: A DIXON
 DRG No: N/A

10.2.6 Tekscan Press



- NOTES:
1. MATERIAL: DELRIN
 2. RADI FOR MACHINING TIPS PERMISSIBLE
 3. BREAK ALL SHARP EDGES

DO NOT SCALE IF UNLBBT ASK	UNLESS OTHERWISE STATED	1) MACHINE AT $\sqrt{}$ TO 3.2 mm Ra MAX 2) TOLERANCE ON MACHINED DIMENSIONS AS FOLLOWS: 0-500: ± 0.2 ; 500-1000: ± 0.4		LUMED THE UNIVERSITY OF LEEDS SCHOOL OF MECHANICAL ENGINEERING	DATE: 09/19 SCALE: 2:1	TITLE: OVINE STUDY SYRINGE SYSTEM TEKSCAN PRESS	DRAWN BY: A DIXON DRG NO: N/A
----------------------------	-------------------------	--	--	---	---------------------------	---	----------------------------------

10.2.7 Blanked syringe attachment

